

Heavy-ion collisions and fission dynamics with the time-dependent Hartree-Fock theory and its extensions

C. Simenel*

Department of Theoretical Physics and Department of Nuclear Physics, Research School of Physics and Engineering, The Australian National University, Canberra ACT 2601, Australia

A.S. Umar

Department of Physics and Astronomy, Vanderbilt University, Nashville, TN 37235, USA

Abstract

Microscopic methods and tools to describe nuclear dynamics have considerably been improved in the past few years. They are based on the time-dependent Hartree-Fock (TDHF) theory and its extensions to include pairing correlations and quantum fluctuations. The TDHF theory is the lowest level of approximation of a range of methods to solve the quantum many-body problem, showing its universality to describe many-fermion dynamics at the mean-field level. The range of applications of TDHF to describe realistic systems allowing for detailed comparisons with experiment has considerably increased. For instance, TDHF is now commonly used to investigate fusion, multi-nucleon transfer and quasi-fission reactions. Thanks to the inclusion of pairing correlations, it has also recently led to breakthroughs in our description of the saddle to scission evolution, and, in particular, the non-adiabatic effects near scission. Beyond mean-field approaches such as the time-dependent random-phase approximation (TDRPA) and stochastic mean-field methods have reached the point where they can be used for realistic applications. We review recent progresses in both techniques and applications to heavy-ion collision and fission.

Keywords: Time-Dependent Hartree-Fock, Heavy-Ion Fusion, Fission, Nucleus-Nucleus Potential.

*Corresponding author

Email address: `cedric.simenel@anu.edu.au` (C. Simenel)

Preprint submitted to Progress in Particle and Nuclear Physics

August 13, 2018

1. Introduction: nuclear quantum many-body dynamics

The quantum many-body problem is vital to many areas of physics. Indeed, the description of complex quantum objects of interacting particles is of interests for many physical systems, from quarks and gluons in a nucleon to macromolecules, such as fullerenes, to Bose-Einstein condensates. Consequently, major developments in the description of quantum many-body systems are often of interest to many different fields. For instance, the BCS theory introduced to describe superconductivity [1] is also widely used in nuclear physics to incorporate the effect of pairing correlations. Similarly, the tools used to study low-energy fusion with multi-channel tunneling [2] are also used to describe dissociative adsorption of molecules on a surface [3].

The similarity between dynamical processes in quantum many-body systems, whether their constituents are nucleons, electrons, or atoms, is quite striking. It is possible to make such systems vibrate, rotate, fuse, transfer particles, fission and break up. This is of course true for nuclear systems, where each of these processes can be used to learn about specific aspects of quantum many-body dynamics. For instance, the study of nuclear vibrations tells us how single-particles can produce collective motion, what is its interplay with the underlying shell structure, what are the source of non-linearities leading to anharmonicities, and how collective modes get damped and decay. These concepts and many others can also be studied via heavy-ion collisions:

- Heavy-ion fusion could be a tool to understand thermalization of a many-body system initially out of equilibrium. Fusion is also well suited to investigate the quantum tunneling of complex systems over orders of magnitudes in terms of barrier transmission probabilities. This allows to study the coupling between relative motion (the main collective degree of freedom used to characterize fusion) with other internal degrees of freedom (vibrations, rotations, single-particle excitations...). These internal degrees of freedom could also be responsible for dissipation and decoherence processes, whose descriptions remain problematic with fully quantum treatments.
- Transfer reactions between heavy-ions are another example of mechanism strongly driven by quantum dynamical processes. Such reactions produce entangled fragments in coherent superpositions of proton and neutron numbers. The measurement of the properties of one fragment (e.g., particle number or kinetic energy) induces a projection of the quantum state of the other fragment. Transfer reactions are also ideal to investigate clustering and superfluidity (via, e.g., the excitation of pairing vibrations). In addition, they are thought to be a doorway to dissipation in heavy-ion collisions. Interesting questions regarding the indistinguishability in the transfer of identical particles could also be raised.
- At higher energies, deep-inelastic collisions (DIC) can be used to investigate quantum fluctuations, via, e.g., the measurement of fragment mass and charge distributions. In addition, dissipation and fluctuations are correlated in a dynamical way. The finite contact times between the fragments give access to equilibration times of initial asymmetries between the collision partners (e.g., mass and isospin asymmetries). DIC and quasi-fission reactions can also be used to test the persistence of the quantum shell corrections (responsible, e.g., for the formation of magic fragments) with respect to the excitation energy of the fragments.

- Finally, nuclear fission is probably the mechanism which has the most to teach us about the diversity of quantum many-body dynamical aspects. It is then not surprising that, in turns, it is the most complicated reaction to describe. Not only it is a large amplitude collective motion which involves the overcoming of one or several barriers (where quantum tunneling could happen), it is also strongly affected by shell effects, superfluidity, fluctuations and dissipation. Naively, it could be seen as the reverse process of fusion. However, the mechanisms which produce fission fragments are often much more difficult to describe than in the fusion case. It has to do essentially with the adiabatic (slow motion in a space of collective degrees of freedom where the other internal degrees of freedoms are assumed to be at equilibrium) to non-adiabatic transition occurring between the fission saddle point and the scission point where the entangled fragments are formed.

Table 1: Examples of many-body systems and their environments.

	Nuclei	Atoms	Molecules
Size	$\sim 10^{-14}$ m	$\sim 10^{-10}$ m	$\sim 10^{-9}$ m
Time scale	10^{-21} s=1 zs	10^{-18} s=1 as	10^{-15} s=1 fs
Environment	none	EM	EM+gas
Equation of motion	<i>Quantum</i>	<i>Quantum</i> (<i>Classical</i>)	<i>Classical</i> (<i>Quantum</i>)

In addition to the diversity of phenomena accessible in heavy-ion collisions, what makes them special to test predictions of quantum many-body theories is their almost complete isolation from external environments. It is well known that the coupling of a system to an external environment induces a decoherence process which is responsible for the quantum to classical transition [4, 5]. Atoms and molecules have different sizes and native time scales than atomic nuclei and, in turn, do not interact with the same environments (see Tab. 1). In particular, atomic and molecular dynamics are easily affected by the coupling to electromagnetic field (and to collisions with the particles of the surrounding gas for the largest systems). The typical time scale for the collision of atomic nuclei, however, is of the order of few zeptoseconds (1 zs= 10^{-21} s), which is usually too short to emit or absorb photons. The quantum coherence built up during the collision is then preserved until after the outcome of the collision has been decided. In other words, no major decoherence processes are expected to occur and affect the quantum nature of the reaction. Heavy-ion collisions are then ideal to study fundamental concepts of quantum physics, such as the existence of collective motion in many-particle systems [6], the interplay between quantum tunneling and dissipation [7], coupled reaction channels effects [3], and entanglement properties [8].

Nuclear physicists can put together up to about 500 interacting nucleons over a very short time (few zeptoseconds) thanks to actinide collisions. (Of course, many more nucleons may interact in astrophysical systems such as neutron stars.) Describing such reactions and predicting their outcomes is of course a great challenge. As discussed above, several reactions could occur, which are sometimes in competition with each other for a given collision energy. Ideally, the same theoretical model should be able to describe all types of nuclear dynamics. To some extent, this is possible at the mean-field level, where the particles evolve independently in the mean-field generated by the ensemble of

particles. For fermions, this is described by the time-dependent Hartree-Fock (TDHF) theory proposed by Dirac in 1930 [9].

In his original work, Dirac introduced the TDHF equation to describe the electrons in atoms. The first applications of the TDHF formalism to nuclear systems was due to Bonche and co-workers in 1976 [10]. Since then, several groups have developed and used TDHF codes to study nuclear dynamics, with a strong revival of the approach in the past ten years as it became clear that the TDHF theory was a tool of choice to describe low-energy reactions to be studied with the upcoming radioactive beam facilities. Indeed, applications to heavy-ion collisions at energies close to the Coulomb barrier with stable nuclei have led to realistic description of nuclear dynamics, motivating new TDHF studies focussing on reactions with exotic nuclei at low-energy. Although the applicability of the TDHF approach at low-energy has been demonstrated, it is not clear how high in energy one can go before the mean-field approximation breaks down. TDHF calculations of heavy-ion collisions at more than twice the barrier energy have given realistic results [11] as long as one focusses on expectation values of one-body observables for which TDHF is optimised [12]. Collisions up to 40 MeV/nucleon have also been simulated with TDHF to investigate charge equilibration [13] and reactions leading to supranormal density [14]. However, all applications presented in this review are much lower in energy. Nevertheless, it would be interesting in the future to investigate the energy range for applicability of the TDHF theory to heavy-ion collisions.

Earlier investigations of nuclear dynamics within the TDHF framework have been summarized in previous reviews [15–17]. Nevertheless, several new techniques have been developed and new applications have been made in the past few years. These new techniques include the extraction of microscopic nucleus-nucleus potentials in fusion reactions, the development of projection techniques to better characterize the fragment properties, the inclusion of time-dependent pairing correlations, beyond mean-field quantum fluctuations, optimization of collective coordinates, improvement of boundary conditions, etc. These led to new applications such as to better understand fusion with exotic nuclei, multi-nucleon transfer reactions, dissipative processes in DIC, the role of shell effects in quasi-fission, non-adiabatic effects in fission, etc. The present review will focus on these recent works.

2. Formalism

2.1. Introduction

Various formalisms have been developed in the past to describe the dynamics of quantum many-body systems (see Fig. 1). Some of these approaches are based on variational principles, while others rely on perturbation theory. Interestingly, at the lowest level of approximation they usually lead to the time-dependent Hartree-Fock self-consistent mean-field theory [9]. The fact that the TDHF equation can be derived in so many ways illustrates its universality. It is also interesting to see what are the underlying approximations used in deriving the TDHF equation in these various approaches as they inform us on the domain of applicability of the theory. For instance, the Thouless theorem [18] can be used to extract the mean-field contribution to the dynamics (see, e.g., [19]), while the approach of Blaizot and Ripka is optimized to scattering amplitudes [20]. The next section describes how the TDHF equation is obtained in different approaches.

In the following, we give only a brief description of standard approaches to microscopic dynamics based on the mean-field approximation. For more details, see earlier reviews [15–17, 19].

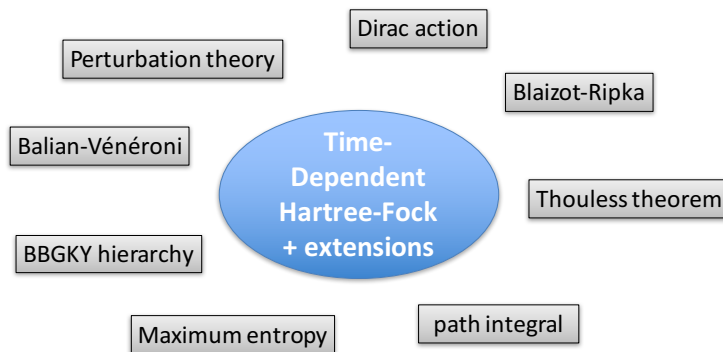


Figure 1: Various approaches leading to the TDHF equation and to its extensions.

For non-relativistic systems, the evolution of the state $|\Psi(t)\rangle$ is given by the Schrödinger equation

$$i\hbar \frac{\partial}{\partial t} |\Psi(t)\rangle = \hat{H} |\Psi(t)\rangle. \quad (1)$$

In the case of a two-body interaction $\hat{v}(1, 2)$, the Hamiltonian can be written as

$$\hat{H} = \sum_{i=1}^A \frac{\hat{\mathbf{p}}(i)^2}{2m} + \sum_{i>j=1}^A \hat{v}(i, j) \equiv \sum_{ij} t_{ij} \hat{a}_i^\dagger \hat{a}_j + \frac{1}{4} \sum_{ijkl} \bar{v}_{ijkl} \hat{a}_i^\dagger \hat{a}_j^\dagger \hat{a}_l \hat{a}_k, \quad (2)$$

where A is the total number of particles and \bar{v} denotes antisymmetrized matrix elements. The many-body state $|\Psi\rangle$ contains all the information on the system, including all types of correlations between the nucleons. We often require only a small subset of this information. For instance, we can often content ourselves with the knowledge of one-body

observables of the form $\hat{F} = \sum_{i=1}^A \hat{f}(i)$, such as particle number operators, kinetic energy, momentum, multipole moment among others. If our focus is on the expectation value of such an operator, then its time evolution is given by the Ehrenfest theorem

$$\frac{\partial}{\partial t} \langle \hat{F} \rangle_\psi = \frac{i}{\hbar} \langle [\hat{H}, \hat{F}] \rangle_\psi. \quad (3)$$

The above equation is exact and valid for any (correlated or not) state. The expectation value of \hat{F} ,

$$\langle \hat{F} \rangle = \sum_{\alpha\beta} f_{\alpha\beta} \rho_{\beta\alpha} = \text{tr}(\rho f), \quad (4)$$

only requires the knowledge of the one-body density matrix ρ with matrix elements

$$\rho_{\alpha\beta} = \langle \Psi | \hat{a}_\beta^\dagger \hat{a}_\alpha | \Psi \rangle, \quad (5)$$

where \hat{a}_α (\hat{a}_α^\dagger) annihilates (creates) a particle in the single-particle state $|\alpha\rangle$. It is therefore not surprising that the one-body density matrix plays a central role in the various approximation schemes discussed below.

2.2. Quantum many-body perturbation theory

Quantum many-body perturbation theory offers an elegant way to derive the Hartree-Fock equation (see, e.g., [21]). In particular, the origin of the self-consistency of the theory is relatively clear in this approach: It is due to the fact that the propagation of a particle is affected by its interaction with other particles, which are themselves interacting particles. An important quantity is then $\langle \Psi_0 | \hat{\psi}_H(x' s' q') \hat{\psi}_H^\dagger(x s q) | \Psi_0 \rangle$ in the Heisenberg representation¹. It is associated with the amplitude of probability for a nucleon with spin s and isospin q created at space-time position $x = (\mathbf{x}, t)$ on top of the interacting ground-state Ψ_0 to propagate and be found at $x' = (\mathbf{x}', t' > t)$ with s' and q' where it is annihilated². Similarly, the quantity $\langle \Psi_0 | \hat{\psi}_H^\dagger(x' s' q') \hat{\psi}_H(x s q) | \Psi_0 \rangle$, where the annihilation occurs before the creation, plays also an essential role.

Both terms are combined in the single-particle Green's function or Feynman propagator

$$\begin{aligned} iG(x, x') &= \langle \Psi_0 | T[\hat{\psi}_H(x) \hat{\psi}_H^\dagger(x')] | \Psi_0 \rangle \\ &= \langle \Psi_0 | \hat{\psi}_H(x) \hat{\psi}_H^\dagger(x') | \Psi_0 \rangle \Theta(t - t') - \langle \Psi_0 | \hat{\psi}_H^\dagger(x') \hat{\psi}_H(x) | \Psi_0 \rangle \Theta(t' - t), \end{aligned} \quad (6)$$

where T is the time ordering operator, and where spin and isospin indices have been dropped for simplicity³. The minus sign in front of the last term is due to the fermionic nature of the system. The Green's function is central in quantum field theory as it can be used to compute important quantities such as the one-body density matrix (in the interacting ground-state): $\rho(\mathbf{r}, \mathbf{r}'; t) = \langle \Psi_0 | \hat{\psi}^\dagger(\mathbf{r}' t) \hat{\psi}(\mathbf{r} t) | \Psi_0 \rangle = -iG(\mathbf{r} t, \mathbf{r}' t^+)$.

¹In the case of a time-independent Hamiltonian, we have $\hat{F}_H(t) = e^{i\hat{H}t/\hbar} \hat{F} e^{-i\hat{H}t/\hbar}$.

²Of course, nucleons are indistinguishable fermions and there is no guarantee that the nucleon which is annihilated is the same as the one which is created. In fact, the question of "which one" is created or annihilated does not make sense.

³See, e.g., Ref. [21] for a derivation including spin.

The perturbation theory is based on the separation of the Hamiltonian (which we assume to be time independent) into $\hat{H} = \hat{H}_0 + \hat{V}$ where \hat{H}_0 is the non interacting Hamiltonian (kinetic energy plus an eventual external one-body potential) and \hat{V} is the interaction [see eq. (2)]. It is then more convenient to use the interaction representation where the operators evolve according to the non-interacting Hamiltonian only: $\hat{F}_I(t) = e^{i\hat{H}_0 t/\hbar} \hat{F} e^{-i\hat{H}_0 t/\hbar}$. The Green's function can then be written as

$$iG(x, y) = \sum_{n=0}^{\infty} \left(\frac{-i}{\hbar}\right)^n \frac{1}{n!} \int_{-\infty}^{+\infty} dt_1 \cdots dt_n \frac{\langle \Phi_0 | T [\hat{V}_I(t_1) \cdots \hat{V}_I(t_n) \hat{\psi}_I(x) \hat{\psi}_I^\dagger(y)] | \Phi_0 \rangle}{\langle \Phi_0 | \hat{U}(-\infty, +\infty) | \Phi_0 \rangle} \quad (7)$$

where Φ_0 is the non-interacting ground-state of \hat{H}_0 and \hat{U} the evolution operator (with interaction).

Feynman diagrams (see Appendix) provide a powerful way to calculating the terms in the expansion of $G(x, y)$. In particular, all non-connected diagrams in the numerator can be factorised and cancelled by the denominator, leading to

$$iG(x, y) = \sum_{n=0}^{\infty} \left(\frac{-i}{\hbar}\right)^n \frac{1}{n!} \int_{-\infty}^{+\infty} dt_1 \cdots dt_n \langle \Phi_0 | T [\hat{V}(t_1) \cdots \hat{V}(t_n) \hat{\psi}(x) \hat{\psi}^\dagger(y)] | \Phi_0 \rangle_{connect.} \quad (8)$$

where only connected diagrams remain. Here and in the following, the subscript I of the interaction representation is dropped to simplify the notation. The above equation can be expressed as

where the thin lines refer to the non-interacting system with the propagator $iG^0(x, y) = \langle \Phi_0 | T [\hat{\psi}(x) \hat{\psi}^\dagger(y)] | \Phi_0 \rangle$, the curly lines correspond to interaction terms $\mathcal{V}(x, x')$, and Σ is the self energy of the interacting system. The first and second diagrams with an interaction line are the “direct” and “exchange” contributions to the first order term of the expansion, respectively. Using Feynman rules (see Appendix), the direct and exchange terms are respectively

$$\frac{i}{\hbar} \int d^4 z d^4 z' (-1) G^0(x, z) \mathcal{V}(z, z') G^0(z, y) G^0(z', z')$$

and

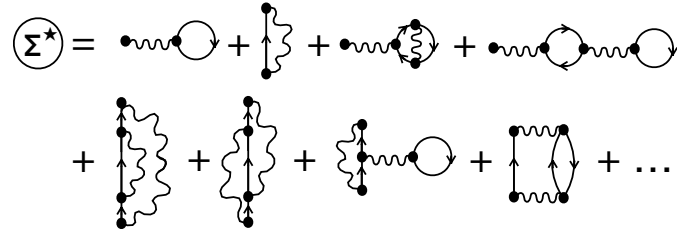
$$\frac{i}{\hbar} \int d^4 z d^4 z' G^0(x, z) \mathcal{V}(z, z') G^0(z, z') G^0(z', y).$$

We see that each diagram involves single-particle non-interacting Green's function G^0 , which can easily be calculated, as well as matrix elements of the interaction.

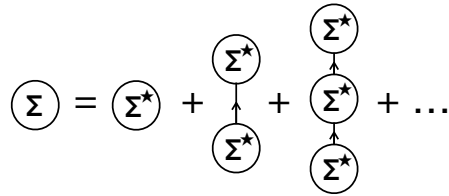
There is of course an infinite number of diagrams to calculate which makes the perturbation theory useless unless the interaction is small enough to neglect diagrams above a given order in the expansion. One could for instance neglect diagrams above the first

order. We see that, in this case, the particle propagating between x and y space-time positions interacts with another particle which itself propagates without interaction as its propagator is G^0 . The resulting theory is therefore not self-consistent.

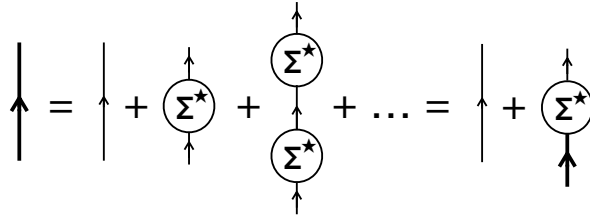
It is possible to construct a self-consistent theory by rewriting the self energy Σ in terms of “proper self energy” insertions, i.e., diagrams with an incoming and an outgoing particle and which cannot be cut into two pieces by cutting a single-particle line. The proper self energy Σ^* is the sum of these diagrams:



The self energy can then be written as



leading to Dyson's equation for $G(x, y)$:



or equivalently

$$G(x, y) = G^0(x, y) + \int d^4 z d^4 z' G^0(x, z) \Sigma^*(z, z') G(z', y). \quad (9)$$

We see that the interacting single-particle Green's function G is now present on both sides of the equation.

So far no approximations have been made and the problem remains impractical as the proper self energy Σ^* contains an infinite number of diagrams. A possible approximation is to keep only the first order diagrams in Σ^* :

$$\textcircled{\Sigma^*} \approx \textcircled{\Sigma_{(i)}^*} = \textcircled{\text{wavy line}} + \textcircled{\text{self-energy}}$$

However, this again leads to a lack of self consistency as the particle line is the non-interacting one.

In the self-consistent Hartree-Fock approximation, the above diagrams are replaced by

$$\textcircled{\Sigma^*} \approx \textcircled{\Sigma_{HF}^*} = \textcircled{\text{wavy line}} + \textcircled{\text{self-energy}}$$

where the interaction occurs with an interacting particle (i.e., with the propagator G instead of G^0). For simplicity, we consider an interaction of the form $\mathcal{V}(x, x') = V(\mathbf{x} - \mathbf{x}')\delta(t - t')$. Using Feynman rules, we get

$$\Sigma_{HF}^*(x, x') = \frac{-i\delta(t - t')}{\hbar} \left[\delta(\mathbf{x} - \mathbf{x}') \int d^3x'' G(\mathbf{x}''t, \mathbf{x}''t^+) V(\mathbf{x} - \mathbf{x}'') - V(\mathbf{x} - \mathbf{x}') G(\mathbf{x}t, \mathbf{x}'t^+) \right]. \quad (10)$$

The first term in the right hand side is the direct (Hartree) contribution and the last term is the exchange (Fock) one. The Dyson's equation for $G(x, y)$ in the self-consistent Hartree-Fock approximation becomes

$$\textcircled{\uparrow} \approx \textcircled{\uparrow} + \textcircled{\uparrow \text{ wavy line } \uparrow} + \textcircled{\uparrow \text{ self-energy } \uparrow}$$

that is,

$$G(x, y) \approx G^0(x, y) + \int d^4z d^4z' G^0(x, z) \Sigma_{HF}^*(z, z') G(z', y). \quad (11)$$

Rewriting the proper self energy as $\Sigma_{HF}^*(x, y) = \delta(t_x - t_y) \Sigma_{HF}^*(\mathbf{x}, \mathbf{y})$ and using Fourier transform in the time domain defined as

$$G(x, y) = \frac{1}{2\pi} \int_{-\infty}^{+\infty} d\omega e^{-i\omega(t_x - t_y)} G(\mathbf{x}, \mathbf{y}, \omega) \quad (12)$$

we get

$$G(\mathbf{x}, \mathbf{y}, \omega) = G^0(\mathbf{x}, \mathbf{y}, \omega) + \int d^3z d^3z' G^0(\mathbf{x}, \mathbf{z}, \omega) \Sigma_{HF}^*(\mathbf{z}, \mathbf{z}') G(\mathbf{z}', \mathbf{y}, \omega). \quad (13)$$

It is convenient to use the single-particle states φ_i^0 with single-particle energy e_i^0 associated with eigenstates of the non-interacting Hamiltonian \hat{H}_0 . Using $\hat{\psi}(x) = \sum_i \varphi_i^0(\mathbf{x}) \hat{a}_i(t)$ and its Hermitian conjugate, the non-interacting single-particle Green's function can be written as

$$\begin{aligned} iG^0(x, x') &= \langle \Phi_0 | T \left[\sum_{ij} \varphi_i^0(\mathbf{x}) \varphi_j^{0*}(\mathbf{x}') \hat{a}_i(t) \hat{a}_j^\dagger(t') \right] | \Phi_0 \rangle \\ &= \langle \Phi_0 | T \left[\sum_{ij} \varphi_i^0(\mathbf{x}) \varphi_j^{0*}(\mathbf{x}') e^{i\hat{H}_0 t/\hbar} \hat{a}_i e^{-i\hat{H}_0(t-t')/\hbar} \hat{a}_j^\dagger e^{-i\hat{H}_0 t'/\hbar} \right] | \Phi_0 \rangle \\ &= \sum_i \varphi_i^0(\mathbf{x}) \varphi_i^{0*}(\mathbf{x}') e^{-ie_i^0(t-t')/\hbar} [\Theta(t-t')\Theta(e_i^0 - \epsilon_F^0) - \Theta(t'-t)\Theta(\epsilon_F^0 - e_i^0)] \end{aligned}$$

where we have used $\langle \Phi_0 | \hat{a}_i \hat{a}_j^\dagger | \Phi_0 \rangle = \delta_{ij} \Theta(e_i^0 - \epsilon_F^0)$ and $\langle \Phi_0 | \hat{a}_j^\dagger \hat{a}_i | \Phi_0 \rangle = \delta_{ij} \Theta(\epsilon_F^0 - e_i^0)$ with the Fermi energy ϵ_F^0 . This leads to the time-Fourier transform

$$\begin{aligned} G^0(\mathbf{x}, \mathbf{y}, \omega) &= \sum_i \varphi_i^0(\mathbf{x}) \varphi_i^{0*}(\mathbf{y}) \left[\frac{\Theta(e_i^0 - \epsilon_F^0)}{\omega - \frac{e_i^0}{\hbar} + i\eta} + \frac{\Theta(\epsilon_F^0 - e_i^0)}{\omega - \frac{e_i^0}{\hbar} - i\eta} \right] \\ &= \sum_i \varphi_i^0(\mathbf{x}) \varphi_i^{0*}(\mathbf{y}) \frac{1}{\omega - \frac{e_i^0}{\hbar} + \text{sign}(e_i^0 - \epsilon_F^0) i\eta}. \end{aligned} \quad (14)$$

By analogy with $G^0(\mathbf{x}, \mathbf{y}, \omega)$ and using the fact that Σ_{HF}^* does not depend on ω , we can search for solutions of the Dyson's equation of the form

$$G(\mathbf{x}, \mathbf{y}, \omega) = \sum_i \varphi_i(\mathbf{x}) \varphi_i^*(\mathbf{y}) \frac{1}{\omega - \frac{e_i}{\hbar} + \text{sign}(e_i - \epsilon_F) i\eta}, \quad (15)$$

where $\varphi_i(\mathbf{x})$ is a single-particle eigenstate of the correlated system with single-particle energy e_i and Fermi energy ϵ_F . Note that, by construction, the many-body ground-state of the interacting system is approximated by a Slater determinant, with single-particle states fully occupied below ϵ_F and empty above. However, unlike the expression for G^0 where φ_i^0 and e_i^0 are assumed to be known, the single-particle states φ_i and energies e_i are unknown in the interacting system.

To find an equation for $\varphi_i(\mathbf{x})$ and e_i , we first apply $\hbar\omega - H_0$ to the left of Eq. (13). Noting that

$$(\hbar\omega - H_0) G^0(\mathbf{x}, \mathbf{y}, \omega) = \hbar \sum_i \varphi_i^0(\mathbf{x}) \varphi_i^0(\mathbf{y})^* = \hbar \delta(\mathbf{x} - \mathbf{y}),$$

we get

$$(\hbar\omega - H_0) G(\mathbf{x}, \mathbf{y}, \omega) = \hbar \delta(\mathbf{x} - \mathbf{y}) + \int d^3z \hbar \Sigma_{HF}^*(\mathbf{x}, \mathbf{z}) G(\mathbf{z}, \mathbf{y}, \omega). \quad (16)$$

Using expression (15) for G , multiplying by $\varphi_j(\mathbf{y})$ and integrating over \mathbf{y} gives

$$H_0 \varphi_i(\mathbf{x}) + \int d^3y \hbar \Sigma_{HF}^*(\mathbf{x}, \mathbf{y}) \varphi_i(\mathbf{y}) = e_i \varphi_i(\mathbf{x}). \quad (17)$$

For a system of fermions without external potential, the non-interacting Hamiltonian is just the kinetic energy, i.e., $H_0 = \frac{-\hbar^2 \nabla^2}{2m}$. The self-energy in Eq. (17) acts as a mean-field potential induced by the interactions between particles. We then recognise a single-particle Schrödinger equation $h\varphi_i = e_i\varphi_i$ with the single-particle Hamiltonian $h = \frac{\mathbf{p}^2}{2m} + \hbar\Sigma_{HF}^*$. Using the expressions (12) and (15) for G , we can show that the one-body density matrix $\rho(\mathbf{x}, \mathbf{y}) = -iG(\mathbf{x}t, \mathbf{y}t^+)$ in the HF ground-state is expressed as $\rho(\mathbf{x}, \mathbf{y}) = \sum_{i=1}^A \varphi_i(\mathbf{x})\varphi_i(\mathbf{y})$ with the sum running over the occupied single-particle states with $e_i < \epsilon_F$. We then get the HF equation in its usual form

$$[h, \rho] = 0. \quad (18)$$

The expression for the mean-field potential can be obtained from Eq. (10):

$$\begin{aligned} \hbar\Sigma_{HF}^*(\mathbf{x}, \mathbf{x}') &= -\delta(\mathbf{x} - \mathbf{x}') \int d^3x'' iG(\mathbf{x}''t, \mathbf{x}''t^+)V(\mathbf{x} - \mathbf{x}'') + V(\mathbf{x} - \mathbf{x}') iG(\mathbf{x}t, \mathbf{x}'t^+) \\ &= \delta(\mathbf{x} - \mathbf{x}') \int d^3x'' \rho(\mathbf{x}'', \mathbf{x}'')V(\mathbf{x} - \mathbf{x}'') - V(\mathbf{x} - \mathbf{x}') \rho(\mathbf{x}, \mathbf{x}'). \end{aligned} \quad (19)$$

The above equation leads to the usual expression for the mean-field

$$\begin{aligned} \hbar\Sigma_{HF}^*(\mathbf{x}, \mathbf{y}) &= \int d^3z d^3z' \rho(\mathbf{z}', \mathbf{z}) V(\mathbf{x} - \mathbf{z}) [\delta(\mathbf{x} - \mathbf{y}) \delta(\mathbf{z} - \mathbf{z}') - \delta(\mathbf{x} - \mathbf{z}') \delta(\mathbf{z} - \mathbf{y})] \\ &= \int d^3z d^3z' \rho(\mathbf{z}', \mathbf{z}) \langle 1 : \mathbf{x}, 2 : \mathbf{z} | \hat{V}(1, 2) [| 1 : \mathbf{y}, 2 : \mathbf{z}' \rangle - | 1 : \mathbf{z}', 2 : \mathbf{y} \rangle] \\ &= \langle \mathbf{x} | \text{tr}_2 \left[\hat{\bar{V}}(1, 2) \hat{\rho}(2) \right] | \mathbf{y} \rangle \end{aligned} \quad (20)$$

where tr_2 denotes the partial trace over the degrees of freedom of the particle “2”, and \bar{V} is antisymmetrised. We see that the mean-field is self-consistent as it depends on ρ .

This derivation from the quantum many-body perturbation theory gives a natural explanation for the self-consistency of the HF mean-field. We see that it assumes an independent particle form of the many-body state, i.e., written as a Slater determinant of occupied single-particle wave-functions. It is interesting to see that the approach includes diagrams to all orders in the self energy Σ . However, the proper self energy Σ^* , which is used to build Σ , contains only a subset of diagrams. The validity of this approximation is not *a priori* straightforward. In fact, like the truncation of the BBGKY hierarchy which we see next, one drawback of this approach is that it is based on the approximation that some terms in the exact expansion can be neglected. This is in contrast with variational approaches which provide an optimal description within a subspace of states (e.g., approximating the state by a single Slater determinant).

2.3. Truncation of the BBGKY hierarchy

A one-body operator can be written as a linear combination of $\hat{a}_i^\dagger \hat{a}_j$. Therefore, it is sufficient to follow the expectation values of $\langle \hat{a}_i^\dagger \hat{a}_j \rangle$, which are nothing but the matrix elements of the one-body density matrix ρ . Using Erhenfest’s theorem in Eq. (3), we get

$$\frac{\partial}{\partial t} \langle \hat{a}_i^\dagger \hat{a}_j \rangle_\psi = \frac{\partial}{\partial t} \rho_{ji} = \frac{i}{\hbar} \langle [\hat{H}, \hat{a}_i^\dagger \hat{a}_j] \rangle_\psi. \quad (21)$$

Using the expression (2) for the Hamiltonian, we can rewrite the above equation as

$$i\hbar \frac{\partial}{\partial t} \rho(t) = [h[\rho], \rho] + \text{tr}_2 \left[v_{(1,2)}^{(res)}, C_{(1,2)} \right], \quad (22)$$

where C_{12} is the two-body correlation matrix with elements

$$C_{ijkl} = \langle \hat{a}_l^\dagger \hat{a}_k^\dagger \hat{a}_i \hat{a}_j \rangle_\psi - \rho_{jl} \rho_{ik} + \rho_{il} \rho_{jk}. \quad (23)$$

The partial trace is taken over the degrees of freedom of the particle “2”,

$$\text{tr}_2 \{ v_{(1,2)} C_{(1,2)} \}_{\alpha\beta} = \sum_{\gamma\delta\epsilon} v_{\alpha\delta\gamma\epsilon} C_{\gamma\epsilon\beta\delta}. \quad (24)$$

The Hartree-Fock single-particle Hamiltonian $h[\rho]$ is a matrix with elements

$$h_{\alpha\beta}[\rho] = \frac{\delta \langle \Psi | \hat{H} | \Psi \rangle}{\delta \rho_{\beta\alpha}}. \quad (25)$$

In the energy density functional (EDF) formalism⁴, the above equation is replaced by

$$h_{\alpha\beta}[\rho] = \frac{\delta E[\rho]}{\delta \rho_{\beta\alpha}}, \quad (26)$$

where the functional $E[\rho]$ is directly fitted for a set of observables (nuclear matter equation of state, masses, radii, spin-orbit splitting, etc.).

Equation (22) contains two unknown quantities, namely the one-body density matrix ρ and the two-body correlation matrix C . According to the Bogoliubov-Born-Green-Kirkwood-Yvon (BBGKY) hierarchy [22–24], the evolution of C depends on the three-body correlation matrix and so on. The mean-field approximation is obtained by truncating the BBGKY hierarchy to the lowest order, i.e., assuming $C = 0$ at all time. We end up with the time-dependent Hartree-Fock (TDHF) equation proposed by Dirac [9]

$$i\hbar \frac{\partial}{\partial t} \rho(t) = [h[\rho], \rho]. \quad (27)$$

As the two-body correlations have been neglected, the state of the system reduces to an independent particle-state at all times. Thus, the TDHF equation describes the evolution of independent particles in the mean-field generated by all the particles.

2.4. Beyond TDHF correlations

The above approach, where the TDHF equation is obtained by truncating the BBGKY hierarchy at lowest order, tells us that the TDHF approach neglects two-body correlations at all time. For the mean-field approximation to be valid, it is therefore necessary for the two-body correlations to remain a small perturbation during the dynamics. These correlations include, e.g., nucleon-nucleon collisions, pairing and quantum fluctuations of collective observables:

⁴As shown in section 2.8, the EDF and Hamiltonian approaches are equivalent, in the sense that there is no need to assume an explicit expression of the Hamiltonian [as in Eq. (2)] to get the TDHF equation.

- *Nucleon-nucleon collisions* are expected to be small at low energy due to the Pauli exclusion principle. Indeed, due to conservation of energy when two nucleons collide, one nucleon has an increased energy while the other one would go to a lower energy state which is likely to be already occupied. As a result of this Pauli blocking, the collision is forbidden and the mean-free path of the nucleon is increased to the order of the size of the nucleus. The above argument is in fact simplistic as it assumes that the nucleons have a well defined energy. Unlike in the static HF case, where h and ρ commute and thus have the same eigenstates, in TDHF an occupied single-particle state (eigenstate of ρ) does not have a well defined single-particle energy. As a result, collisions (neglected in TDHF) could happen even at low energy. Ultimately, the theoretical approach has to be validated by detailed comparison with experimental data.
- *Pairing correlations*, however, which are known to play an important role in structure, could affect some reaction mechanisms such as multi-nucleon transfer. The inclusion of pairing dynamics at the BCS or Bogoliubov levels has been the subject of recent works [25–28] which will be discussed in section 3.2.
- *Quantum fluctuations* of observables are sometimes poorly described in TDHF. This is the case, for instance, with the fluctuation of the particle number in deep-inelastic collisions [29]. Beyond TDHF methods which rely on existing codes have thus been developed, based on the time-dependent RPA [30] approach or on the stochastic mean-field method [31]. Recent applications will be discussed in section 3.4.

2.5. Variational principle with the Dirac action

The Dirac action is defined as

$$S \equiv S_{t_0, t_1}[\Psi] = \int_{t_0}^{t_1} dt \langle \Psi(t) | \left(i\hbar \frac{d}{dt} - \hat{H} \right) | \Psi(t) \rangle. \quad (28)$$

If the many-body state $|\Psi(t)\rangle$ is free to explore the entire Hilbert space, then requesting stationarity of the action leads to the exact Schrödinger equation.

If, however, the variational space is restricted to independent particle states $|\phi\rangle$ corresponding to Slater determinants of the occupied single-particle states $|\varphi_i\rangle$, then the action can be expressed as

$$S = \int_{t_0}^{t_1} dt \left(i\hbar \sum_{i=1}^N \int dx \varphi_i^*(x, t) \frac{d}{dt} \varphi_i(x, t) - E[\rho(t)] \right) \quad (29)$$

where $E[\rho] = \langle \phi | \hat{H} | \phi \rangle$. For simplicity, the equations are written in one-dimension and spin is omitted. The stationarity of the action imposes

$$\frac{\delta S}{\delta \varphi_\alpha^*(x, t)} = i\hbar \frac{d}{dt} \varphi_\alpha(x, t) - \int_{t_0}^{t_1} dt' \frac{\delta E[\rho(t')]}{\delta \varphi_\alpha^*(x, t)} = 0. \quad (30)$$

The variation of E can be expressed as

$$\frac{\delta E[\rho(t')]}{\delta \varphi_\alpha^*(x, t)} = \int dy dy' \frac{\delta E[\rho(t')]}{\delta \rho(y, y'; t')} \frac{\delta \rho(y, y'; t')}{\delta \varphi_\alpha^*(x, t)} = \int dy h(x, y; t) \varphi_\alpha(y, t') \delta(t - t'), \quad (31)$$

where we have defined the single-particle Hartree-Fock Hamiltonian h as

$$h(x, y; t) = \frac{\delta E[\rho(t)]}{\delta \rho(y, x; t)}. \quad (32)$$

The TDHF equation for the occupied states finally read

$$i\hbar \frac{d}{dt} \varphi_\alpha(x, t) = \int dy h(x, y; t) \varphi_\alpha(y, t), \quad (33)$$

or, equivalently,

$$i\hbar \frac{\partial}{\partial t} \varphi_i(t) = h[\rho(t)] \varphi_i(t) \quad \text{for } 1 \leq i \leq A. \quad (34)$$

This set of non-linear Schrödinger like equations is fully equivalent to the TDHF equation (27).

In practice, TDHF codes usually solve the mean-field dynamics in the canonical basis using Eq. (34) [32–35]. They provide a time-evolution of each single-particle wavefunction $\varphi_i(t)$ which can be used to compute expectation values of one body observables, as well as single-particle properties such as the transfer from specific single-particle states [36].

We see from the above derivation that a restriction to independent particle states at all times, which is equivalent to neglecting the effect of two-body correlations on the dynamics, leads to the TDHF formalism. Interestingly, neither the BBGKY truncation nor the Dirac variational principle impose any restriction on the type of observables which could in principle be computed within the TDHF framework.

2.6. Balian-Vénéroni variational principle

The Balian-Vénéroni action differs from the Dirac one as it considers both the state of the system, represented by its density matrix operator $\hat{D}(t)$ (in the Schrödinger picture), and the observable $\hat{A}(t)$ (in the Heisenberg picture) to be variational quantities. Their action is written as [12]

$$J = \text{Tr} [\hat{A}(t_1) \hat{D}(t_1)] - \int_{t_0}^{t_1} dt \text{Tr} \left[\hat{A}(t) \left(\frac{d\hat{D}(t)}{dt} + i[\hat{H}(t), \hat{D}(t)] \right) \right], \quad (35)$$

where $\hbar = 1$. The boundary conditions are given by

$$\hat{D}(t_0) = \hat{D}_0, \quad (36)$$

where \hat{D}_0 is the initial state, and

$$\hat{A}(t_1) = \hat{A}_1, \quad (37)$$

where \hat{A}_1 is the operator at the final time. We see that, unlike the previous methods, the choice of the observable to compute plays a crucial role in this approach.

The TDHF equation is obtained by constraining the variation δ_A to leave \hat{A} in the space of one-body operators, which is achieved with

$$\delta_A \hat{A}(t) \equiv \hat{a}_\alpha^\dagger \hat{a}_\beta \quad (38)$$

and $\delta\hat{A}(t_1) = 0$ due to the boundary condition in Eq. (37). Imposing the stationarity of the action with respect to variations of A , i.e., $\delta_A J = 0$, we get

$$\text{Tr} \left[\hat{a}_\alpha^\dagger \hat{a}_\beta \left(\frac{\partial \hat{D}}{\partial t} + i[\hat{H}, \hat{D}] \right) \right] = 0. \quad (39)$$

As before, we also restrict the variational space for \hat{D} to independent particle states, i.e., $\hat{D}(t) = |\phi(t)\rangle \langle \phi(t)|$ where $|\phi(t)\rangle$ is a Slater determinant.

Using $\rho_{\alpha\beta} = \langle \phi | \hat{a}_\beta^\dagger \hat{a}_\alpha | \phi \rangle$, we get

$$i \frac{\partial \rho_{\beta\alpha}(t)}{\partial t} = \langle \phi(t) | \left[\hat{a}_\alpha^\dagger \hat{a}_\beta, \hat{H} \right] | \phi(t) \rangle. \quad (40)$$

This is Eq. (21) with the additional restriction that $|\phi\rangle$ is a Slater determinant. As a result, the two-body correlation matrix C is zero and we get the TDHF equation (27).

The Balian-Vénéroni variational principle tells us that, in addition to being an approach to independent particles, the TDHF theory is optimized to expectation values of one-body observables. In principle, the TDHF approach is not adequate to compute two-body operators or fluctuations of one-body operators. For the latter, the TDRPA equation has been derived from the same variational principle with a larger variational space for the observable [30] (see section 3.4.1).

2.7. Path integral formulation

In his many-path formulation of quantum mechanics [37], Feynman showed that the amplitude of probability for a particle to go from a position q_i at time t_i to a position q_f at time t_f can be expressed as

$$\langle q_f | \hat{U}(t_f, t_i) | q_i \rangle = \int \mathcal{D}[q] e^{iS[q]/\hbar},$$

where $S[q] = \int_{t_i}^{t_f} dt L(q, \dot{q})$ is the action and $L = \frac{m}{2} \dot{q}^2 - V(q)$ is the Lagrangian of the particle. The stationary phase approximation (SPA), valid for classical systems where $S \gg \hbar$, leads to $\int \mathcal{D}[q] e^{iS[q]/\hbar} \sim e^{iS[q_c]/\hbar}$ with the classical path obeying the variational principle $\delta S[q]|_{q=q_c} = 0$.

Starting from the Hamiltonian $\hat{H} = \sum_{i=1}^A \hat{K}_i + \frac{1}{2} \sum_{i,j=1}^A V(\hat{x}_i - \hat{x}_j)$, Levit showed that the amplitude of probability to go from the many-body state $|i\rangle$ to $|f\rangle$ could be written as a similar path integral [38],

$$\langle f | \hat{U}(t_f, t_i) | i \rangle = \int \mathcal{D}[\sigma] e^{iS_{eff}[\sigma]},$$

where $\sigma(x, t)$ is the scalar auxiliary field arising from the use of Hubbard-Stratonovich transformation and the effective action is given by ($\hbar = 1$)

$$S_{eff}[\sigma] = \frac{1}{2} \int_{t_i}^{t_f} dt \int dx dx' \sigma(x, t) V(x - x') \sigma(x', t') - i \ln \langle f | \hat{U}_\sigma | i \rangle.$$

Here, $\hat{U}_\sigma(t_f - t_i)$ is the evolution operator in the interaction representation with Hamiltonian

$$\hat{H}_\sigma = \sum_{i=1}^A \left[\hat{K}_i - \frac{V(0)}{2} + \int dx V(\hat{x}_i - x) \sigma(x, t) \right].$$

Imposing $|i\rangle$ and $|f\rangle$ to be Slater determinants and using the SPA, i.e., requiring $\delta S_{eff}[\sigma] = 0$, lead to the mean-field equation

$$i \frac{\partial \varphi_i(x)}{\partial t} = \left(\frac{p^2}{2m} - \frac{V(0)}{2} + \int dx' \rho(x', t) V(x - x') \right) \varphi_i(x).$$

This is the time-dependent Hartree equation. Going to the next order beyond the SPA leads to the Fock term, gets rid of the self-interaction energy term $\frac{V(0)}{2}$, and also contains some RPA corrections [39].

We see that the SPA applied to the path integral formulation leads to classical physics for one-particle system while it produces a mean-field approach for many-particle systems. We then understand the classical behavior of the TDHF equation in terms of collective coordinates as well as its lack of quantum fluctuations. In particular, this is a possible explanation for the inability of TDHF to incorporate quantum many-body tunneling of strongly interacting systems like nuclei.

2.8. Equivalence between Hamiltonian and energy density functional approaches

We conclude the formalism section by showing the equivalence between Hamiltonian and energy density functional approaches. It is indeed interesting to note that the derivation of the TDHF equation from the variational principle with the Dirac action (see section 2.5) does not require an explicit expression for the Hamiltonian \hat{H} . This is because the Dirac action can be directly defined with the energy density functional $E[\rho] = \langle \phi | \hat{H} | \phi \rangle$ in it [see Eq. (29)]. On the contrary, other derivations of the TDHF equation from the truncation of the BBGKY hierarchy (section 2.3) or from the Balian-Vénéroni variational principle (section 2.6) require an explicit expression of the Hamiltonian, as in Eq. (2), in order to compute the quantity $\langle [\hat{a}_i^\dagger \hat{a}_j, \hat{H}] \rangle$ appearing in Eqs. (21) and (40). Here, we show that such an explicit expression of \hat{H} is, in fact, not necessary.

Our goal is to show that

$$\langle \phi | [\hat{a}_\beta^\dagger \hat{a}_\alpha, \hat{H}] | \phi \rangle = [h, \rho]_{\alpha\beta} \quad (41)$$

for any Hamiltonian \hat{H} and Slater $|\phi\rangle$, with

$$h_{\alpha\beta} = \frac{\delta \langle \phi | \hat{H} | \phi \rangle}{\delta \rho_{\beta\alpha}} = \frac{\delta E[\rho]}{\delta \rho_{\beta\alpha}}. \quad (42)$$

Indeed, using Eq. (41) in Eqs. (21) or (40) would give the TDHF equation (27).

We can rewrite the left hand side of Eq. (41) using the basis $\{|\nu\rangle\}$ of eigenstates of \hat{H} as

$$\begin{aligned} \langle \phi | [\hat{a}_\beta^\dagger \hat{a}_\alpha, \hat{H}] | \phi \rangle &= \langle \phi | \left[\hat{a}_\beta^\dagger \hat{a}_\alpha, \sum_\nu |\nu\rangle \langle \nu | \hat{H} \right] | \phi \rangle \\ &= \sum_\nu E_\nu \langle \phi | [\hat{a}_\beta^\dagger \hat{a}_\alpha, |\nu\rangle \langle \nu |] | \phi \rangle, \end{aligned} \quad (43)$$

where E_ν is the eigenenergy of the state $|\nu\rangle$. Let us write $|\nu\rangle$ in the n -particle n -hole basis built from the Slater $|\phi\rangle$ as

$$|\nu\rangle = C_0^\nu |\phi\rangle + \sum_{ph} C_{ph}^\nu \hat{a}_p^\dagger \hat{a}_h |\phi\rangle + \sum_{pp'hh'} C_{pp'hh'}^\nu \hat{a}_p^\dagger \hat{a}_{p'}^\dagger \hat{a}_h \hat{a}_{h'} + \dots, \quad (44)$$

with $C_{ph}^\nu = \langle \phi | \hat{a}_h^\dagger \hat{a}_p |\nu\rangle$. (Note that $C_{hp}^\nu = 0$.) This leads to

$$\langle \phi | [\hat{a}_\beta^\dagger \hat{a}_\alpha, \hat{H}] | \phi \rangle = \sum_\nu E_\nu (C_{\alpha\beta}^\nu C_0^{\nu*} - C_0^\nu C_{\beta\alpha}^{\nu*}). \quad (45)$$

We now look for an expression for the term $[h, \rho]$ as a function of the same quantities. Using $\rho_{\alpha\beta} = \langle \phi | \hat{a}_\beta^\dagger \hat{a}_\alpha | \phi \rangle \equiv \langle \hat{a}_\beta^\dagger \hat{a}_\alpha \rangle$, we can write

$$\begin{aligned} [h, \rho]_{\alpha\beta} &= \sum_\gamma \left(\frac{\delta E[\rho]}{\delta \rho_{\gamma\alpha}} \rho_{\gamma\beta} - \rho_{\alpha\gamma} \frac{\delta E[\rho]}{\delta \rho_{\beta\gamma}} \right) \\ &= \sum_\gamma \left(\frac{\delta \langle \hat{H} \rangle}{\delta \langle \hat{a}_\alpha^\dagger \hat{a}_\gamma \rangle} \langle \hat{a}_\beta^\dagger \hat{a}_\gamma \rangle - \langle \hat{a}_\gamma^\dagger \hat{a}_\alpha \rangle \frac{\delta \langle \hat{H} \rangle}{\delta \langle \hat{a}_\gamma^\dagger \hat{a}_\beta \rangle} \right). \end{aligned} \quad (46)$$

Notice that, in the canonical basis, γ has to be a hole state. Using, again, the eigenbasis $\{|\nu\rangle\}$, we have $\langle \hat{H} \rangle = \sum_\nu E_\nu \langle \phi | \nu \rangle \langle \nu | \phi \rangle$. Using this and Eq. (44), we see that the functional derivatives in Eq. (46) include terms like

$$\begin{aligned} \frac{\delta(\langle \phi | \nu \rangle \langle \nu | \phi \rangle)}{\delta \langle \hat{a}_\alpha^\dagger \hat{a}_\gamma \rangle} &= \sum_{ph} C_{ph}^\nu \frac{\delta \langle \hat{a}_p^\dagger \hat{a}_h \rangle}{\delta \langle \hat{a}_\alpha^\dagger \hat{a}_\gamma \rangle} \langle \nu | \phi \rangle + \sum_{ph} C_{ph}^{\nu*} \langle \phi | \nu \rangle \frac{\delta \langle \hat{a}_h^\dagger \hat{a}_p \rangle}{\delta \langle \hat{a}_\alpha^\dagger \hat{a}_\gamma \rangle} \\ &= C_{\alpha\gamma}^\nu \langle \nu | \phi \rangle + C_{\gamma\alpha}^{\nu*} \langle \phi | \nu \rangle, \end{aligned} \quad (47)$$

where $C_{\alpha p} = C_{h\alpha} = 0$, i.e., only C_{ph} terms are non zero. Similarly, for a Slater determinant we have $\langle \hat{a}_\alpha^\dagger \hat{a}_p \rangle = \langle \hat{a}_p^\dagger \hat{a}_\alpha \rangle = 0$, i.e., the only non-zero terms are $\rho_{hh'} = \delta_{hh'}$. Consequently, terms like $C_{\gamma\alpha}^\nu \rho_{\gamma\beta}$ and $C_{\gamma\alpha}^\nu \rho_{\beta\gamma}$ are equal to zero because γ cannot be a particle and a hole at the same time. Equation (46) then becomes

$$\begin{aligned} [h, \rho]_{\alpha\beta} &= \sum_\nu E_\nu \sum_\gamma (C_{\alpha\gamma}^\nu \langle \nu | \phi \rangle \rho_{\gamma\beta} - \rho_{\alpha\gamma} C_{\beta\gamma}^{\nu*} \langle \phi | \nu \rangle) \\ &= \sum_\nu E_\nu (C_{\alpha\beta}^\nu C_0^{\nu*} - C_{\beta\alpha}^{\nu*} C_0^\nu), \end{aligned} \quad (48)$$

which, according to Eq. (45), is equal to $\langle \phi | [\hat{a}_\beta^\dagger \hat{a}_\alpha, \hat{H}] | \phi \rangle$. Equation (41) is then verified, implying that derivations of the TDHF equation from Hamiltonian approaches such as the truncation of the BBGKY hierarchy or the Balian-Vénéroni variational principle do not depend on the specific expression of the Hamiltonian.

3. New Techniques and their applications

A number of new techniques have been recently developed to utilize HF and TDHF calculations to extract information that could be directly compared with experimental observations. These include the microscopic calculation of fusion barriers and cross-sections, methods to use TDHF to study scission dynamics with and without pairing, projection methods to compute fluctuation of various observables, beyond mean-field methods based on TDHF, improvements in effective interactions and boundary conditions. In this section, we examine the theoretical underpinnings of these new developments.

3.1. Nucleus-nucleus potentials and fusion reactions

In the absence of a practical many-body approach to study sub-barrier fusion, the problem is transformed to that of a nucleus-nucleus interaction barrier or a series of barriers to incorporate other degrees of freedom such as static deformations. Historically, phenomenological ion-ion potentials such as the Bass potential [40, 41], the proximity potential [42–45], or potentials obtained via the double-folding method [46, 47] have been some of the popular choices. Some of these potentials have been fitted to experimental fusion barrier heights and have been quite successful in describing scattering data with stable nuclei.

The reduction of the many-body dynamics to a two-body problem is a serious approximation. It is needed to describe quantities which are outside the range of applicability of TDHF, such as sub-barrier fusion, or the coherence between reaction channels associated with different barriers (where TDHF reduces the problem to an average barrier). Microscopic approaches can then be used to provide inputs to such two-body calculations, in particular the nucleus-nucleus potential, the coordinate dependent mass (which differs from the asymptotic reduced mass when the densities overlap), the moment of inertia and the friction parameter. In principle, one needs all of these to compute fusion cross-sections. The potential will be discussed at length. By construction, potentials extracted from TDHF dynamics are real as they incorporate (at the mean-field level) all reaction channels. The coordinate dependent mass is discussed in section 3.1.7 where the method to calculate cross-sections are introduced. In principle, this is all we need to compute fusion cross-sections if one makes the isocentrifugal approximation, i.e., neglecting non-central effects, and if dissipation is small. The isocentrifugal approximation is very common (e.g., in most coupled-channel calculations) and will be discussed in section 3.1.7. If dissipation is neglected (see section 3.1.8) the reduction of the dynamics to a two-body problem leads to a Schrödinger equation, as in the coupled-channel framework.

Traditionally, the nucleus-nucleus potential is used to calculate fusion cross-sections with a quantum mechanical barrier penetration model [41, 48, 49], or the coupled-channels approach [50–52], for the transmission coefficients. The coupled-channels method includes various excitations of the target and/or projectile, as well as a simplified description of neutron transfer (see, e.g., [53]), and can be consistently applied at energies above and below the barrier [49, 51] (see [3] for a review).

One possible way to construct a nucleus-nucleus potential from microscopic densities is via the double-folding model. In this approach, static densities of the two nuclei, separated by a relative coordinate \mathbf{R} , are folded with a phenomenological effective

nucleon-nucleon interaction to compute the interaction barrier:

$$V_F(R) = \int d\mathbf{r}_1 d\mathbf{r}_2 \rho_1(\mathbf{r}_1) \rho_2(\mathbf{r}_2) v(\mathbf{r}_{12}), \quad (49)$$

where R is the norm of \mathbf{R} and $\mathbf{r}_{12} = \mathbf{R} - (\mathbf{r}_1 - \mathbf{r}_2)$. The double-folding potential allows the use of microscopic approaches, such as the Hartree-Fock-Bogoliubov (HFB) or the relativistic mean-field model (RMF), to compute the nuclear densities in Eq. (49). Double-folding potentials have also been used in conjunction with the São Paulo barrier penetration model to simulate the energy dependence of barriers [54, 55] for astrophysical fusion cross-sections. Note that the interaction used in the structure part and the one used in the calculation of the potential often differ, introducing a lack of consistency in the method. In this section, we discuss microscopic approaches to compute nucleus-nucleus potentials which overcome this limitation as both potentials and densities are computed from the same Skyrme EDF.

One common physical assumption used in many of these calculations is the frozen density (or “sudden”) approximation. In this approximation the nuclear densities are unchanged during the computation of the ion-ion potential as a function of the internuclear distance. This leads to a *bare* nucleus-nucleus potential. Methods to compute bare potentials from HF densities will be discussed in sections 3.1.1 and 3.1.3. Of course, the possibility for the nuclei to change their shape dynamically must be accounted for one way or another. Indeed, in principle the bare potential provides a realistic description of the interaction between the nuclei at high energy only (where the time scale of the reaction is too short for the nuclei to polarise), and at distances large enough so that the overlap between the densities of the fragments is not unrealistic (typically with a density in the neck between the fragments that does not exceed the saturation density).

Dynamical change of shapes of the nuclei is accounted for in coupled-channels calculations via the couplings to low-lying collective states. This means that coupled-channels calculations require properties of low-lying collective states in the projectile and target nuclei such as excitation energies and reduced transition probabilities $B(EL)$ which are usually taken from experiment, but not always available (in particular for exotic nuclei). RPA strength functions (e.g., computed from TDHF response in the small amplitude limit) can also be used to provide these inputs to coupled-channels calculations, as illustrated in section 3.1.2. Although these couplings may accurately represent the early stages of the collision process, the situation may become more complicated when the nuclei overlap due to a modification of the collective excitations [56]. An alternative approach to coupled-channels method is to incorporate dynamical effects directly in the potential by calculating the latter from TDHF densities (see section 3.1.4).

Issues with the two-body approach to heavy-ion collisions become much more prevalent when studying fusion at deep sub-barrier energies. In particular, the large overlap of the frozen nuclear densities lead to an unphysical attraction in the inner barrier region. To remedy this drawback, various modifications of the nucleus-nucleus potential have been suggested. These include the addition of a repulsive core resulting in a *shallow potential* pocket [57] or a two-step model for fusion in which the effects of neck formation are approximately included [58]. Microscopic approaches discussed here provide a physical insight into the mechanisms at play when the nuclei overlap. For instance, they can be used to account for the repulsion in the bare potential induced by the Pauli exclusion principle between nucleons of different collision partners (see section 3.1.3). This Pauli

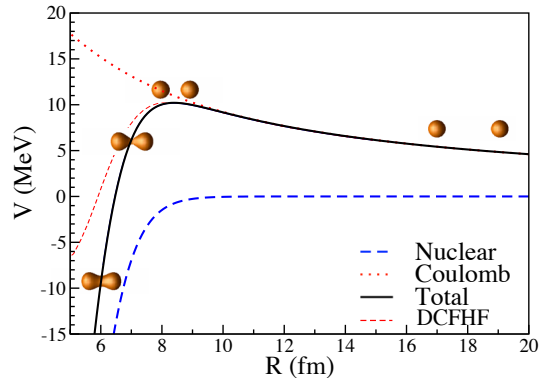


Figure 2: Nuclear (long-dashed line), Coulomb (dotted line) and total (solid line) contributions to the Frozen Hartree-Fock (FHF) potential calculated for the $^{16}\text{O}+^{16}\text{O}$ system with the SLy4d parametrization of the Skyrme EDF. The density-constrained FHF (DCFHF) potential including Pauli repulsion is shown with a short dashed line. Isodensities at half the saturation density $\rho_0/2 = 0.08 \text{ fm}^{-3}$ from a TDHF calculation at centre of mass energy $E_{cm} = 12 \text{ MeV}$ are also shown.

repulsion is of course naturally included in TDHF which describes the dynamics of a fully antisymmetrised many-body state.

In recent years, a number of new developments have been introduced to employ HF or TDHF calculations to compute nucleus-nucleus potentials and fusion cross-sections in a more microscopic and self-consistent manner. In this section, we review these new methods and present some selected applications.

3.1.1. Frozen Hartree-Fock Approach

A procedure for computing nucleus-nucleus potentials microscopically using frozen static HF densities has been developed. Construction of such microscopic bare potentials could provide input to coupled-channels calculations since frozen densities are used and no excitations have been accounted for. The approach is based on energy density functional (EDF) $E[\rho]$ written as an integral of an energy density $\mathcal{H}[\rho(\mathbf{r})]$ [59, 60], i.e.,

$$E[\rho] = \int d\mathbf{r} \mathcal{H}[\rho(\mathbf{r})]. \quad (50)$$

One can adopt the idea of Brueckner *et al.* [61] to derive the bare potential from an EDF. The bare potential is obtained by requiring frozen ground-state densities ρ_i of each nucleus ($i = 1, 2$), which we compute using the HF mean-field approximation.

Typically, the Skyrme EDF [62] is used both in HF calculations and to compute the bare potential. This ensures that all of the structure information contained in the EDF is part of the bare potential, such as the effects of neutron skin for neutron-rich nuclei [63]. Neglecting the Pauli exclusion principle between nucleons in different nuclei leads to the usual frozen Hartree-Fock (FHF) potential [16, 64–66]

$$V_{FHF}(\hat{\mathbf{R}}) = \int d\mathbf{r} \mathcal{H}[\rho_1(\mathbf{r}) + \rho_2(\mathbf{r} - \hat{\mathbf{R}})] - E[\rho_1] - E[\rho_2], \quad (51)$$

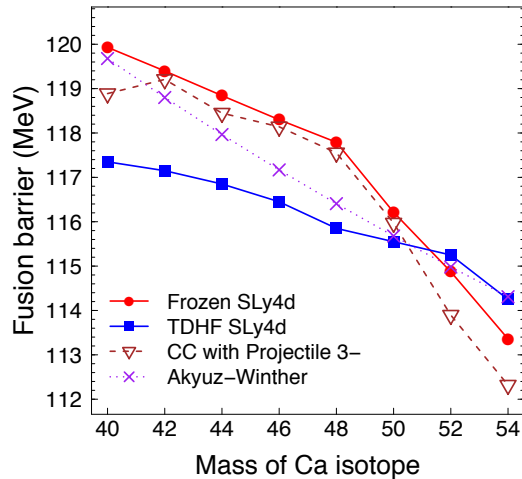


Figure 3: Fusion barriers in $^A\text{Ca}+^{116}\text{Sn}$ obtained from the Akyüz-Winther potential [68] (crosses), FHF (circles), coupled-channel calculations (triangles) and TDHF (squares).

where $\hat{\mathbf{R}}$ is the distance vector between the centres of mass of the nuclei.

The first term in the r.h.s. of Eq. (51) is calculated by placing the two static HF solutions at a distance R from each other in a TDHF code without a boost and computing the energy of the combined system, including the Coulomb contribution. An example of FHF potential for the $^{16}\text{O}+^{16}\text{O}$ reaction is shown in Fig. 2.

Figure 3 shows the change of the bare potential barrier using FHF (circles) with the mass of calcium projectiles incident on a ^{116}Sn target [67]. A clear change of slope is observed near ^{48}Ca which is interpreted as an effect of the neutron skin in neutron rich calcium isotopes which increases the barrier radius, and then reduces the Coulomb repulsion as well as the barrier height. This effect is not observed in the phenomenological Akyüz-Winther potential (crosses) [68]. This shows that microscopic potentials like FHF are more promising for reactions with exotic beams.

3.1.2. Couplings to collective vibrations

Computing fusion cross-sections via a one-barrier penetration model with bare FHF potentials usually underestimates fusion cross-sections at near and below barrier energies. This is because couplings to low-lying states, which are known to enhance fusion at these energies⁵, are not accounted for. FHF potentials have then been used in coupled-channels calculations in order to take into account these couplings in the calculations of cross-sections [67, 69, 70].

In addition to the nucleus-nucleus potential, coupled-channels calculations require the energy and transition probability of the collective states. Such information on low-lying rotational and vibrational states may not be readily available for exotic nuclei.

⁵ Couplings between relative motion and internal excitations leads to off-diagonal terms in the Hamiltonian. After diagonalisation, the new eigenchannels correspond to mixture of ground and excited states. The new eigenchannel with lowest energy is pushed down in energy with respect to the uncoupled ground-state channel. See Ref [3] for a review.

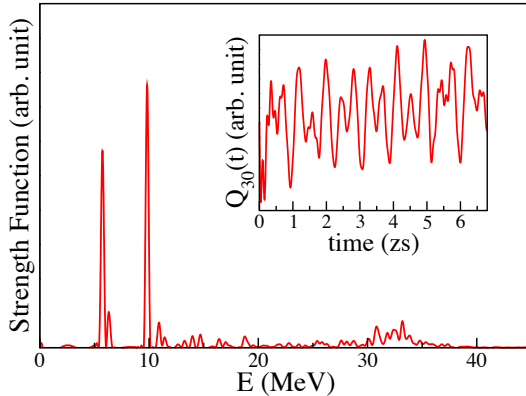


Figure 4: Strength function of the octupole response in ^{48}Ca obtained from the small amplitude limit of TDHF with the SLy4 functional. The time-evolution of the octupole moment following the octupole boost is shown in the inset.

Consequently, it is also essential to develop methods to calculate collective excitation energies and transition probabilities as input to these codes. For vibrational states, these properties can be computed using the TDHF approach in the small amplitude response limit [25, 33, 34, 67, 69–80] which is equivalent to the random-phase approximation (RPA).

This makes use of the linear response theory where the evolution of the wave-function after a boost of the form $|\Psi(t=0)\rangle = e^{-i\varepsilon\hat{Q}}|\Psi_0\rangle$, applied on the ground state $|\Psi_0\rangle$, leads to

$$\Delta Q(t) = \langle \Psi(t) | \hat{Q} | \Psi(t) \rangle - \langle \Psi_0 | \hat{Q} | \Psi_0 \rangle = -2\varepsilon \sum_{\nu} |q_{\nu}|^2 \sin \omega_{\nu} t + O(\varepsilon^2), \quad (52)$$

where $q_{\nu} = \langle \Psi_{\nu} | \hat{Q} | \Psi_0 \rangle$ is the transition amplitude. The strength function is then defined as

$$R_Q(\omega) = \lim_{\varepsilon \rightarrow 0} \frac{-1}{\pi\varepsilon} \int_0^{\infty} dt \Delta Q(t) \sin(\omega t) = \sum_{\nu} |q_{\nu}|^2 \delta(\omega - \omega_{\nu}). \quad (53)$$

An example of RPA octupole strength function computed in the small amplitude limit of a TDHF evolution following an octupole excitation with the SLy4 Skyrme functional [81] is shown in Fig. 4. The time-evolution of the octupole moment used to compute the strength function from Eq. (53) is shown in the inset. Such strength function can be directly used to extract the energy of the low-lying collective vibrations (position of the peaks) as well as their transition amplitude (area of the peaks).

Low-lying collective vibrational modes can get easily excited in heavy-ion collisions at near-barrier collisions. This is illustrated in Fig. 5 comparing $^{40}\text{Ca}+^{40}\text{Ca}$ and $^{56}\text{Ni}+^{56}\text{Ni}$ near-barrier central collisions with TDHF [69]. At the stage when the neck forms in $^{40}\text{Ca}+^{40}\text{Ca}$, the fragments have acquired a strong octupole shape due to the coupling to the 3_1^- state which is predicted at $E_{3_1^-}^{TDHF} = 3.44$ MeV in the strength function, in good agreement with the experimental energy $E_{3_1^-}^{exp} \simeq 3.74$ MeV [82]. In the $^{56}\text{Ni}+^{56}\text{Ni}$ reaction, however, such octupole deformation is not observed, which is consistent with

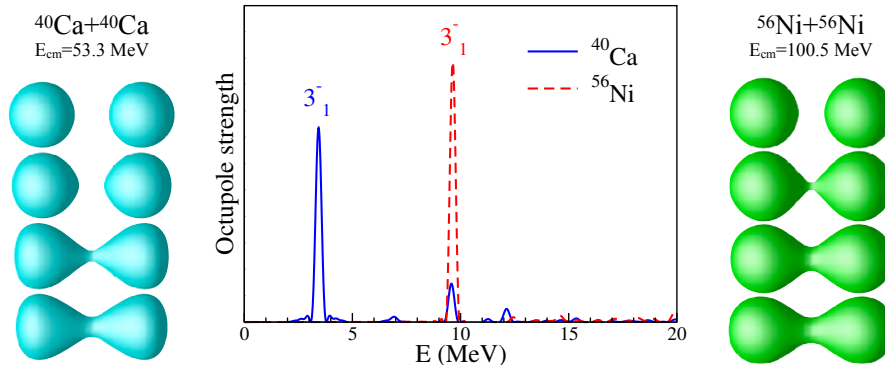


Figure 5: Evolution of isodensities at half the saturation density $\rho_0/2 = 0.08 \text{ fm}^{-3}$ in TDHF calculations of $^{40}\text{Ca}+^{40}\text{Ca}$ (left) and $^{56}\text{Ni}+^{56}\text{Ni}$ (right) central collisions at $E_{cm} = 53.3$ MeV and $E_{cm} = 100.3$ MeV, respectively, with the SLy4d Skyrme functional. The middle panel shows the RPA octupole strength function in ^{40}Ca (solid line) and ^{56}Ni (dashed line). The 3_1^- states are the low-lying collective octupole vibrations used in coupled-channels calculations.

the fact that the 3_1^- state is predicted at much higher energy in ^{56}Ni , and thus it is less excited in the collision.

The impact of the coupling to octupole modes on the fusion barriers of $^A\text{Ca}+^{116}\text{Sn}$ systems has been computed with the CCFULL code [51] in Ref. [67]. The results are shown in Fig. 3 (triangles). It is observed that the couplings to these octupole modes systematically lower the average barrier. (This fact is well known from standard coupled-channels calculations, see, e.g., [3]). Nevertheless, the effect of the neutron skin on the barrier is still present. It is interesting to see, however, that the effect of the neutron skin is completely washed out in direct TDHF calculations (squares) of the fusion thresholds (corresponding to the fusion barriers once all dynamics has been accounted for at the mean-field level). Indeed, the change of slope at $A = 48$ is not observed in the TDHF calculations. This was interpreted as an effect of transfer channels in [67].

Of course, the TDHF linear response (RPA) only provides an approximate description to basic vibrational modes in the harmonic limit. Anharmonicities can be studied by investigating, e.g., non-linear response in TDHF [71, 75, 83] or boson mapping techniques [84]. An alternative approach based on the multireference covariant density functional theory (MCDFT) has also been used to compute the properties of low-lying collective excitations and their effect on fusion via coupled-channel calculations [85, 86].

3.1.3. Density Constrained FHF

While constructing the FHF potential, we have neglected all of the dynamical effects as well as the Pauli principle between the nucleons belonging to different nuclei. It is obvious that the Pauli exclusion principle will generate a repulsion between the two nuclei as they begin to overlap. The use of Pauli orthogonalization results in altering the single-particle states in the overlap region to minimize their overlap and would have the effect of a static rearrangement. The importance of Pauli orthogonalization was also recognized in the earlier work concerning α -nucleus scattering studies [87], where specialized normalization operators were introduced to reconstruct the states following

a Gram-Schmidt procedure. However, these techniques could only be applied using semi-analytic methods. In the same spirit, the Pauli repulsion should be included in the nucleus-nucleus potentials used to model reactions such as (in)elastic scattering, (multi)nucleon transfer, and fusion.

Pauli repulsion is ignored in double-folding and FHF potentials: The argument has been that the outcome of a collision between nuclei is mostly determined at a distance where the nuclei do not overlap much, and thus the effects of the Pauli exclusion principle are negligible. This is definitely the case in $^{16}\text{O}+^{16}\text{O}$ as we see in Fig. 2 that the barrier is reached with very little overlap between the nuclei. This argument is based on the assumption that nuclei do not necessarily probe the inner part of the fusion barrier. However, at energies well above the barrier, the system could reach more compact shapes where one cannot neglect the effect of the Pauli principle anymore, as was shown by several authors in the 1970's [88–92]. Similarly, for deep sub-barrier energies, the inner turning-point of the fusion barrier entails significant overlap between the two nuclei [93, 94].

The question then arises if one can construct a bare frozen-density nucleus-nucleus potential while incorporating the Pauli exclusion principle at the same time. An answer to this question can be found in the density-constrained method [95, 96]. The density-constrained FHF (DCFHF) approach introduced in [97] facilitates the computation of the bare potential by using the self-consistent HF mean-field with exact frozen densities. The Pauli exclusion principle is included exactly by allowing the single-particle states, constituting the combined nuclear density, to reorganize to attain their minimum energy configuration and be properly antisymmetrized as the many-body state is a Slater determinant of all the occupied single-particle wave-functions. The HF minimization of the combined system is thus performed subject to the constraint that the local proton (p) and neutron (n) densities do not change:

$$\delta \langle H - \sum_{q=p,n} \int d\mathbf{r} \lambda_q(\mathbf{r}) [\rho_{1_q}(\mathbf{r}) + \rho_{2_q}(\mathbf{r} - \mathbf{R})] \rangle = 0, \quad (54)$$

where the $\lambda_{n,p}(\mathbf{r})$ are Lagrange parameters at each point of space constraining the neutron and proton densities. This equation determines the state vector (Slater determinant) $|\Phi(\mathbf{R})\rangle$. The DCFHF potential, assumed to be central, is then defined as

$$V_{\text{DCFHF}}(R) = \langle \Phi(\mathbf{R}) | H | \Phi(\mathbf{R}) \rangle - E[\rho_1] - E[\rho_2]. \quad (55)$$

An example of DCFHF potential in the $^{16}\text{O}+^{16}\text{O}$ system is shown in Fig. 2 (short dashed line). We see that the effect of the Pauli repulsion is to widen the barrier. In a light system such as $^{16}\text{O}+^{16}\text{O}$, the effect is relatively minor, though it is expected to induce a fusion hindrance at deep sub-barrier energies [97]. In particular, Pauli repulsion could have an important effect at energies relevant for astrophysical processes, i.e., in the Gamow window. In heavier systems, Pauli repulsion is expected to have a stronger effect at larger internuclear distance, and could even impact the barrier height. This is illustrated in Figure 6 where the nucleus-nucleus potentials for several systems are compared. We see that a potential pocket is produced inside the barrier, which becomes shallower in heavier systems.

Of course, the proper inclusion of the Pauli exclusion principle induces an apparent excitation of the system, e.g., increasing the local kinetic energy density in the overlap

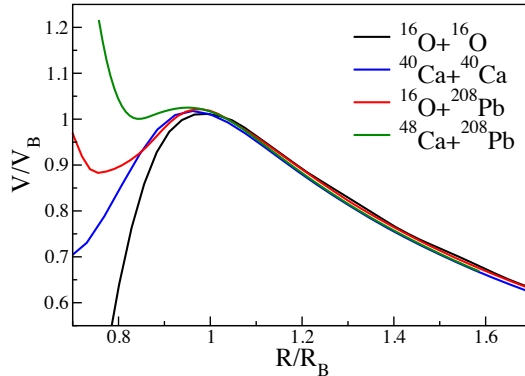


Figure 6: DCFHF potentials in various systems. R_B and V_B denote the FHF barrier radius and height, respectively.

region. Nevertheless, this type of excitation would have strictly no effect on the shape as the density is frozen (coupled-channel calculations incorporate effects of collective excitations via a change of density, so frozen densities have no effect on the dynamics). The only place where the excitation induced by the inclusion of the Pauli principle could in principle affect the coupled-channel equations is in the increase of the excitation energy which acts in the diagonal part of the coupled-channel Hamiltonian and thus effectively corresponds to a modification of the potential. But this is exactly what the Pauli repulsion potential does.

However, the fact that the nuclei cannot stay in their ground-states when they strongly overlap due to the Pauli exclusion principle raises another question concerning the validity of the coupled-channel approach. In usual coupled-channel applications, a description of the internal states of the nuclei in terms of a ground-state and few low-lying collective excited states is assumed. When the overlap between the densities is significant, this assumption breaks down because of the change of internal structure induced by the Pauli exclusion principle and because of the transition toward an adiabatic potential for the compound system [98]. Thus, we expect two effects from the Pauli exclusion principle: an increase of the potential (Pauli repulsion) and a reduction of the coupling strength.

To summarize, the DCFHF potential is a bare potential which can, in principle, be used in coupled-channel calculations if one neglects the modification of the internal states induced by the Pauli principle. The excitation induced by the inclusion of the Pauli principle has no other effect on the couplings as the density is frozen, and its excitation energy is already accounted for by the Pauli repulsion potential. The latter corresponds to the difference between the DCFHF and FHF potentials because (i) they use exactly the same density and (ii) FHF neglects the Pauli principle as the potential is obtained by adding the densities of the nuclei while in DCFHF the total state is described by a fully antisymmetrized Slater determinant.

3.1.4. Density Constrained TDHF

The TDHF method is probably the most established microscopic theory for studying the low-energy collisions of nuclei. In a direct TDHF calculation of a heavy-ion collision,

two static many-body states calculated in the HF approximation are boosted with a relative kinetic energy to initiate a nuclear collision. This evolution results in a self-organizing system which selects its evolutionary path by itself following the microscopic dynamics. Some of the effects naturally included in the TDHF calculations are: neck formation (see, e.g., Fig. 5), mass exchange, internal excitations, deformation effects to all orders, as well as the effect of nuclear alignment for deformed nuclei [99–102]. The main disadvantage of using TDHF directly to calculate fusion cross-sections, however, is the fact that due to its semi-classical character sub-barrier tunneling is not possible. This limits the fusion calculations to above barrier energies. In direct TDHF calculations, the fusion probability can then be either 0 or 1.

The use of nucleus-nucleus potentials is currently the only way to calculate sub-barrier fusion cross-sections. As discussed above, the FHF and DCFHF potentials do not incorporate dynamical rearrangements of the density. One possibility mentioned earlier is to include some dynamical effects via the coupled-channel method. Alternatively, one can compute potentials which incorporate the effects of the dynamics to some level. These “polarization potentials” are often energy dependent.

A natural generalization of the FHF and DCFHF methods can be accomplished by using the dynamical nuclear densities obtained from TDHF along with the density constraint to extract ion-ion interaction potentials directly from the TDHF time-evolution of the nuclear system. This density-constrained time-dependent Hartree-Fock (DCTDHF) method has been widely discussed and used in the literature [94, 100, 103–107].

The procedure for the DCTDHF method is as follows; TDHF time-evolution takes place with no restrictions. At certain times, corresponding to a nuclear distance $R(t)$ between the two nuclei during the evolution, the instantaneous density is used to perform a static Hartree-Fock minimization while holding the neutron and proton densities constrained to be the corresponding instantaneous TDHF densities,

$$E_{DC}(t) = \min_{\rho} \left\{ E[\rho_n, \rho_p] + \int d\mathbf{r} \lambda_n(\mathbf{r}) [\rho_n(\mathbf{r}) - \rho_n^{TDHF}(\mathbf{r}, t)] \right. \\ \left. + \int d\mathbf{r} \lambda_p(\mathbf{r}) [\rho_p(\mathbf{r}) - \rho_p^{TDHF}(\mathbf{r}, t)] \right\}.$$

Here, $E[\rho_n, \rho_p]$ is the EDF used in the HF and TDHF calculations. We refer to this minimized energy as the “density constrained energy”, E_{DC} . It is clear that the density constrained energy plays the role of a collective potential, except for the fact that it contains the binding energies of the two colliding nuclei. One can thus define the ion-ion potential as [103]

$$V_{DCTDHF}(R) = E_{DC}(R) - E[\rho_1] - E[\rho_2]. \quad (56)$$

This nucleus-nucleus potential is asymptotically correct since at large initial separations it exactly reproduces $V_{Coulomb}(R_{max})$. All of the dynamical features included in TDHF are naturally included in the DCTDHF potentials. These effects include neck formation, particle exchange [36, 108, 109], internal excitations, and deformation effects to all order, among others.

Examples of DCTDHF potentials are shown in Fig. 7 for $^{40}\text{Ca}+^{40}\text{Ca}$ at various TDHF energies [106]. The DCTDHF barriers are lower than the bare potential barriers obtained with the static FHF and DCFHF approaches. This is interpreted as a manifestation of the couplings to low-lying vibrational states which enhance fusion near the barrier. Indeed,

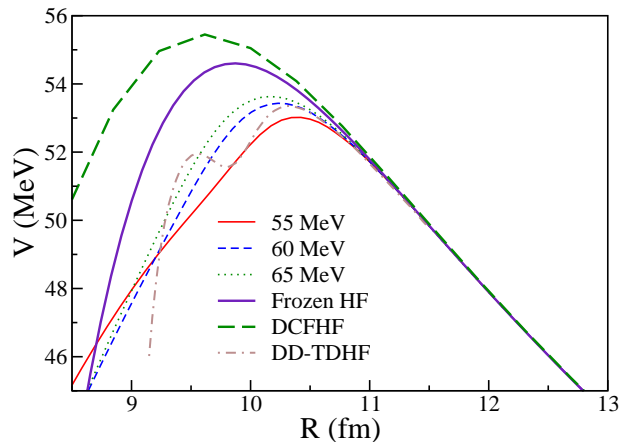


Figure 7: DCTDHF potentials in $^{40}\text{Ca}+^{40}\text{Ca}$ obtained from TDHF central collisions at $E_{cm} = 55, 60$ and 65 MeV, together with the FHF and DCFHF potentials. The dissipative dynamics TDHF (DD-TDHF) potential at $E_{cm} = 55$ MeV from [65] is also shown.

couplings between relative motion and internal structures are known to affect fusion barriers by dynamically modifying the densities of the colliding nuclei (see Fig. 5).

An energy dependence is also observed, with an increase of the barrier with collision energy. The lowering of the barrier due to the couplings is indeed expected to be stronger at energies near the barrier top, where changes in density have longer time to develop than at higher energies. A similar energy dependence is observed with the dissipative dynamics TDHF (DD-TDHF) method [65]. Note that at high energy the polarization potential should converge towards the bare potential. In fact, it is expected to converge towards the FHF potential and not the DC-FHF potential as nucleons of one fragment have very different momentum vectors than the nucleons in the other fragments, therefore reducing the Pauli repulsion [97].

There are different view points as to why DCTDHF works well. TDHF density evolution does contain the relevant collective degrees of freedom as well as single-particle dynamics during the early stages of the collision. Unlike static approaches, the DCTDHF method incorporates collision dynamics at the mean-field level, such as pre-equilibrium excitations, neck formation, and transfer. Naturally, the TDHF evolution takes place above the static potential energy surface. However, despite this, single-particle friction can quickly absorb this energy and lead to a configuration that may be considered a doorway state. As long as the average single-particle excitation energy per nucleon in this doorway state is less than the shell energy (about 4-8 MeV), the details of the ground-state potential-energy surface are still felt, and shell-correction energies influence the TDHF dynamics. As a result, DCTDHF calculations reproduce ion-ion interaction barriers for heavy-ion collisions.

3.1.5. Isovector and isoscalar contributions to the potential

It is sometimes convenient to separate isoscalar and isovector contributions to observables. This is often particularly useful when one wants to investigate specific effects with exotic nuclei, such as the evolution of the fusion barrier with nuclei along isotopic

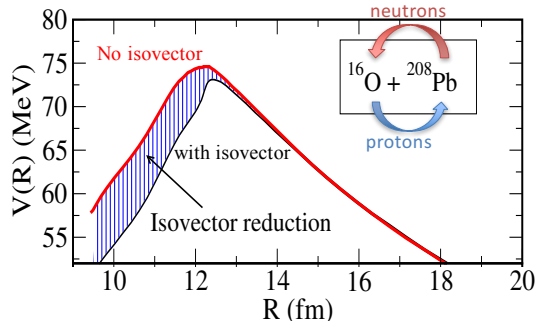


Figure 8: DCTDHF potential in $^{16}\text{O}+^{208}\text{Pb}$ with (black) and without (red) isovector contribution v_1 using TDHF densities from a central collision at $E_{cm} = 75$ MeV.

chains.

The isoscalar and isovector contributions in building up the nucleus-nucleus interaction barrier have recently been isolated. This is possible because the Skyrme EDF can be decomposed as [110];

$$\mathcal{H}(\mathbf{r}) = \frac{\hbar^2}{2m}\tau_0 + \mathcal{H}_0(\mathbf{r}) + \mathcal{H}_1(\mathbf{r}) + \mathcal{H}_{Coulomb}(\mathbf{r}). \quad (57)$$

The isospin index $I = 0, 1$ stands for isoscalar and isovector energy densities, respectively. The isoscalar (isovector) energy density, $\mathcal{H}_0(\mathbf{r})$ ($\mathcal{H}_1(\mathbf{r})$), depends on the isoscalar (isovector) particle density, $\rho_0 = \rho_n + \rho_p$ ($\rho_1 = \rho_n - \rho_p$), with analogous expressions for other densities and currents. The use of this decomposition in Eq. (56) allows us to write

$$V(R) = \sum_{I=0,1} v_I(R) + V_C(R), \quad (58)$$

where $v_I(R)$ denotes the potential computed by using the isoscalar and isovector parts of the Skyrme EDF [111].

In the static case the isovector potential v_1 is found to be small, and even vanishes in the FHF approximation. The isovector potential is then mostly induced by dynamical effects. Figure 8 illustrates the impact of the isovector contribution to the potential in the $^{16}\text{O}+^{208}\text{Pb}$ system [111]. An isovector reduction is observed in the inner part of the barrier. The origin of this reduction is interpreted as an effect of transfer of protons from ^{16}O to ^{208}Pb and of neutrons in the opposite direction. This is compatible with recent experiments of multi-nucleon transfer at sub-barrier energies [112, 113]. The fact that protons and neutrons do not flow in the same direction induces a non-zero isovector density at the origin of the observed variation of the potential at short distances.

3.1.6. Interplay between transfer and fusion

This approach has been employed to investigate the influence of transfer on fusion for a number of systems [111], including on heavy systems such as $^{40,48}\text{Ca}+^{132}\text{Sn}$ in which the experimental signatures are not so clear [114, 115]. As shown in several works using

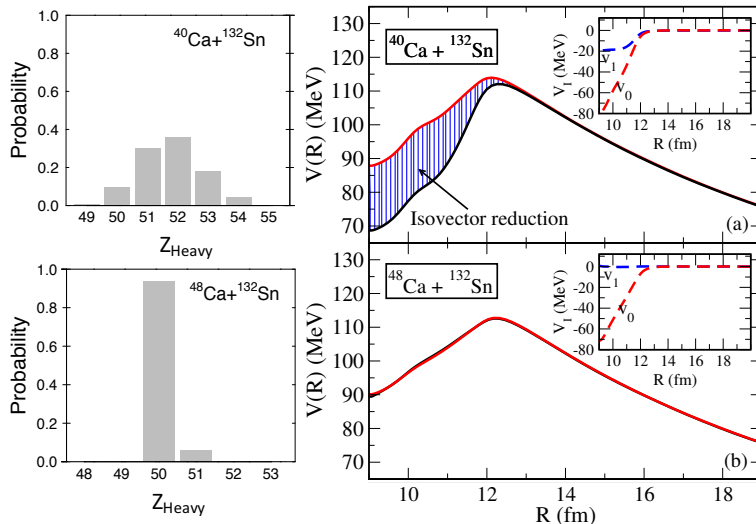


Figure 9: Charge distributions in the heavy fragments following a central collision with TDHF just below the barrier (left) and DCTDHF potentials (right) without (solid red line) and with (solid black line) isovector contributions in $^{40}\text{Ca} + ^{132}\text{Sn}$ (top) and in $^{48}\text{Ca} + ^{132}\text{Sn}$ (bottom). The insets show the isoscalar and isovector contributions to the nuclear part of the potential.

TDHF [13, 116–120], systems with N/Z asymmetries encounter a rapid charge equilibration (transfer of protons and neutrons in opposite directions). This charge equilibration has a strong impact on v_1 [111].

The isovector reduction of the potential due to transfer depends naturally on the presence of positive Q -value transfer channels [121]. As shown in Fig. 9, an isovector reduction is observed in $^{40}\text{Ca} + ^{132}\text{Sn}$ which has several positive Q -value transfer channels, but not in $^{48}\text{Ca} + ^{132}\text{Sn}$ which has only negative Q -value transfer channel. Another confirmation of this effect is obtained from the proton number distributions in the heavy fragments when the collision occurs just below the barrier (i.e., with two outgoing fragments in the TDHF evolution). These distributions are obtained from a particle number projection technique [108] (see section 3.3). As a result, almost no charge transfer is observed in $^{48}\text{Ca} + ^{132}\text{Sn}$ while significant transfer probabilities are found in $^{40}\text{Ca} + ^{132}\text{Sn}$.

Standard coupled-channels calculations without couplings to transfer channels then reproduce the $^{48}\text{Ca} + ^{132}\text{Sn}$ system relatively well [122]. However, similar calculations underpredict the fusion cross sections in $^{40}\text{Ca} + ^{132}\text{Sn}$. This is interpreted as a fusion enhancement at and below the barrier from couplings to transfer channels in the latter system. In DCTDHF, the origin of this enhancement is a reduction of the barrier width as seen in Fig. 9-a). As a result, sub-barrier fusion cross-sections calculated from such potentials (see next section) are in relatively good agreement with experiment for these systems [104] despite the fact that these calculations have no adjustable parameters.

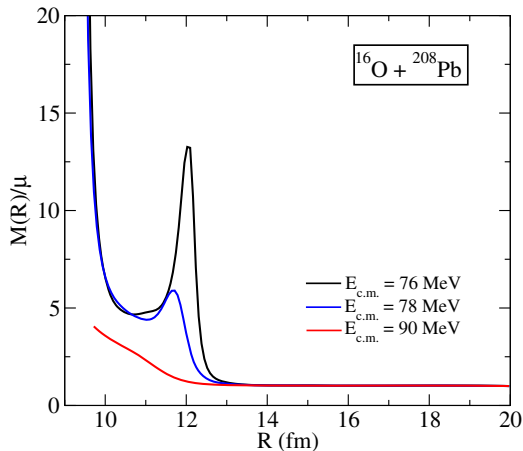


Figure 10: Ratio of the coordinate-dependent mass $M(R)$ over the constant reduced mass obtained from TDHF $^{16}\text{O}+^{208}\text{Pb}$ central collisions at various energies [124].

3.1.7. Fusion cross-sections

The nucleus-nucleus potential is of course an essential ingredient to compute fusion cross-sections. As the DCTDHF potentials already account for effects of the dynamics (at the mean-field level), they should not be used in coupled-channels calculations as this would double count the effect of the couplings. Fusion probabilities can then be computed with DCTDHF potentials using a series of one-barrier penetration calculations. In principle, one needs to do one calculation per incident energy as the DCTDHF potential is energy dependent. In practice, potentials computed at few energies in steps of few MeV near the barrier are usually sufficient for the calculation of fusion cross-sections [106, 123, 124]. Note that one drawback of the approach is that it cannot provide barrier potentials from TDHF collisions at sub-barrier energies, as in this case the TDHF trajectory does not lead to fusion. Sub-barrier fusion cross-sections are then estimated with DCTDHF potentials computed with a near-barrier energy.

Another important quantity entering the calculation of cross-sections is the coordinate-dependent mass $M(R)$. The latter can be obtained from TDHF evolutions using energy conservation for a central collision

$$M(R) = \frac{2[E_{\text{cm}} - V(R)]}{\dot{R}^2}, \quad (59)$$

where the collective velocity \dot{R} is directly obtained from the TDHF evolution. Examples of evolutions of $M(R)$ at various energies are shown in Fig. 10 for the $^{16}\text{O}+^{208}\text{Pb}$ reaction [124]. The R -dependence of this mass at lower energies is very similar to the one found in constrained Hartree-Fock calculations [125] with a constraint on the quadrupole moment. On the other hand, at higher energies the coordinate dependent mass essentially becomes flat, which is again a sign that most dynamical effects are contained at lower energies. The peak at small R values is due to the fact that the centre-of-mass energy is above the barrier and the denominator of Eq. (59) becomes small due to the slowdown of the ions.

The fusion barrier penetrabilities $T_L(E_{\text{cm}})$ can be obtained by numerical integration of the Schrödinger equation for the collective distance coordinate R , using the heavy-ion potential $V(R)$ with coordinate dependent mass parameter $M(R)$. Alternatively, we can instead use the constant reduced mass μ and transfer the coordinate-dependence of the mass to a scaled potential using the well known exact point transformation [124, 125]

$$dR \longrightarrow \left(\frac{M(R)}{\mu} \right)^{\frac{1}{2}} dR. \quad (60)$$

The potential $V(R)$, which includes the coordinate-dependent mass effects differs from the original only in the interior region of the barrier. Further details can be found in Ref. [124]. Using the transformed potential the fusion barrier penetrabilities $T_L(E_{\text{cm}})$ are obtained by numerical integration of the Schrödinger equation

$$\left[\frac{-\hbar^2}{2\mu} \frac{d^2}{dR^2} + \frac{L(L+1)\hbar^2}{2\mu R^2} + V(R) - E_{\text{cm}} \right] \psi(R) = 0, \quad (61)$$

using the incoming wave boundary condition (IWBC) method [126]. IWBC assumes that once the minimum of the potential is reached fusion will occur. In practice, the Schrödinger equation is integrated from the potential minimum, R_{min} , where only an incoming wave is assumed, to a large asymptotic distance, where it is matched to incoming and outgoing Coulomb wavefunctions. The barrier penetration factor, $T_L(E_{\text{cm}})$, is the ratio of the incoming flux at R_{min} to the incoming flux at large distance. Here, we implement the IWBC method exactly as it is formulated for the coupled-channel code CCFULL described in Ref. [51]. However, since the DCTDHF potential already includes excitations present at the mean-field level it can no longer be considered as a bare nucleus-nucleus potential. Consequently, it would not be appropriate to employ channel couplings using this potential and the potential must be directly used. This gives us a consistent way for calculating fusion cross-sections at energies below and above the barrier via

$$\sigma_f(E_{\text{cm}}) = \frac{\pi}{k^2} \sum_{L=0}^{\infty} (2L+1) T_L(E_{\text{cm}}). \quad (62)$$

At energies well above the barrier either the DC-TDHF method or direct TDHF calculations [where $T_L(E_{\text{cm}}) = 0$ or 1] can be used to determine the fusion cross-sections.

An example of calculations of fusion cross-sections in $^{16}\text{O}+^{16}\text{O}$ is shown in Fig. 11 [79]. The oscillations observed in the cross-sections result from overcoming angular momentum dependent fusion barriers. Cross-sections computed directly from TDHF agree relatively well with those computed from DCTDHF potential, except at the highest energies, which could possibly indicate a breakdown of the isocentrifugal approximation used in the one-barrier penetration approach. The calculations match well the experimental data near and below the barrier. Above the barrier, there is a strong dependence in the experimental results, with cross-sections found to be smaller than in the calculations. It would be interesting to perform new measurements on this system at above barrier energies. A similar comparison between TDHF predictions [66] and experimental data [132] in the $^{16}\text{O}+^{208}\text{Pb}$ system shows an overestimation of the fusion cross-sections of $\sim 16\%$ above

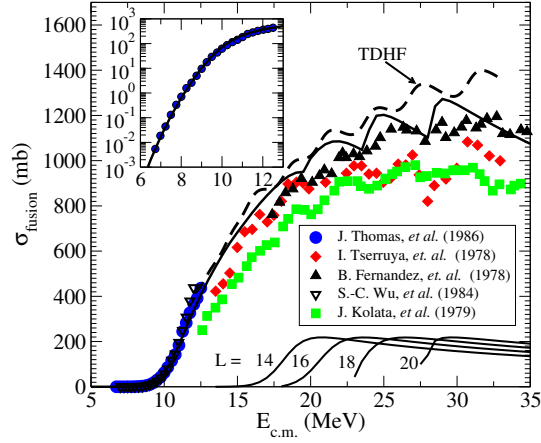


Figure 11: Fusion cross-sections in $^{16}\text{O}+^{16}\text{O}$ in linear scale. Logarithmic cross-sections are shown in the inset for the low energies. Total fusion cross-sections computed from DCTDHF potential and the contributions from various angular momenta are shown with solid lines. The dashed line gives the fusion cross-sections computed directly from TDHF. Experimental data are from [127–131].

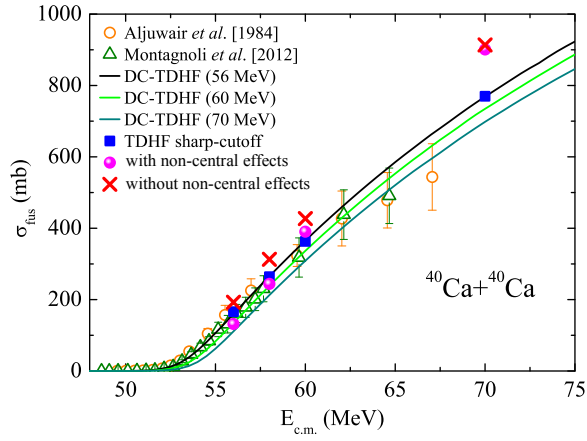


Figure 12: Comparison of fusion cross-sections in $^{40}\text{Ca}+^{40}\text{Ca}$ from experimental data [133, 134] and from TDHF (squares) and DCTDHF predictions with (circles) and without (crosses) non-central effects. Adapted from [105].

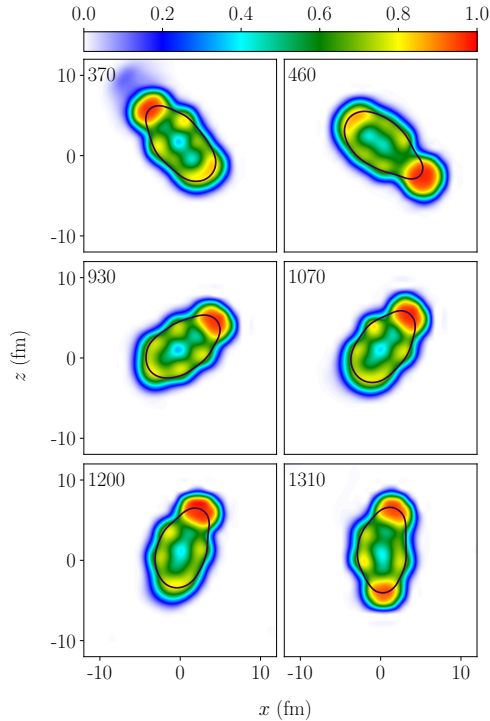


Figure 13: α -localization function in $^{18}\text{O}+^{12}\text{C}$ at $E_{cm} = 14$ MeV with an impact parameter of 2 fm [136]. Hot colors indicate the likelihood for the presence of an α -cluster. The numbers indicate time in fm/c. The solid line is an isodensity at 0.05 fm^{-3} .

the barrier, while the position of the barrier is very well reproduced. The origin of this discrepancy remains to be investigated.

The DCTDHF method has been recently implemented within the Sky3D solver [35] by X. Jiang and collaborators [105]. In particular, they investigated non-central effects on the potential by computing the DCTDHF potentials at finite impact parameters [105, 135]. They found that these non-central effects have a significant effect near the barrier, reducing the fusion cross-sections in this energy region and improving the agreement with experiment, as shown in Fig. 12. At higher energies, however the non-central effects on the potential are shown to be negligible.

Other examples of comparisons between DCTDHF predictions and experimental fusion cross-sections include reactions with radioactive beams. DCTDHF calculations predict a large enhancement of fusion with neutron-rich light nuclei, such as $^{24}\text{O}+^{16}\text{O}$ [94] which could have an impact on reaction rates in dense stellar matter such as neutron star crusts [137]. In the same mass region, the reaction $^{20}\text{O}+^{12}\text{C}$ has been measured [138] and compared with DCTDHF calculations [139]. While for this system the calculations underestimate the fusion cross-sections, it is interesting to note that a good agreement is obtained for the $^{19}\text{O}+^{12}\text{C}$ system [140]. A poor agreement is obtained for the $^{18}\text{O}+^{12}\text{C}$ stable system [141]. This could be due to the fact that ^{18}O has a strong $^{14}\text{C}+\alpha$ cluster

configuration, as shown by the strong probability for α -transfer in $^{18}\text{O}+^{208}\text{Pb}$ [113, 142]. These cluster configurations are difficult to account for in TDHF calculations, unless they are already present in the initial HF wave-function, as in the $^8\text{Be}+\alpha$ reaction [143] or with rod-shape configurations [144, 145]. Note that Schuetrumpf and collaborators have recently developed a nucleon localization technique for nuclear systems [146] which they applied to identify the presence of α -clustering in heavy-ion collisions [136]. An example is shown in Fig. 13, where we see that an α -cluster is likely to be found on one hedge of the rotating compound system. This technique could form the basis for a beyond TDHF approach to incorporate cluster effects in the dynamics.

3.1.8. Dissipation on the way to fusion

The ability for the nuclei to deform and get excited during a collision induces a dissipation mechanism where the kinetic energy for the relative motion is transformed into internal excitation energy. It is possible to use time-dependent microscopic calculations to compute parameters associated with dissipative dynamics, e.g., friction coefficient entering the Langevin equation [147–149]. The dissipation mechanism has also been investigated using the DCTDHF technique in [150, 151].

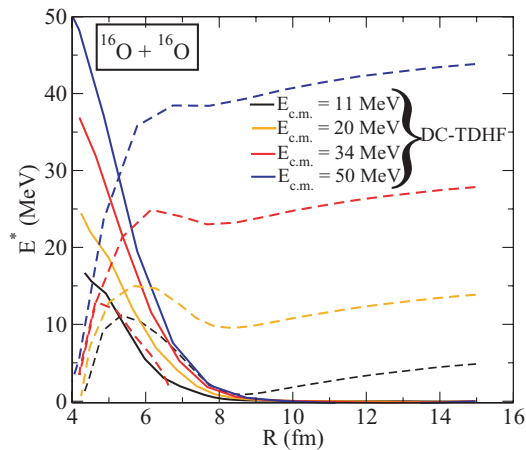


Figure 14: Excitation energy in $^{16}\text{O}+^{16}\text{O}$ from DCTDHF (solid lines) and corresponding collective kinetic energy (dashed lines) at various centre of mass energies [150].

Using the DCTDHF method, it is indeed possible to calculate dynamical excitation energies by making the premise that the TDHF energy can be divided into a collective and an intrinsic part [150]

$$E^*(t) = E_{TDHF} - E_{coll}(\rho(t), \mathbf{j}(t)) , \quad (63)$$

where E_{TDHF} is the total energy of the dynamical system, which is a conserved quantity, and E_{coll} represents the collective energy of the system

$$E_{coll}(t) = E_{kin}(\rho(t), \mathbf{j}(t)) + E_{DC}(\rho(t)) . \quad (64)$$

Here E_{kin} is the collective kinetic part and is given by

$$E_{kin}(\rho(t), \mathbf{j}(t)) = \frac{m}{2} \int d\mathbf{r} \mathbf{j}^2(\mathbf{r}, t) / \rho(\mathbf{r}, t) , \quad (65)$$

which is asymptotically equivalent to the kinetic energy of the relative motion, $\frac{1}{2}\mu\dot{R}^2$, where μ is the reduced mass and $R(t)$ is the ion-ion separation distance.

An example of evolution of the excitation energy as a function of the relative distance between the nuclei is shown in Fig. 14 for $^{16}\text{O}+^{16}\text{O}$ central collisions [150]. The barrier radius is approximately 8.3 fm in this system (see Fig. 2). We see in Fig. 14 that, with such light collision partners, the excitation energy increases rapidly inside the barrier. The situation is different in heavier systems, e.g., in those used to form superheavy nuclei. Indeed, DCTDHF calculations show that, in such systems, the excitation energy increases before capture [151], thus increasing the probability for the systems to encounter a quasi-fission process. These calculations also show that, in the case of reactions with actinides, the evolution of the excitation energy depends strongly on the orientation of the deformed target.

3.1.9. Adiabatic potentials for sub-barrier fusion

As mentioned in section 3.1.7, one difficulty of the DCTDHF method is to determine the potential seen by the nuclei at sub-barrier energies when tunneling through the barrier. This is because DCTDHF is a method to extract the potential from TDHF trajectories, yet the latter do not lead to fusion at sub-barrier energies. This problem could be overcome with constrained Hartree-Fock potentials obtained by minimizing the HF energy under a collective constraint (e.g., a fixed value of the quadrupole and octupole moments) [152]. This technique is bread and butter in fission studies [153] as it leads to adiabatic potentials well suited for fission. However, the choice of the constraint may sometime be problematic, in particular in asymmetric collisions where an octupole constraint may not be sufficient to ensure the correct asymmetry in the approach phase.

The adiabatic self-consistent collective coordinate (ASCC) method provides an alternative approach to describe the fusion path and potential without relying on a specific choice of the collective coordinates [17, 154]. The method determines the optimal collective path which may differ from the constrained HF one [155]. Another advantage of the ASCC method is to self-consistently determine the inertial mass to be used. Wen and Nakatsukasa have applied the method recently to $\alpha, ^{16}\text{O}+^{16}\text{O}$ collisions [156]. Although the calculations still use a simple functional (BKN), the method shows some promise in automatically selecting the collective degrees of freedom which are relevant for the chosen reaction path (e.g., fusion).

3.2. Superfluid dynamics for heavy-ion collisions and fission reactions

It is well known that pairing plays a vital role in studies of structure of ground and excited states of nuclei [157]. The inclusion of pairing degrees of freedom in structure calculations is implemented via the Hartree-Fock-Bogoliubov (HFB) or the Hartree-Fock combined with BCS (HF+BCS) approaches (see, e.g., [158–164]). Importance of pairing in nuclear fission has been the subject of a number of recent studies of multi-dimensional potential energy surfaces (PES) [153, 165–168]. It was also recognized as an essential ingredient to investigations of the evolution from saddle to scission in fissioning nuclei with time-dependent microscopic approaches [169]. One of the most important contributions of pairing to self-consistent mean-field calculations is the ability of the system to allow for level crossings, which results in fragments establishing their identity between the saddle and scission points [166, 167, 170–173]. Pairing is also expected to play a

role as a residual interaction in dynamical calculations of heavy-ion collisions, giving flexibility to the system to attain more compact shapes in fusion, influence transfer and breakup, or lowering the effect of spherical magic shells and open other magic numbers for final fragment formation in fission and quasifission studies [174]. While it is clear that pairing interaction plays an important role in multi-nucleon transfer reactions and for fission fragments acquiring their identity after passing the saddle point, the influence of pairing in fusion, which involves high excitation, is not so well established and is still under investigations [175–180].

3.2.1. Time-dependent Hartree-Fock Bogoliubov calculations

Formally, the time-dependent Hartree-Fock-Bogoliubov (TDHFB) theory should be the tool of choice for treating pairing in dynamical calculations. To date, most applications of TDHFB have been confined to the small amplitude limit as linear response calculations [17, 25, 26, 28, 181–183]. The direct coordinate space implementation of TDHFB equations for large amplitude reaction phenomena appears to be very complicated [184], requiring a vast computational effort, albeit recently significant progress has been done in application to scission dynamics [185], neutron star crust vortex dynamics [186], and heavy-ion collisions [178, 179, 187].

In the traditional method to solve the HFB equations we express the many-body wavefunction in terms of the Bogoliubov quasiparticle vacuum [162, 164, 188, 189], resulting in the HFB supermatrix. As for the TDHF equation, the TDHFB equation can be derived starting from the action between an initial and final time t_i and t_f

$$S = \int_{t_i}^{t_f} dt \langle \Psi(t) | i\hbar \frac{\partial}{\partial t} - \hat{H} | \Psi(t) \rangle \quad (66)$$

(see section 2.5). The difference with the independent particle case (TDHF) is that now the state $|\Psi(t)\rangle$ is constrained to be a quasiparticle vacuum instead of a Slater determinant. The basis of quasiparticle annihilators $\{\hat{\beta}\}$ is defined such that $\hat{\beta}_\mu |\Psi\rangle = 0$ for all μ [157] and can be related to the particle creation and annihilation operators $\{\hat{a}^\dagger, \hat{a}\}$ through the Bogoliubov transformation [190]

$$\hat{\beta}_\mu = \sum_\nu (U_{\nu\mu}^* \hat{a}_\nu + V_{\nu\mu}^* \hat{a}_\nu^\dagger). \quad (67)$$

The variational principle $\delta S = 0$ leads to the TDHFB equation [191]

$$i\hbar \frac{\partial}{\partial t} \mathcal{R} = [\mathcal{H}, \mathcal{R}], \quad (68)$$

with the generalized one-body density matrix

$$\mathcal{R}(t) = \begin{pmatrix} \rho(t) & \kappa(t) \\ -\kappa^*(t) & 1 - \rho^*(t) \end{pmatrix} \quad (69)$$

and the generalised Hamiltonian

$$\mathcal{H} = \begin{pmatrix} h & \Delta \\ -\Delta^* & -h^* \end{pmatrix}. \quad (70)$$

In addition to the one-body density matrix ρ and the single-particle Hamiltonian h , we now have to account for the pairing tensor $\kappa_{\mu\nu} = \langle \psi | \hat{a}_\nu \hat{a}_\mu | \psi \rangle$ as well as the pairing field

$$\Delta_{\mu\nu} = \frac{\delta \mathcal{E}[\rho, \kappa, \kappa^*]}{\delta \kappa_{\mu\nu}^*}, \quad (71)$$

where $\mathcal{E}[\rho, \kappa, \kappa^*]$ is the energy density functional accounting for pairing. In practice, the TDHFB equation is solved as a function of the quasiparticle components U and V following

$$i\hbar \frac{\partial}{\partial t} \begin{pmatrix} U_{\nu\mu} \\ V_{\nu\mu} \end{pmatrix} = \sum_{\eta} \begin{pmatrix} h_{\nu\eta} & \Delta_{\nu\eta} \\ -\Delta_{\nu\eta}^* & -h_{\nu\eta}^* \end{pmatrix} \begin{pmatrix} U_{\eta\mu} \\ V_{\eta\mu} \end{pmatrix}. \quad (72)$$

In calculations based on the Skyrme energy density functional, the dependence of the EDF on the pairing tensor is often written as a local pairing functional (see, e.g., [161] and references therein)

$$\mathcal{E}_{pair} = \int d\mathbf{r} \frac{g}{4} \left[1 - \left(\frac{\rho_0(\mathbf{r})}{\rho_c} \right)^\gamma \right] \sum_q \tilde{\rho}_q^*(\mathbf{r}) \tilde{\rho}_q(\mathbf{r}) \quad (73)$$

where $\rho_q(\mathbf{r}) = \sum_s \rho_q(\mathbf{r}s, \mathbf{r}s)$ and $\tilde{\rho}_q(\mathbf{r}) = \sum_s \tilde{\rho}_q(\mathbf{r}s, \mathbf{r}s)$, and $\tilde{\rho}_q(\mathbf{r}s, \mathbf{r}'s') = -2s'\kappa_q(\mathbf{r}s, \mathbf{r}'s')$ is the anomalous density (q and s are the nucleon isospin and spin, respectively). However, this choice of pairing functional leads to divergences [158, 192, 193] and it is necessary to introduce a regularization scheme, e.g., by using a cutoff in the quasiparticle spectrum. For instance, a quasiparticle energy window of 80 MeV (allowing for two-quasiparticle excitations up to 160 MeV) was necessary to ensure a good convergence in a study of pairing vibrations with the TDHFB equation solved in spherical symmetry [25]. Such high energy cutoff is often prohibitive in symmetry unrestricted calculations.

Because it is not an eigenstate of the particle number operator, a HFB ground state is defined up to a gauge angle. As a result, heavy-ion collisions computed in TDHFB exhibit a dependence with the relative gauge angle between the collision partners [178, 179, 187]. In particular, fusion thresholds are shown to increase significantly when the gauge angles do not match in these calculations for symmetric head-on collisions. As shown by an analysis of frozen nucleus-nucleus potentials, this phenomenon is partly due to static effects [178]. Nevertheless, dynamical effects such as solitonic excitations could contribute to the dissipation process [179]. Comparing fusion in superfluid and non-superfluid systems could lead to experimental evidence of these effects [180].

3.2.2. Time-dependent BCS approximation

An alternate and much simplified approach can be obtained by expressing HFB solutions in the BCS form [26, 194–196]

$$|\Psi(t)\rangle = \prod_{k>0} \left(u_k(t) + v_k(t) a_k^\dagger(t) a_{\bar{k}}^\dagger(t) \right) |0\rangle, \quad (74)$$

where a_k^\dagger is the creation operator of a nucleon in the k -th HFB canonical or natural basis state. The quantities $u_k(t)$ and $v_k(t)$ establish the link between the canonical states and

the quasiparticle states. This assumption results in a diagonal one-body density matrix as well as a diagonal pairing density. The corresponding time-dependent equations can then be written in terms of the occupation numbers $n_k(t) = v_k^2(t)$ of single-particle states [26, 196] and anomalous density components $\kappa_k(t) = u_k^*(t)v_k(t)$

$$i\hbar \frac{dn_k}{dt} = \Delta_k^* \kappa_k - \Delta_k \kappa_k^*, \quad i\hbar \frac{d\kappa_k}{dt} = \kappa_k(\epsilon_k - \epsilon_{\bar{k}}) + \Delta_k(2n_k - 1), \quad (75)$$

where Δ_k is the pairing field.

There are numerous advantages of using the TDHF+BCS (also called TDBCS or canonical basis TDHFB in the literature) approach instead of TDHFB. First, the canonical states are localized and therefore instead of dealing with a very large number of states proportional to the box volume we can deal with a much smaller number of states proportional to the nuclear volume. Second, the evolution of the system closely resembles TDHF equations

$$i\hbar \frac{d}{dt} |\varphi_k\rangle = (h[\rho] - \epsilon_k(t)) |\varphi_k\rangle, \quad (76)$$

where $h[\rho]$ is the self-consistent mean-field and $\epsilon_k(t) = \langle \varphi_k | h[\rho] | \varphi_k \rangle$ [196].

Although the TDHF+BCS approach has been introduced a long time ago [197], it was applied with a simple “constant G” pairing interaction. Without an energy cut-off, this leads to only one degree of freedom for the pairing which is the pairing gap Δ . In modern TDHF+BCS calculations with density-dependent interactions, the pairing field in the canonical basis $\Delta_{i\bar{i}}$ changes during the evolution and presents a non-integrable phase evolution different for each state i .

A word of caution when using the BCS approximation is necessary regarding the single-particle states with positive energy. Use of these states should be avoided as they create an artificial low-density gas in the numerical box and interfere with the time-evolution of the system by introducing an artificial damping due to the interaction with box boundaries. It is also important to note that TDHF+BCS violates the one-body continuity equation. This can lead to spurious transfer between fragments [196]. In realistic calculations, one needs to monitor the effect. Although it can lead to uncertainties in transfer reactions [27], it does not have a significant impact in fission studies [171, 198, 199]. In addition, as discussed in section 3.2.1, in TDHF+BCS or TDHFB approaches the initial superfluid collision partners can each have different gauge angles. Realistic calculations of heavy ion collisions would then require to sum these gauge angles coherently, thus calling for beyond mean-field techniques [187].

An interesting question is whether the TDHF+BCS approximation would capture the main features observed in TDHFB calculations. As an example, Fig. 15 shows a comparison of density evolutions obtained from TDHF and TDHF+BCS in $^{22}\text{O} + ^{52}\text{Ca}$ at $E_{cm} = 25$ MeV and for impact parameter $b = 4.1$ fm [176]. It is observed that the inclusion of pairing dynamics at the BCS level prevents the system to fuse. Similar observations were also made by the full TDHFB calculations [178, 179] discussed in section 3.2.1. This is an indication that TDHF+BCS contains at least part of the dissipative mechanisms induced by the pairing correlations. Of course, the BCS approximation is much simpler than TDHFB, and some effects present in TDHFB could be missed in TDHF+BCS, e.g., effects induced by the non-uniformity of the pairing field [179].

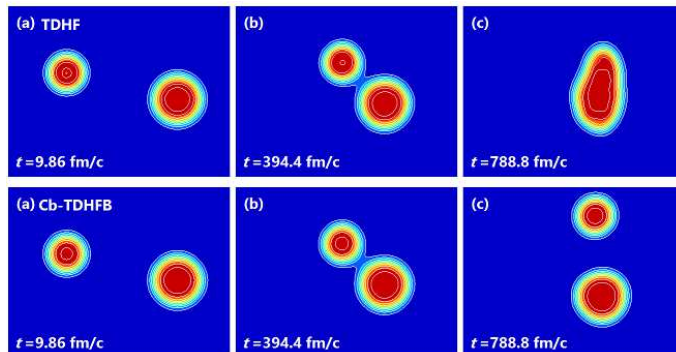


Figure 15: TDHF (top) and TDHF+BCS (bottom) neutron density evolutions in $^{22}\text{O}+^{52}\text{Ca}$ at $E_{cm} = 25$ MeV and $b=4.1$ fm [176].

3.2.3. TDHF+BCS with the frozen occupation approximation

When static pairing correlations are important for a proper description of the initial state (e.g., to have a realistic deformation of the collision partners) but are not expected to play a crucial role during the dynamics, then the so-called *frozen occupation approximation* (FOA) is sometimes used. The FOA further simplifies the BCS approach by freezing the occupation numbers for the time-evolution. The FOA is expected to be a good approximation at the early stages of heavy-ion collisions, up to the capture of the collision partners. For instance, TDHF+FOA calculations have been used to investigate above-barrier capture cross-sections with exotic nuclei [200].

In Ref. [196] a comprehensive model study of TDHF+BCS and TDHFB approaches showed that the TDHF+BCS approximation with time-dependent occupation numbers violates the continuity equation and results in unphysical results for particle emission, while the FOA approximation is found to be stable and provide reasonable outcomes. The parallel TDHFB study was found to give a good description of particle emission for short times but also suffered from unphysical oscillations at later times.

Applications of TDHF+BCS to study isovector dipole [201] and isoscalar and isovector quadrupole vibrations [78, 80] were performed without the FOA approximation. However, in [78, 80] Scamps and Lacroix performed a comparison between full TDHF+BCS results and calculations using the FOA approximation. An almost perfect agreement was found between the two levels of approximation. Comparison to cases without pairing was not straightforward since without pairing most of these nuclei are deformed. To remedy this problem the filling approximation was used. It was found that the mean collective energy depends strongly on the energy density functional, while other effects such as pairing resulted in local fluctuations about this mean. However, the pairing was found to be essential when considering low-lying states. Note also that an excellent comparison between the TDHF+BCS and QRPA (which is obtained by linearizing the full TDHFB equation) approaches was obtained.

Another example of application of the FOA is to study transfer reactions (see also section 3.3). The effect of pairing on two-particle transfer has been investigated by Scamps and Lacroix [27, 177]. It was found that the pairing had a little effect on one-particle transfer but significant effect on two-particle transfer, albeit still not enough

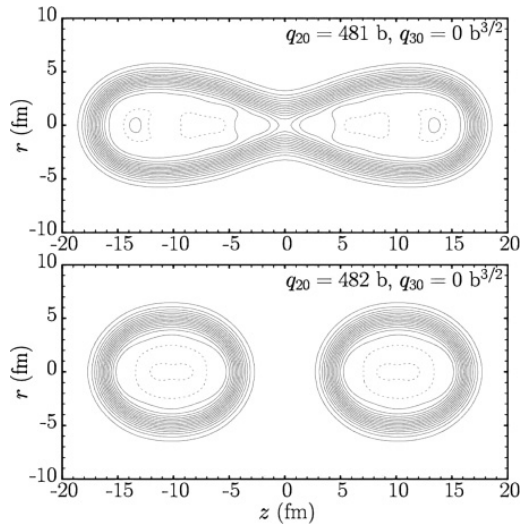


Figure 16: Symmetric scission configurations of ^{226}Th before (up) and after (down) scission [205]. The quadrupole and octupole moments q_{20} and q_{30} , respectively, are used as external constraints in the HFB calculations.

transfer was obtained. The primary source of the increase in two-particle transfer was traced to the partial occupations of the single-particle states. This suggests that beyond mean-field approaches may be necessary for a proper description of two-particle transfer.

3.2.4. Applications to fission

Perhaps the most striking example of recent applications of TDHF and its extensions in the past few years has been to fission [170, 171, 185, 198, 199, 202–204] studies. These works have been performed with different level of approximation to the many-body dynamical problem, including standard TDHF, TDHF with BCS pairing correlations at the FOA level, and dynamical pairing with TDHF+BCS and TDHFB approaches.

The description of fission with time-dependent microscopic theories has been a long-standing problem (see [153] for a recent review). One approach is to construct a fully microscopic potential energy surface (PES) using deformation constrained HFB states and to solve the time-dependent generator coordinate method (TDGCM) equation with the Gaussian overlap approximation (GOA) to predict the dynamical evolution of the collective wave-function [206, 207]. This approach is well suited to describe the overcoming of the barrier as well as fluctuations and repartition between fission valleys. However, the underlying adiabatic assumption used to construct the static constrained HFB states should break down close to scission where non-adiabatic effects are expected to play a role. As an illustration, Fig. 16 [205] shows the two consecutive HFB states obtained just before and just after scission (notice the very small difference in the quadrupole moment q_{20}). If pushed to the extreme, the adiabatic approximation would lead to the spurious description that the systems evolves from the pre-scission to the post-scission state in one step, while what is expected is a rapid but continuous evolution at scission. The idea is then to use TDHF based approaches to improve the description of the microscopic

states near scission.

Fission dynamics along the mass symmetric valley of ^{264}Fm has been investigated with TDHF calculations [170]. As the ^{132}Sn fragments are doubly magic, it is expected that pairing correlations disappear somewhere between the saddle and scission configurations, with the formation of magic gaps in the single-particle energy spectra signaling the pre-formation of the fragments, as shown in Fig. 17. Before the magic gap is formed, jumps in the single particle energies are observed due to single particle levels crossing the Fermi surface and inducing a change of the shape of the system [208]. These jumps are often associated with barriers in the PES which cannot be overcome in mean-field based descriptions (even if one uses the more elaborate TDHFB treatment) due to lack of quantum many-body tunneling. Time-dependent mean-field calculations then need to be started at configurations outside these barriers.

The ^{264}Fm symmetric fission is a special case as it can be studied at the TDHF level. However, in the vast majority of systems, the inclusion of pairing correlations at some level is mandatory. Goddard, Stevenson and Rios have investigated the dynamics of deformation and boost induced fission with the FOA [202, 203]. Although the systems could be made to fission in some cases, it was shown that the properties of the fragments (mass, charge, kinetic energies) were depending on the choice of the initial configuration used in the time-dependent calculation. Nevertheless, a reasonably good agreement with experiment was achieved, showing promise for the technique.

The dependence of the fission fragment properties with the initial configuration in the saddle to scission potential energy descent is to a large extent reduced when pairing is accounted for in a dynamical fashion. Scamps and collaborators have used the TDHF+BCS approach to study the fission dynamics of ^{258}Fm [171]. The time-dependent pairing correlations are able to describe the fact that when a single particle level leaves the Fermi surface, its occupation number goes to zero, as shown in Fig. 18. The reorganisation of the neutron occupation numbers in the symmetric fission of ^{258}Fm is also shown in Fig. 19 together with the density evolution and the repartition of the energy in terms of kinetic and Coulomb potential energies. One particular advantage of these time-dependent descriptions of fission dynamics is that the final properties of the fission fragments do not depend on how the scission configuration is defined.

In particular, this leads to unambiguous determination of the total kinetic energy (TKE) of the fragments. The TKE is obtained from the sum of the Coulomb and kinetic energies after scission. Indeed, the nuclear interaction between the fragments has vanished when the fragments are well separated and the sum of the Coulomb and kinetic energies remains constant. (Of course, asymptotically, all the Coulomb potential energy is transformed into kinetic energy.) This allows direct comparison of the predicted average mass and TKE of the fragments with experimental distributions as illustrated in Fig. 20.

Recently, Bulgac and collaborators have used their TDHFB code to investigate fission dynamics of ^{240}Pu [185]. An interesting finding is that the saddle to scission time seems to be longer than in the earlier studies described above. The explanation invoked in [185] is that the system is allowed to explore more degrees of freedom as the pairing field has less spatial restrictions than in TDHF+BCS. However, it has since been shown that TDHF+BCS could lead to similarly long saddle-to scission times [199, 204].

A drawback of the present mean-field approaches is that they do not account for the fluctuations of collective variables. If included, these fluctuations would allow a

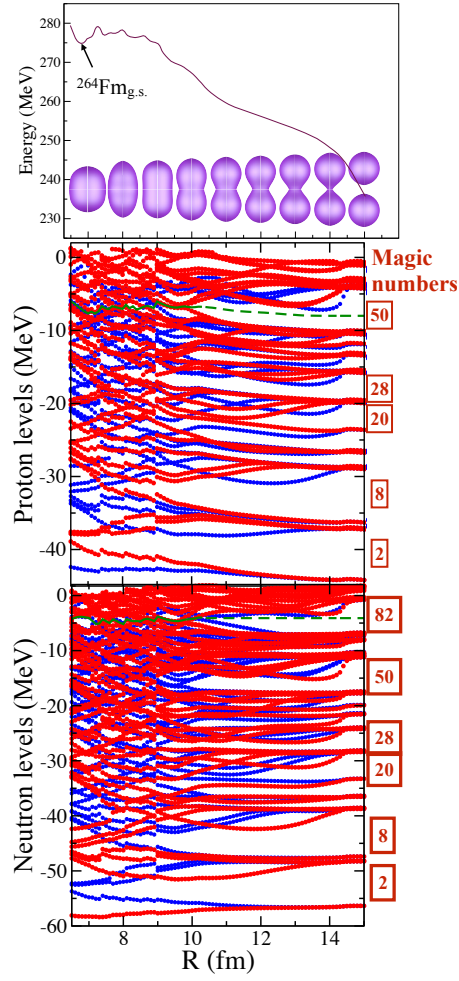


Figure 17: Constrained HF+BCS calculations of ^{264}Fm symmetric fission valley with the SLy4d Skyrme functional and surface pairing as a function of the distance between the fragments R . (top) Adiabatic potential and isodensities at half the saturation density $\rho_0/2 = 0.08 \text{ fm}^{-3}$. Single-particle levels are plotted for protons and neutrons in the middle and bottom panels, respectively. Positive and negative parity states are shown in red and blue, respectively. Adapted from [170].

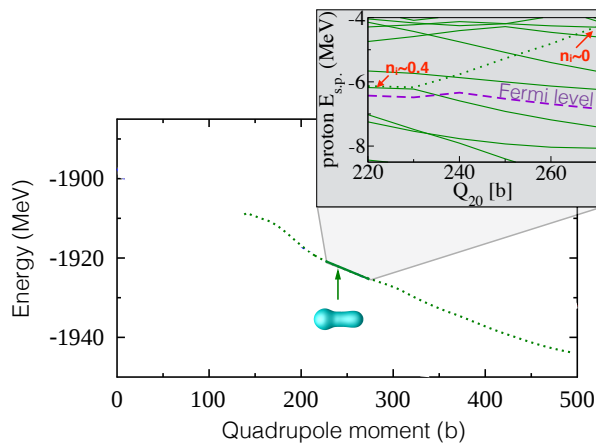


Figure 18: Potential energy in the asymmetric fission valley of ^{258}Fm . The inset shows the single-proton energies for a smaller range of deformations, with the Fermi energy shown by the dashed line and a specific level leaving the Fermi surface shown with a dotted line. Occupation numbers for this level are indicated. Adapted from [171].

direct a comparison with the experimental distributions, i.e., not only the averages. The difficulty is that a large part of the fluctuations is expected to come from the early stage of the fission process, when the barriers are overcome and where the evolution is essentially slow and adiabatic. Nevertheless, Tanimura, Lacroix and Ayik have recently applied their stochastic mean-field method (see section 3.4) to the symmetric fission of ^{258}Fm and they showed that large fluctuations could be expected in the saddle to scission evolution [199].

3.2.5. Applications to quasi-fission

Applications of time-dependent microscopic methods to quasi-fission has also attracted lots of efforts in the past few years [107, 200, 210–218]. Quasi-fission is a mechanism in which two fragments are emitted after capture and before the formation of a fully equilibrated compound nucleus could be achieved [219]. It occurs in reactions with heavy nuclei (typically with a product of the charges $Z_1 Z_2 > 1600$), and it is the main obstacle for the formation of a compound superheavy nucleus. One major difficulty in experimental studies of quasi-fission is that the outgoing fragments share many similarities with fragments formed in fusion-fission (i.e., where an equilibrated compound nucleus has actually been formed), making it difficult to separate both mechanisms.

TDHF calculations have then been used with the FOA to provide theoretical guidance and support in data analysis. TDHF calculations can also be used to predict the energy threshold for fusion which is found to be higher than the static Coulomb barrier [16, 220, 221]. Figure 21 shows a typical shape evolution observed in TDHF calculations of quasi-fission in the $^{40}\text{Ca}+^{238}\text{U}$ system [212]. The contact time between the fragments of ~ 20 zs is typical to quasi-fission. Another characteristic of quasi-fission is the partial mass equilibration also observed in the final fragments ($^{103}\text{Mo}+^{175}\text{Yb}$) in Fig. 21.

An interesting finding of these TDHF studies of quasi-fission is the prediction of the role of shell effects which favour the formation of magic fragments, in particular in the

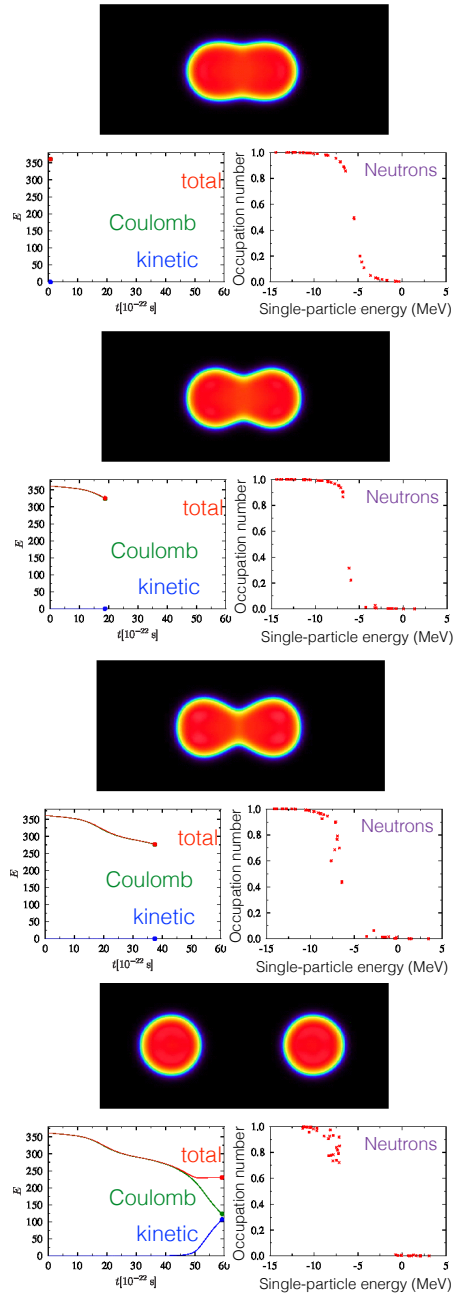


Figure 19: Density, energy repartition, and neutron occupation numbers in ^{258}Fm symmetric fission with TDHF+BCS. Adapted from [171].

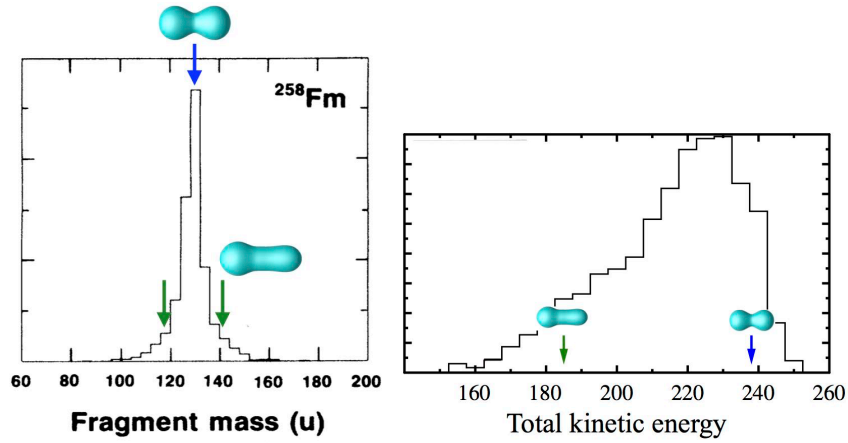


Figure 20: Experimental mass (left) and TKE (right) distributions in ^{258}Fm compared with TDHF+BCS predictions for the symmetric compact and asymmetric modes. Experimental data are from [209]. Adapted from [171].

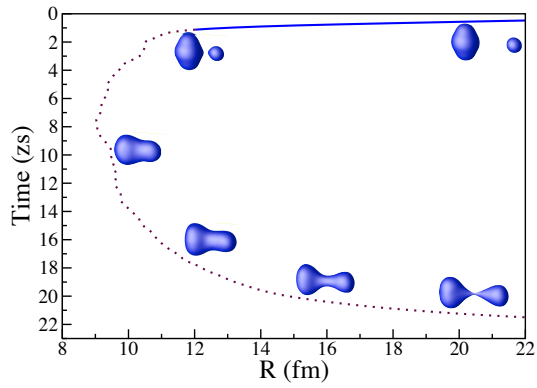


Figure 21: Time evolution of the distance between the centres of mass of the fragments in the $^{40}\text{Ca}+^{238}\text{U}$ central collision at $E_{cm} = 205.2$ MeV [212]. The snapshots show densities at half the saturation density.

$Z = 82$ region in reactions involving an actinide collision partner [212]. This prediction has been later confirmed experimentally by Morjean and collaborators [218]. In addition, the calculations show that these shell effects strongly depend on the orientation of deformed actinide. Another finding is that only collisions with the side of the actinide can eventually lead to fusion.

It would be interesting to apply the full TDHFB formalism to study quasi-fission reactions. Indeed, TDHFB seems to predict long saddle to scission times [185]. The quasi-fission time distributions are relatively well known thanks to extensive experimental measurements of the correlations between the mass and the angle of the fragments [219, 222] and are thus ideal to benchmark microscopic theories.

3.3. Fragment particle number distributions in time-dependent mean-field theories

Predicting the properties of fragments formed in heavy-ion collisions or in fission, such as their mass, charge, angular momentum and kinetic energies, is particularly challenging when one wants to extract distributions for these observables. According to the Balian-Vénéroni variational principle, the TDHF equation is optimized for the prediction of expectation values of one-body observables, while their distributions (which involve quantum fluctuations) are in principle outside the range of application of the TDHF theory. Nevertheless, mean-field approaches based on the TDHF theory have been used to compute multi-nucleon transfer probabilities [11, 27, 108, 109, 187, 216, 223–228] and to investigate particle number distributions in fission fragments [171, 199, 229].

In TDHF calculations, the single-particle states are evolved according to Eq. (34). Depending on the reaction, they can eventually spread in space once the fragments are formed. While the single-particle wave functions are initially localized in a nuclear fragment at the beginning of a reaction, they may partially transfer to the collision partner during the TDHF evolution [36, 223, 230]. This process may result in a variation of the average particle number for each fragment, indicating that nucleon transfer has taken place during the reaction [66].

In quantum mechanics, a system can be found in a coherent superposition of channels associated with different repartitions of particle numbers between its fragments. Formally, such a state is written as

$$|\Psi\rangle = \sum_N C_N |\Psi_N\rangle, \quad (77)$$

where $|\Psi_N\rangle$ are eigenstates of a particle number operator \hat{N} counting the particles in a fragment:

$$\hat{N}|\Psi_N\rangle = N|\Psi_N\rangle. \quad (78)$$

In the case of a nuclear reaction, the final fragments are entangled. For instance, measuring the number of particles in one fragment projects out the state of the other fragment.

Note that, although the eigenvalue N is an integer, $\langle\hat{N}\rangle \equiv \langle\Psi|\hat{N}|\Psi\rangle$ can be a real number, in particular when several coefficients C_N are non-zero. Therefore, “counting” the particles involves the determination of the distribution of probabilities $\mathcal{P}(N) = |C_N|^2$. In particular, a non-integer value of $\langle\hat{N}\rangle = \bar{N} = \sum_N N|C_N|^2$ is a clear signature that the system is in a superposition of different eigenstates of \hat{N} .

3.3.1. Evolution of single-particle states

An example of evolution of single-particle states is given in Fig. 22 for a sub-barrier central collision of two ^{16}O nuclei. The figure shows a set of probability distributions $|\varphi_i(\mathbf{r}, t)|^2$ at various times. Only neutron wave-functions initially located on the left fragment are shown. By symmetry, the same dynamics occurs with the wave functions initially in the right fragment. A partial transfer is observed to the collision partner for each wave-function. As expected, the transfer is more important for the least bound wave-functions (p -states in ^{16}O)

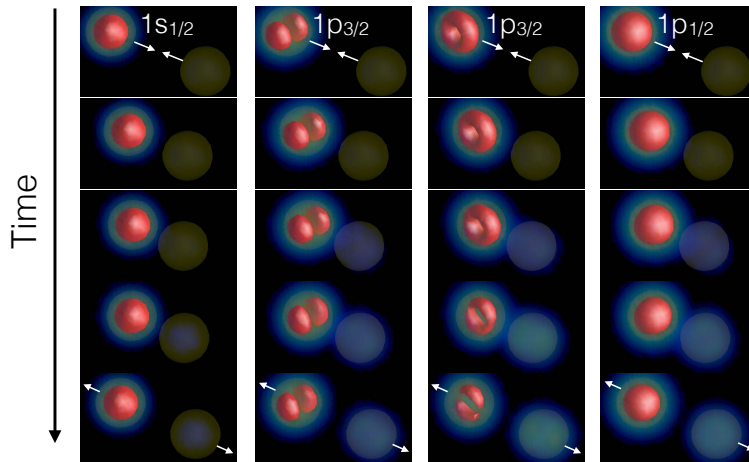


Figure 22: Time-evolution of single-particle probability spatial distributions associated with initial ^{16}O neutron wave-functions in a near-barrier $^{16}\text{O}+^{16}\text{O}$ central collision at $E_{cm} = 10$ MeV.

In a semi-classical transport approach, we could approximate the variance $\sigma_N^2 = \overline{N^2} - \overline{N}^2$ of particle number in the fragments by the total number N_{exc} of exchanged nucleons (in both directions) [231]:

$$\sigma_N^2 \simeq N_{exc}. \quad (79)$$

Applying Eq. (79) to the collision of two ^{16}O shown in Fig. 22, we get $\sigma_N^2 \simeq 0.6$. In fact, this classical result is clearly unphysical as it does not account for the indistinguishability of identical particles. Consider a simple example where a single-particle state $|L\rangle$, initially in the left fragment, is partially transferred to the same state $|R\rangle$ in the right fragment:

$$|L\rangle \rightarrow \alpha|L\rangle + \beta|R\rangle.$$

We can choose the phase such that α is real. If the collision is symmetric, we also have

$$|R\rangle \rightarrow \alpha'|R\rangle + \beta'|L\rangle,$$

with $|\alpha'| = \alpha$ and $|\beta'| = |\beta|$. Orthogonality of the states imposes $\alpha\beta' + \beta^*\alpha' = 0$. Thus, we have up to an irrelevant global phase

$$|R\rangle \rightarrow \alpha|R\rangle - \beta^*|L\rangle.$$

For identical fermions, the state is antisymmetric. Up to a global phase and normalisation, we have

$$|L, R\rangle - |R, L\rangle \rightarrow (\alpha^2 + |\beta|^2) (|L, R\rangle - |R, L\rangle).$$

Thus, the state is unchanged up to a global phase. As a consequence, we have $\sigma_N^2 = 0$ in this example. However, if we apply the semi-classical formula in Eq. (79), we get $\sigma_N^2 \simeq 2|\beta|^2$. Therefore, Eq. (79) is expected to overestimate the fluctuations of particle numbers in the fragments.

We see from the above example that we need a quantum approach in order to estimate the distribution of probability $\mathcal{P}(N)$ to find N nucleons in a fragment.

3.3.2. Variance

Following Ref. [29], we can calculate the variance σ_N^2 in TDHF using anticommutation relations for fermions as well as the property

$$\langle \hat{a}_i^\dagger \hat{a}_j^\dagger \hat{a}_k \hat{a}_l \rangle = n_i n_j (\delta_{il} \delta_{jk} - \delta_{ik} \delta_{jl})$$

for a Slater determinant where i and j denote states in the canonical basis. The variance then reads

$$\sigma_N^2 = \langle \hat{N}_V \rangle - \sum_{i,j=1}^A |\langle \varphi_i | \varphi_j \rangle_V|^2, \quad (80)$$

where

$$\hat{N}_V = \int_V d^3r \hat{a}^\dagger(\mathbf{r}) \hat{a}(\mathbf{r}) \quad (81)$$

counts the number of particles in the volume V and

$$\langle \varphi_i | \varphi_j \rangle_V = \int_V d^3r \varphi_i^*(\mathbf{r}) \varphi_j(\mathbf{r}) \quad (82)$$

is the overlap of the single-particle wave-functions φ_i and φ_j over the volume V . Spin and isospin degrees of freedom are omitted for simplicity. Note that the expectation value of \hat{N}_V can also be written with this notation as

$$\langle \hat{N}_V \rangle = \sum_{i=1}^A \langle \varphi_i | \varphi_i \rangle_V. \quad (83)$$

Applying Eq. (80) to compute the variance of the number of nucleons in the final fragments of the collision shown in Fig. 22, we get σ_N^2 of the order of 10^{-5} , which is orders of magnitude smaller than the classical result obtained from Eq. (79) as the indistinguishability of identical particles has been taken into account. Note that when the numerical value of the variance gets so small, it could easily be affected by an accumulation of numerical errors leading to small changes of the norm of the single-particle wave-functions during the evolution.

3.3.3. Combinatory approach

We can go a step further and calculate the probability $\mathcal{P}(N)$ to find N particles in a volume V and the remaining $A - N$ particles in the complementary volume \bar{V} using a simple combinatory approach [223]:

$$\mathcal{P}(N) = \frac{A!}{N!(A-N)!} \int_V d^3r_1 \cdots d^3r_N \int_{\bar{V}} d^3r_{N+1} \cdots d^3r_A |\Psi(\mathbf{r}_1 \cdots \mathbf{r}_A)|^2. \quad (84)$$

In the TDHF framework, the many-body wave-function is a Slater determinant of occupied single-particle wave-functions at all time. In this case, Eq. (84) leads to [109, 223]

$$\mathcal{P}(N) = \sum_{s(\{\tau_i\}: V^N \bar{V}^{A-N})} \det\{\langle \varphi_i | \varphi_j \rangle_{\tau_i}\}, \quad (85)$$

where $\tau_i = V$ or \bar{V} [see Eq. (82)]. The notation $s(\{\tau_i\}: V^N \bar{V}^{A-N})$ stands for all possible combinations of N volumes V and $A - N$ volumes \bar{V} . Equation (85) becomes rapidly difficult to solve numerically when the number of particles A increases due to the large number of determinants [109].

3.3.4. Particle number projection technique

It is also possible to compute the probability to form a fragment with a given number of nucleons by employing the particle-number projection technique introduced in [108], resulting in a distribution of multi-particle transfer probabilities. The projection method has long been utilized in structure studies to resolve the particle-number symmetry violation [157, 232–236]. To calculate transfer probabilities in heavy-ion collisions one can project the post-collision TDHF wave function, in a spatial volume V containing the fragment, onto N protons or neutrons that represent a certain transfer channel. The projection operator may be written as an integral over the gauge angle θ in the form [161]

$$\hat{P}_V^q(N) = \frac{1}{2\pi} \int_0^{2\pi} d\theta e^{i\theta(\hat{N}_V^q - N)}, \quad (86)$$

where \hat{N}_V^q counts the number of particles in the region V with an isospin q . The probability of finding N particles of isospin q in the region V is [108]

$$\langle \Psi | \hat{P}_V^q(N) | \Psi \rangle = \frac{1}{2\pi} \int_0^{2\pi} d\theta e^{-i\theta N} \langle \Psi | e^{i\theta \hat{N}_V^q} | \Psi \rangle. \quad (87)$$

The expectation value in the integral of Eq. (87) is the determinant of the overlap matrix

$$\langle \Psi | \Psi_V(\theta) \rangle = \det(\mathbf{O}), \quad (88)$$

with the state $|\Psi_V(\theta)\rangle = e^{i\theta \hat{N}_V^q} |\Psi\rangle$ representing a rotation in the gauge-space associated with the particle number degree of freedom. The overlap matrix, \mathbf{O} , is given by

$$(\mathbf{O})_{ij} = \sum_{\sigma} \int d\mathbf{r} \varphi_i^*(\mathbf{r}\sigma q) \varphi_j(\mathbf{r}\sigma q) e^{i\theta \Theta(\mathbf{r})} = \delta_{ij} + \langle i | j \rangle_V (e^{i\theta} - 1). \quad (89)$$

The function $\Theta(\mathbf{r})$ takes the value of 1 in region V and 0 elsewhere. The method allows one to obtain the particle number probability distributions for fragments by performing this procedure for differing values of N in V .

Recently, the projection technique has been employed by Sekizawa and Yabana in the calculation of the expectation values of one-body and two-body operators using the particle-number projected states [237]. This extension allows for an analysis of other reaction observables associated with the target and projectile-like fragments that correspond to specific transfer channels, such as the excitation energy and intrinsic angular momenta of the number-projected states [226]. While the particle-number projection approach is a useful tool for obtaining fragment mass and charge distributions, it often underestimates these in dissipative collisions [11, 29]. This suggests that other beyond mean-field correlations may be important.

3.3.5. Numerical implementation

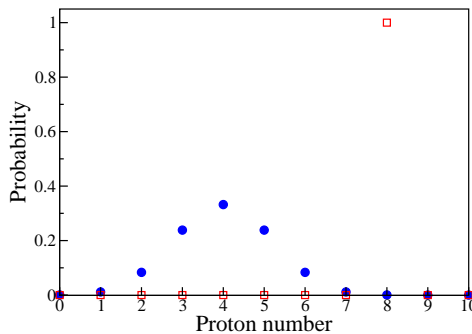


Figure 23: Proton number probability distribution with V containing the entire ^{16}O nucleus (open squares) and only half of it (full circles).

Unlike expression (85), the number of determinants to compute in Eq. (87) only depends on the number of discretised gauge angles θ . Numerical applications using Eqs. (85) and (87) lead to almost identical results [109]. In fact, the application of Eq. (87) is rather straightforward.

The shape and normalisation of the probability distribution $\mathcal{P}(N)$ should be first tested in a simple case. Let us consider the HF ground-state of a single ^{16}O nucleus. Figure 23 shows the proton probability distribution when (i) V contains the entire nucleus (open squares) and (ii) V includes only half of the nucleus (full circles). We verify that both distributions have a norm one. As expected, when V includes the entire nucleus, we find all the 8 protons with a probability one, while, when only half the nucleus is in V , we find an average of 4 protons. Note that both cases give a probability zero (up to numerical noise) to find more than 8 protons.

The distribution which is obtained for half the nucleus is particularly wide, with a variance of ~ 1.4 protons. It would correspond to the distribution of fragments formed in a collision where the nucleus is suddenly cut in half. One would expect such a violent

process to lead to the maximum possible variance. We see from Eq. (80) that the variance is maximum when the overlap (restricted to the volume V) between different single-particle wave-functions is zero, i.e., when $\langle \varphi_i | \varphi_j \rangle_V \propto \delta_{ij}$. Then, the maximum variance can be expressed as a binomial distribution [29]

$$\sigma_N^2 \leq \sum_{i=1}^A \langle \varphi_i | \varphi_i \rangle_V (1 - \langle \varphi_i | \varphi_i \rangle_V). \quad (90)$$

This gives an upper limit for the variance

$$\sigma_N^2 \leq \langle \hat{N}_V \rangle \left(1 - \frac{\langle \hat{N}_V \rangle}{A} \right) \leq A/4. \quad (91)$$

This upper limit is an intrinsic limitation of independent particle systems. Considering a binary partition of an oxygen nucleus, we see that the maximum variance of the proton number is 2, which is larger than, but of the same order of magnitude as the “half-oxygen” example (see Fig. 23).

3.3.6. Multi-nucleon transfer probabilities with TDHF

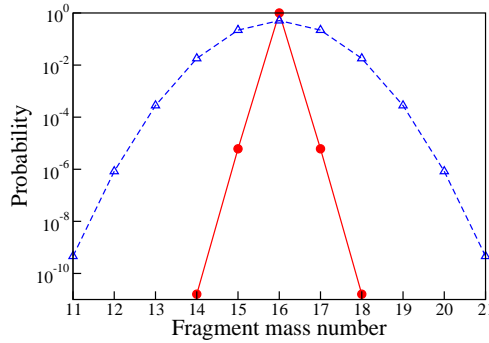


Figure 24: Fragment mass number probability distribution in $^{16}\text{O}+^{16}\text{O}$ central collisions at $E_{cm} = 10$ MeV. The TDHF result with the particle number projection technique is shown with solid line. The dashed line shows the probability distribution obtained from the semi-classical transport approach assuming a Gaussian distribution with $\sigma_N^2 = N_{exc} = 0.6$.

We now consider the application of the particle number projection method to the case of sub-barrier transfer reactions studied with TDHF. Applying the method to the final state of the $^{16}\text{O}+^{16}\text{O}$ central collision shown in Fig. 22, we obtain the distribution of probabilities given in Fig. 24 with a solid line. As expected, this distribution is much narrower than the one obtained from the semi-classical transport approach of Ref. [231] (dashed line). In fact, the transfer probability of one nucleon is smaller than 10^{-5} , which would be at the limit of current experimental detection setups.

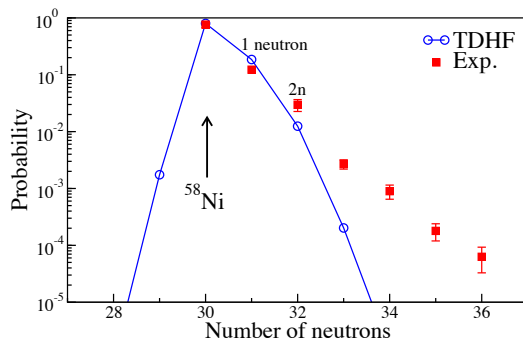


Figure 25: Neutron number distribution of the light fragment in the exit channel of the $^{58}\text{Ni}+^{124}\text{Sn}$ central collision at $E_{cm} = 144.7$ MeV computed with TDHF (circles). The squares show experimental data extracted from Ref. [238] at $E_{cm} = 153$ MeV $\simeq 0.96V_B$ and $\theta_{cm} = 127.5$ deg leading to the same distance of closest approach.

The quantum mechanical effects responsible for the strong hindrance of transfer are expected to be less important in non-symmetric systems. Figure 25 shows an example of experimental near-barrier neutron transfer probabilities (filled squares) in $^{58}\text{Ni}+^{124}\text{Sn}$ [238]. Positive Q -values for neutron stripping in this system allow for observation of up to 6 neutrons transferred from ^{58}Ni to ^{124}Sn . In particular, a relatively large one-neutron transfer probability of ~ 0.1 is observed.

The one-neutron stripping probability is relatively well reproduced by TDHF calculations (open circles). However, these calculations strongly underpredict transfer of more than one neutron. This discrepancy comes from the mean-field approximation. Indeed, it is assumed that all transfer channels evolve in the same average mean-field. This approximation may be reasonable for the transfer of a very small number of particles (with respect to the total number of particles in the collision partners). However, it is doomed to fail to describe reaction channels with very different mass and charge partitions than the average one.

Nevertheless, Sekizawa and Yabana have applied this method with some success to investigate multi-nucleon transfer reactions in various systems such as $^{40,48}\text{Ca}+^{124}\text{Sn}$, $^{40}\text{Ca}+^{208}\text{Pb}$, $^{58}\text{Ni}+^{208}\text{Pb}$ [109] and $^{64}\text{Ni}+^{238}\text{U}$ [216]. In principle, the outgoing fragments are still excited at the end of a TDHF calculation. Therefore, they correspond to primary fragments before statistical decay occurs. In order to compare with experimental data, it is then necessary to couple TDHF calculations with statistical decay calculations [120, 226, 240]. An example performed by Sekizawa is shown in Fig. 26 for the $^{40}\text{Ca}+^{124}\text{Sn}$ reaction [226]. Good agreement with experimental data is obtained except for large numbers of protons transferred due to the limitation of the mean-field approximation discussed above. It is also shown that this microscopic method is more reliable than the semi-classical approximation used in calculations with the GRAZING code.

3.3.7. Transfer reactions at sub-barrier energies

Let us now investigate how the transfer of one nucleon evolves when going down in energy. At sub-barrier energies, the collision partners do not get close enough to form a neck through which nucleons can be transferred. In this case, particle transfer occurs

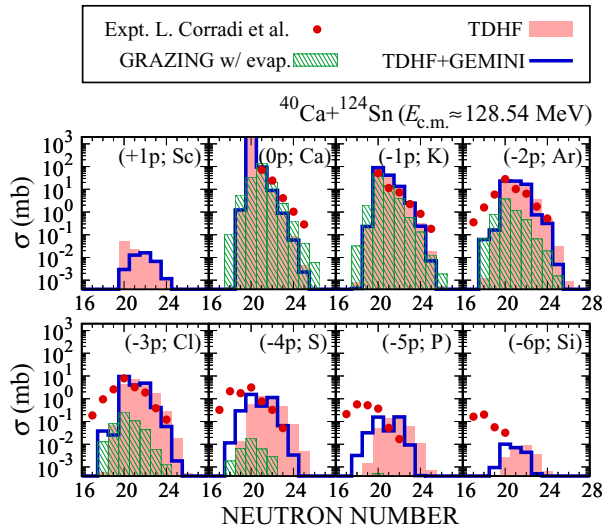


Figure 26: Light fragment production cross sections in the $^{40}\text{Ca}+^{124}\text{Sn}$ reaction at $E_{cm} = 128.54$ MeV as a function of the neutron number and for various elements. Experimental data (circles) are from [239]. TDHF results for primary reaction products are shown with filled areas. Cross sections for secondary reaction products obtained with TDHF+GEMINI are shown by blue solid lines. For comparison, GRAZING results including evaporation are also shown by green shaded histograms. From [226].

only via quantum tunneling. It is therefore dominated by particles near the Fermi surface and it is expected to occur essentially at the distance of closest approach

$$r_{min} \simeq \frac{Z_1 Z_2 e^2}{2E_{cm}} \left(1 + \frac{1}{\sin(\theta_{cm}/2)} \right), \quad (92)$$

where E_{cm} and θ_{cm} are the centre of mass energy and scattering angle, respectively. Due to the exponential decay of wave functions at the surface, the transfer probability of one particle is expected to obey [241, 242]

$$P \sim \exp(-2\kappa r_{min}). \quad (93)$$

Deep sub-barrier transfer has been investigated experimentally, e.g., in the case of one-proton stripping in $^{16}\text{O}+^{208}\text{Pb}$ [112]. The resulting transfer probabilities are reported as a function of r_{min} with filled squares in Fig. 27. We indeed observe an exponential decay of the transfer probability with increasing r_{min} . A fit of the slope parameter for $r_{min} > 13$ fm gives $\kappa \simeq 1.3$ fm $^{-1}$. The same system has been investigated with TDHF calculations [108]. The resulting one-proton transfer probabilities are shown in Fig. 27 with a solid line. Although they overestimate the experimental data, they qualitatively follow the experimental trend. In particular, they confirm the exponential decrease of transfer probabilities expected from Eq. (93). In addition, the value of the slope parameter $\kappa \simeq 1.1$ fm $^{-1}$ is similar to the experimental one.

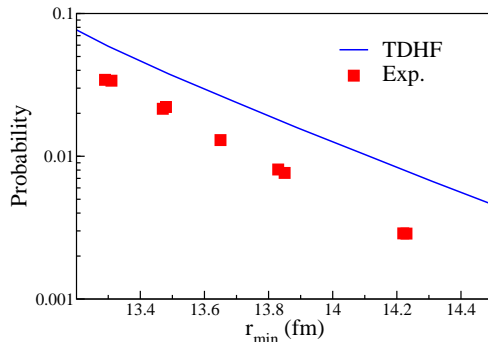


Figure 27: One proton stripping probability in $^{16}\text{O}+^{208}\text{Pb}$ deep sub-barrier central collisions computed with TDHF (solid line) [108]. Filled squares show experimental data from Ref. [112]. The error bars are smaller than the size of the symbols.

3.3.8. Fragment distributions with pairing correlations using the double-projection technique

Two nucleons could be transferred as a correlated Cooper pair in superfluid systems. It is therefore necessary to include pairing correlations at some level in order to investigate transfer in superfluid systems. Pairing correlations are indeed crucial in order to reproduce the transfer of two nucleons which is expected to increase in such systems.

As mentioned earlier, HFB and BCS states do not have a good number of particles. Therefore, the initial fragments of a collision are in a superposition of states with different particle numbers. Applying the particle number projection method to one initial fragment would give a distribution of probabilities even before transfer takes place. This is a spurious effect which prevents the direct use of the particle number projection technique to compute transfer probabilities in superfluid systems.

In models such as TDHFB and TDHF+BCS, where particle-number symmetry is violated, the same particle-number projection technique may be used to restore the symmetry by first projecting the system onto a space with $N_0 = N_V + N_{\bar{V}}$ total particles [27, 177]. Once the initial projection onto N_0 total nucleons has been performed, the above prescription may be followed for the projection of each fragment onto a particle-number N .

Using this idea, Scamps and Lacroix have proposed a double projection technique [27]. Instead of applying Eq. (87) with the BCS state $|\Psi\rangle$, they consider the normalised state with good number of particles N_0 :

$$|N_0\rangle = \frac{\hat{P}'(N_0)|\Psi\rangle}{\sqrt{\langle\Psi|\hat{P}'(N_0)|\Psi\rangle}}, \quad (94)$$

where \hat{P}' is a particle number projector on the entire system, i.e., on the total volume $V + \bar{V}$. Then, they apply the same projection technique as before in order to compute

the particle number distribution in the fragments using

$$\mathcal{P}(N) = \langle N_0 | \hat{P}(N) | N_0 \rangle. \quad (95)$$

The double projection technique has been successfully applied to transfer reactions involving one superfluid nucleus [27]. As a result, the pair transfer is indeed enhanced as compared to calculations without pairing correlations.

3.3.9. Application to superfluid fission fragments

The double projection technique has also been recently applied to investigate fission fragment properties [171]. As discussed in section 3.2.4, the inclusion of dynamics [170, 202] and in particular dynamical pairing correlations [171, 185] is crucial in order to describe fission.

In the TDHF+BCS application to describe the formation and dynamics of fragment produced in ^{258}Fm fission [171], three different valleys [243] were studied: one symmetric valley with compact (quasi-spherical) fragments, one with elongated fragments, and one asymmetric valley. It has been argued that the symmetric compact valley is strongly affected by shell effects due to the $Z = 50$ magic number [209]. This is supported by the quasi-spherical shape of the fragments in this valley.

The TDHF+BCS calculations of Ref. [171] cannot predict what would be the repartition between these valleys. However, the role of shell effects in the particle number distribution can be investigated at the mean-field level thanks to the double projection method. The resulting probability distributions are shown in Fig. 28 for protons and neutrons. We observe that all distributions exhibit similar widths, except for the proton distribution in the symmetric compact mode which is much narrower. This is interpreted as an effect of the spherical magic proton shell in tin isotopes ($Z = 50$). It is interesting to see that the mean-field dynamics, combined with projection techniques, is indeed able to exhibit signatures of magic shells in the fragment properties.

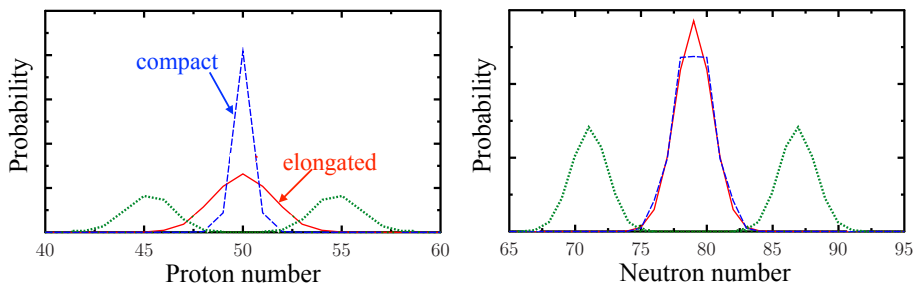


Figure 28: TDHF+BCS prediction of the proton (left) and (neutron) number probability distributions in fission fragments of ^{258}Fm for different fission valleys. Adapted from [171].

3.4. Beyond Mean-Field Methods

One limitation of TDHF lies in the semi-classical nature of the theory. According to the Balian-Vénéroni variational principle [12], only average quantities may in principle be obtained from the study of a reaction with the TDHF theory. In recent years, much effort

has been done to improve the mean-field approximation by incorporating the fluctuation mechanism into the description. At low energies, the one-body fluctuations make the dominant contribution to the fluctuation mechanism of the collective motion. Various extensions have been developed to study the correlation of one-body observables. These include the time-dependent random phase approximation (TDRPA) approach of Balian and Vénéroni [244], the time-dependent generator coordinate method (TDGCM) [206], and the stochastic mean-field (SMF) method [31]. The effects of two-body dissipation on reactions of heavy systems using the time-dependent density-matrix (TDDM) [245, 246] approach have also been recently reported [247–249].

Among the most important observables that are affected by these fluctuations are the widths of nucleon transfer in heavy-ion collisions and fission fragment yields. The mean-field description provides the mean values of the proton and neutron numbers transferred in heavy-ion collisions, sometimes referred to as the drift, as well as the mean-value of the fragment masses and charges in fission reactions.

3.4.1. Time-dependent Random Phase Approximation

In Ref. [12], the Balian-Vénéroni (BV) variational principle is used to show that the TDHF mean-field approach is specially suited for the prediction of one-body observable averages. However, as illustrated in Ref. [29], the limitation of a single-determinant TDHF formalism results in the underestimation of fluctuations and correlations of one-body observables. Indeed, comparisons of TDHF with deep-inelastic collision experiments show that TDHF consistently underestimates experimental mass distributions [223, 250]. The BV approach can be used to better estimate these missing correlations [30].

The general formula for the correlation of two one-body operators, \hat{X} and \hat{Y} , is given by

$$\sigma_{XY} = \sqrt{\langle \hat{X}\hat{Y} \rangle - \langle \hat{X} \rangle \langle \hat{Y} \rangle}, \quad (96)$$

with the same formula providing the fluctuations in the case of $\hat{X} = \hat{Y}$. In TDHF, the expression for the correlation at a final time, t_f , is

$$\sigma_{XY}^2 (TDHF)(t_f) = \text{Tr} \{ Y \rho(t_f) X [I - \rho(t_f)] \}, \quad (97)$$

where I is the identity matrix, X and Y are the matrix representation of the operators \hat{X} and \hat{Y} , and $\rho(t)$ is the one-body density matrix at time t . However, the derivation of the TDHF equation from the Balian-Vénéroni variational principle demonstrates that TDHF is optimized to the expectation values of one-body observables only. Fluctuations of one-body observables involve the expectation value of the square of a one-body operator, for which there is no guarantee that TDHF is predictive. To better recover correlations and fluctuations of one-body operators, the variational space of the observable must be expanded from one-body observables to exponential of one-body operators as detailed in Ref. [30]. In this expanded space, one obtains the following result for the correlation at time t_f (see, e.g., [11] for a detailed derivation)

$$\sigma_{XY}^2(t_f) = \lim_{\epsilon \rightarrow 0} \frac{\text{Tr} \{ [\rho(t_0) - \rho_X(t_0, \epsilon)] [\rho(t_0) - \rho_Y(t_0, \epsilon)] \}}{2\epsilon^2}, \quad (98)$$

where the one-body density matrices $\rho_{X,Y}(t, \epsilon)$ are solutions to the TDHF equation with the boundary condition

$$\rho_{X,Y}(t_f, \epsilon) = e^{i\epsilon X, Y} \rho(t_f) e^{-i\epsilon X, Y}. \quad (99)$$

The result in Eq. (98) considers the fluctuations of the observable about the mean-field evolution at the RPA level [11, 30, 31, 244]. To calculate the correlations, the state at t_f is propagated backwards in time to the initial time t_0 , explaining why the correlations at the time of interest, t_f , depends on the density matrices at the initial time, t_0 .

One useful application of the BV approach is in the investigation of particle number fluctuations for reaction products in deep-inelastic collisions, as in Ref. [11]. In this case, the one-body operator employed in Eq. (98) is the number operator, \hat{N}_V^q

$$\hat{X} = \hat{N}_V^q = \sum_s \int d\mathbf{r} \hat{a}^\dagger(\mathbf{r}sq) \hat{a}(\mathbf{r}sq) \Theta(\mathbf{r}), \quad (100)$$

with $\Theta(\mathbf{r})$ being 1 in the fragment region V and 0 elsewhere. The purpose of this operator is to count all particles with isospin q in the region V . The total number operator is then $\hat{N}_V = \hat{N}_V^{(n)} + \hat{N}_V^{(p)}$. We transform the single-particle states at the final time t_f in accordance with Eq. (99) as follows [251]

$$\psi_i^X(\mathbf{r}\sigma q, t_1; \epsilon) = e^{-i\epsilon \xi_X \Theta_V(\mathbf{r})} \varphi_i(\mathbf{r}\sigma q, t_1), \quad (101)$$

where $\xi_X = 1$ for the total number operator, \hat{N}_V , and $\xi_X = \delta_{qq'}$ for the isospin dependent number operator, $\hat{N}_V^{q'}$. The small parameter ϵ is varied to check convergence [11, 251]. These transformed states are then propagated backwards in time to the initial time t_0 as described above. To obtain the correlations and fluctuations, one must evaluate Eq. (98), which can be reduced to

$$\sigma_{XY}(t_0) = \sqrt{\frac{\eta_{00}(t_0) + \eta_{XY}(t_0) - \eta_{0X}(t_0) - \eta_{0Y}(t_0)}{2\epsilon^2}}, \quad (102)$$

where $\eta_{XX'}$ is

$$\eta_{XX'} = \sum_{ij} \left| \left\langle \psi_i^X | \psi_j^{X'} \right\rangle \right|^2, \quad (103)$$

with the sum over i and j being over occupied states and $X = 0$ and $Y = 0$ denoting the use of untransformed states, φ_i . In practice, the final untransformed states are also propagated backwards in time to reduce numerical inaccuracies introduced by the TDHF evolution, as indicated in Ref. [252].

The BV approach has been used in the past to study mass dispersion from giant resonance decay [253–255] as well as to compute the fluctuation of the particle number in fragments produced in deep-inelastic collisions [11, 229, 251, 252, 255, 256]. This approach was also used to study hot Fermi gas [257], ϕ^4 theory [258], and Boson systems [259–261].

An example of application of the TDRPA to fragment charge distributions in $^{40}\text{Ca}+^{40}\text{Ca}$ deep-inelastic collisions is shown in Fig. 29 [11]. Deep-inelastic collisions are characterised by a strong orbiting of the di-nuclear system, a significant damping of

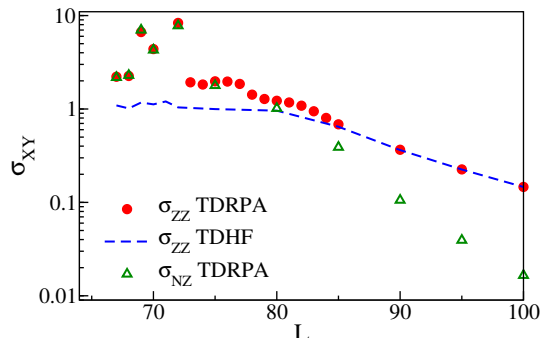


Figure 29: Variance of the fragment charge distribution from TDHF (dashed line) and TDRPA (filled circles) calculations as a function of the angular momentum L in units of \hbar for $^{40}\text{Ca}+^{40}\text{Ca}$ collisions at $E_{cm} = 128$ MeV. Correlations σ_{NZ} between proton and neutron numbers obtained from TDRPA calculations are also shown (open triangles). Adapted from Ref. [11].

the initial relative kinetic energy, and a large width of the fragment mass and charge distributions which are usually underestimated in TDHF. Figure 29 shows the standard deviation of the fragment charge distribution obtained from TDHF (dashed line) and TDRPA (filled circles) as a function of the angular momentum L at $E_{cm} = 128$ MeV (approximately 2.5 times the Coulomb barrier). Both calculations agree at large L , dominated by quasi-elastic scattering. However, TDHF calculations strongly underestimate the fluctuations for more violent collisions at smaller L . The fluctuations predicted by the TDRPA are in better agreement with experimental data of Ref. [262].

Correlations between proton and neutron numbers obtained from TDRPA calculations are also reported in Fig. 29 (open triangles). These correlations are zero in standard TDHF calculations. Although they are negligible for quasi-elastic scattering, they are of similar order as the charge fluctuations for deep-inelastic events. This can be interpreted as an effect of the symmetry energy which favours a transfer of both protons and neutrons in the same direction. This is illustrated in Fig. 30 which shows the expected distribution of fragments in the $N - Z$ plane for various angular momenta assuming Gaussian probability distribution of the form

$$\mathcal{P}(n, z) = \mathcal{P}(0, 0) \exp \left[-\frac{1}{1 - \rho^2} \left(\frac{n^2}{\sigma_N^2} + \frac{z^2}{\sigma_Z^2} - \frac{2\rho n z}{\sigma_N \sigma_Z} \right) \right], \quad (104)$$

where n and z are the number of transferred neutrons and protons, respectively. The correlations between N and Z are quantified by the parameter

$$\rho = \text{sign}(\sigma_{NZ}) \frac{\sigma_{NZ}^2}{\sigma_N \sigma_Z} = \frac{\langle n z \rangle}{\sqrt{\langle n^2 \rangle \langle z^2 \rangle}}. \quad (105)$$

We see that the correlations have a noticeable impact in the $N - Z$ distributions at smaller angular momenta associated with deep-inelastic collisions.

3.4.2. Stochastic Mean Field Approach

As mentioned above the standard TDHF approach provides a deterministic description of a collision process, i.e. the system evolves from a specified initial condition to a

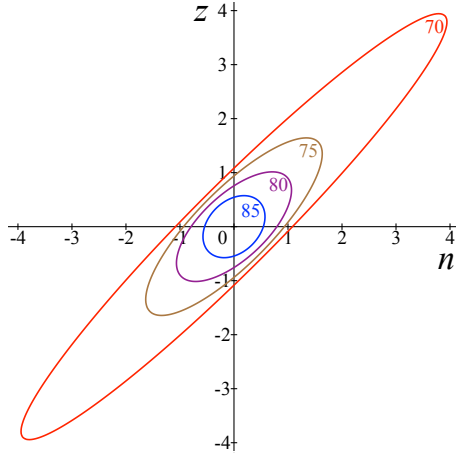


Figure 30: Iso-probabilities $\mathcal{P}(n, z) = \mathcal{P}(0, 0)/2$ for the transfer of n neutrons and z protons in $^{40}\text{Ca}+^{40}\text{Ca}$ at $E_{cm} = 128$ MeV using fluctuations and correlations computed with the TDRPA. The numbers on the curves indicate the angular momentum in units of \hbar .

single final state. In the stochastic mean-field (SMF) approach, the fluctuations in the initial state are incorporated in a stochastic manner by introducing a proper distribution of the initial single-particle density matrices [19, 31]. This results in an ensemble of single-particle density matrices generated by evolving each density in its own mean-field Hamiltonian.

In a single event labeled by λ , the single-particle density matrix is determined by evolving the single-particle wave functions $\phi_j^\lambda(\vec{r}, t)$ according to the self-consistent Hamiltonian in that event. Consequently, in a given event, nucleon density is given by

$$\rho^\lambda(\vec{r}, t) = \sum_{ij} \phi_j^{*\lambda}(\vec{r}, t) \rho_{ji}^\lambda \phi_i^\lambda(\vec{r}, t), \quad (106)$$

where labels (i, j) indicate a complete set of quantum numbers for specifying single-particle wave functions. The mean values of the elements of density matrices are given by $\bar{\rho}_{ji}^\lambda = \delta_{ji} n_j$ and the second moments of fluctuating parts are determined by

$$\overline{\delta\rho_{ji}^\lambda \delta\rho_{i'j'}^\lambda} = \frac{1}{2} \delta_{ii'} \delta_{jj'} [n_i(1 - n_j) + n_j(1 - n_i)], \quad (107)$$

where n_j are the average occupation numbers of the single-particle states. Equation (107) lies at the root of the SMF approach as it can be employed in the study of various reaction phenomena.

By calculating the expectation values of an observable in each event, it is possible to determine probability distributions of observables. In a number of studies [263–270] (see also [19] for a recent review), including studies of mass dispersions in transfer reactions [264, 265, 271], it has been shown that the SMF approach provides a good approximation for the description of quantal fluctuations of the collective motion. In particular, in small amplitude limit, the approach gives rise to the same expression for the dis-

persion of one-body observables familiar from the variational approach of Balian and Vénéroni [244].

Recently, the SMF approach was generalized to include pairing degrees of freedom [272] and subsequently applied to study fission fragment mass and TKE distributions [199]. This study assumed that the fluctuations on the way to scission, at some point after the saddle configuration, arise from fluctuation of states in the vicinity of the Fermi energy. Thus, by considering an ensemble of such states generated by taking ρ_{ji}^λ to be a Gaussian distribution of random numbers, the authors were able to obtain a set of initial conditions, which were then propagated using the TDHF+BCS method mentioned earlier. However, in this case density matrices used in TDHF+BCS equations are no longer diagonal in the canonical basis, due to the fluctuations introduced in Eq. (106) [199]. This requires modification of codes and a higher computational cost. It has been found that the dynamical pairing effects wash out due to the introduction of quantum fluctuations via the initial conditions. In particular, very similar outcomes between the cases of dynamical occupations and the FOA approach were obtained.

In the di-nuclear regime, the SMF approach gives rise to Langevin description for nucleon exchange between projectile-like and target-like nuclei characterized by diffusion and drift coefficients [263]. It is well known that the Langevin description is equivalent to the evolution of the distribution function of the collective variable according to the Fokker-Planck equation. As a result of this equivalence, instead of carrying out stochastic simulations, it is more convenient to calculate the transport coefficients and employ the Fokker-Planck approach. When the drift coefficients are linear functions of mass and charge asymmetry variables, the primary fragment charge and mass distribution $P(N, Z, t)$ is given by Eq. (104). The co-variances σ_{NN} , σ_{ZZ} , and σ_{NZ} are determined by a set of coupled differential equations in which the inputs are provided by the neutron and proton diffusion and drift coefficients.

In the SMF approach these transport coefficients are calculated in terms of the solutions of the TDHF equations. Calculations take into account the full collision geometry and do not involve any fitting parameter other than the standard parameters of the Skyrme interaction. In the earlier investigations, transport coefficients were calculated in the semi-classical approximation in Markovian limit [273, 274]. Recently, it has become possible to calculate these transport coefficients in the quantal framework by including the shell structure and the Pauli blocking in an exact manner [275, 276].

3.5. Nuclear Forces

For all the reaction theories it is desirable to be based on the same footing as the underlying structure theory. The TDHF theory employs the same energy density functional (EDF) developed by the nuclear structure community with no additional parameters. The determination of the parameters of these EDFs contains no reaction information. Almost all TDHF calculations done to date have used the Skyrme energy density functional [62], although recent TDHFB calculations with the Gogny force have been performed [183, 187].

The Skyrme EDF was developed as a zero-range low-momentum expansion of the effective two-body nucleon-nucleon interaction by Skyrme [62, 277]. In recent years, the quality of effective interactions has been substantially improved [81, 278–280]. The Skyrme EDF contains terms which depend on the nuclear density, ρ , kinetic-energy density, τ , vector current density, \mathbf{j} , pseudovector spin density, \mathbf{s} , pseudovector spin

kinetic density, \mathbf{T} , pseudotensor spin-current density, \mathbf{J} , and pseudovector tensor kinetic-density, \mathbf{F} ,

$$\begin{aligned}
E = & \int d^3r \sum_{t=0,1} \left\{ C_t^\rho [\rho_0] \rho_t^2 + C_t^s [\rho_0] \mathbf{s}_t^2 + C_t^{\Delta\rho} \rho_t \nabla^2 \rho_t \right. \\
& + C_t^{\nabla s} (\nabla \cdot \mathbf{s})^2 + C_t^{\Delta s} \mathbf{s}_t \cdot \nabla^2 \mathbf{s}_t + C_t^\tau (\rho_t \tau_t - \mathbf{j}_t^2) \\
& + C_t^T \left(\mathbf{s}_t \cdot \mathbf{T}_t - \sum_{\mu,\nu=x}^z J_{t,\mu\nu} J_{t,\mu\nu} \right) \\
& + C_t^F \left[\mathbf{s}_t \cdot \mathbf{F}_t - \frac{1}{2} \left(\sum_{\mu=x}^z J_{t,\mu\mu} \right)^2 - \frac{1}{2} \sum_{\mu,\nu=x}^z J_{t,\mu\nu} J_{t,\nu\mu} \right] \\
& \left. + C_t^{\nabla \cdot J} (\rho_t \nabla \cdot \mathbf{J}_t + \mathbf{s}_t \cdot \nabla \times \mathbf{j}_t) \right\}, \tag{108}
\end{aligned}$$

where the detailed definitions of densities and currents can be found in Refs. [281–283].

The time-odd densities (\mathbf{j} , \mathbf{s} , \mathbf{T} , \mathbf{F}) vanish for static calculations of even-even nuclei, while they are present for odd mass nuclei, in cranking calculations, as well as in TDHF. The spin-current pseudotensor, \mathbf{J} , is time-even and does not vanish for static calculations of even-even nuclei. It has been shown [77, 284–290] that the presence of these extra time-odd terms are necessary for preserving the Galilean invariance and make an appreciable contribution to the dissipative properties of the collision. Although this one-body dissipation plays an important role in the collisions, it is however not sufficient to lead to a fully equilibrated compound nucleus. This lack of equilibration mechanism has been illustrated by Loebl and collaborators using the Wigner distribution function [291, 292].

The TDHF calculations performed within the last decade have generally incorporated the complete Skyrme interaction with the exception of the tensor part. A comprehensive discussion of the history of the Skyrme tensor force is given in Ref. [282]. Recently, the tensor force was independently incorporated in TDHF calculations by two groups [77, 293] into the Sky3D TDHF code [35]. The effect of the tensor force on vibration has been studied [77, 294] and shown to affect low-energy fusion [295]. In addition, investigation of the high energy limit to fusion in the $^{16}\text{O} + ^{16}\text{O}$ collision found an effect on the fusion threshold energy of the order of several MeV [296]. This suggests that the tensor force can play a non-negligible role in dynamic processes in nuclei. It is also suggested that the tensor force plays a more important role in heavier nuclei [297]. However, there seems to be relatively significant variations among the Skyrme parametrizations including the tensor force [293], which suggests that further studies will be needed before the large scale use of these terms.

3.6. Boundary Conditions

Generally, the numerical solutions of TDHF equation are performed in a box with periodic or static boundary conditions. In few cases, such as 0^+ pairing vibration [25] and giant monopole resonance (GMR) [72, 74, 298–300] studies in spherical nuclei, the system exhibits a spherical symmetry at all time and the TDHF equation can be solved

in one dimension (the radial coordinate), allowing for very large boxes without spurious reflection of the wave functions at the boundaries. In Ref. [300], large spherical grids were then used to perform spectral analyses (via spatial Fourier transforms) of the nucleon wave-functions emitted from unbound GMR direct decay. However, most of TDHF applications (e.g., to heavy-ion collisions), involve Cartesian grids with sizes which are limited by the available computational power.

In TDHF calculations of nuclear reactions, the single-particle states undergo rapid changes which may lead to the development of low-density tails reaching the box boundaries. For hard boundary conditions, this may lead to spurious effects such as a non-conservation of the momentum. For periodic boundary conditions the reflecting single-particle states may cause further damping of the collective motion. Such dependence on the boundary conditions can of course be tested by changing the size of the numerical box. This is not a serious problem in most cases except at higher energies, where the emission of low-density material from the nuclei can interfere with the dynamics in the neighboring box and cause problems in the conservation of energy and angular momentum [301].

Various numerical solutions to this issue have been proposed, including a multigrid approach [302] to extend the boundaries, and methods to remove the emitted particles via radiating or exact boundary conditions [303–306]. However, these methods remain numerically very costly for fully three-dimensional calculations. On the other hand the approach of using absorbing boundary conditions (ABC) [34] offers a feasible alternative, as well as applying a mask function during the TDHF evolution [299].

Recently, the twist-averaged boundary conditions (TABC) have been employed to remove the spurious finite-volume effects for periodic boundary conditions [146, 307]. Periodic boundary conditions (PBC) reflect the boundary condition at one edge of the numerical box to the other edge. However, the Floquet-Bloch theorem states that a wave function in a periodic potential is periodic up to a complex phase shift (twist) between adjacent numerical cells. Bloch boundary conditions do the same but when reflecting also apply a phase correction, which can be averaged to correct for the phase. The TABC Bloch boundary condition for single-particle states is

$$\phi_{\lambda\theta}(\mathbf{r} + \mathbf{L}_i) = e^{i\theta_i} \phi_{\lambda\theta}(\mathbf{r}) , \quad (109)$$

where \mathbf{L}_i are the box lattice vectors ($i = x, y, z$) and $\phi_{\lambda\theta}(\mathbf{r})$ are the solution of HF single-particle equations subject to the above boundary condition

$$\hat{h}_\theta \phi_{\lambda\theta}(\mathbf{r}) = \epsilon_{\lambda\theta} \phi_{\lambda\theta}(\mathbf{r}) . \quad (110)$$

This boundary condition can be implemented by multiplying the original PBC state with a phase, $\phi_{\lambda\theta}(\mathbf{r}) = e^{-i\theta_i x_i/L} \phi_\lambda(\mathbf{r})$. With this substitution, density still remains periodic but the first and second derivatives must be computed with the above form in constructing currents *etc.* In TABC, observables are computed by averaging over different Bloch phases [307]:

$$\langle \hat{O} \rangle = \int \frac{\mathbf{d}\theta}{\pi^3} \langle \Phi_\theta | \hat{O} | \Phi_\theta \rangle , \quad (111)$$

where Φ_θ is the corresponding HF many-body wavefunction. The angles θ_i change between zero (PBC) and π (anti-PBC), as the time-reversal symmetry is assumed. The

integral can be done with Gauss-Legendre quadrature as it was done for the application of calculating nuclear pasta phases found in the structure of the neutron star crust [307].

The treatment of boundary conditions can also be utilized in the study of widths of collective excitations using the time-dependent linear response approach [17]. The total width of giant resonances is comprised of the spreading width, escape width, and the width coming from the Landau damping. The Landau damping is due to the coupling of the collective states incoherently with $1p1h$ excitations, while the escape width is due to continuum excitations or particle emission. The spreading width is due to higher order correlations and requires beyond mean-field methods, such as the TDDM approach [246, 308]. Applications of ABC [34], masking [299], and TABC [146] have all shown that they can effectively reduce the effects of the finite volume discretization in calculating the escape width when using TDHF codes to perform time-dependent linear response calculations.

4. Conclusions and perspectives

Quantum microscopic approaches to time-dependent many-body problems have been discussed within the framework of nuclear dynamics. The time-dependent Hartree-Fock theory, which is obtained via different approaches (variational or based on perturbation schemes), has become the tool of choice to investigate low-energy heavy-ion collisions and fission dynamics. The increase of computational power, the better performance of modern algorithms, as well as the improvement in the nuclear energy density functional (now including spin-orbit and sometimes tensor terms) have made TDHF codes a great tool to help analyze experimental data and guide future experimental programs, e.g., with exotic beams.

Fusion near the barrier is ideal to investigate the interplay between structure and reaction mechanisms. In particular, TDHF calculations, which incorporate all sorts of vibrational modes as well as transfer channels (at the mean-field level), are used to study how these coherent couplings, which are built up during the approach of two nuclei, impact fusion. Microscopic approaches like TDHF are not competitors to coupled-channels models, but instead bring complementary information on the mechanisms at play. It is then natural to attempt to merge both approaches, a program which has been initiated only recently.

By construction, microscopic approaches incorporate the dynamics of single-particles. This allowed studies of nucleon transfer in heavy-ion collisions and the development of new tools such as the particle number projection technique to compute transfer probabilities. The range of applications has been recently extended to include multi-nucleon transfer and quasi-fission reactions. In particular, the ability of mean-field dynamics to capture the influence of magic shell effects in the formation of quasi-fission fragments has been a surprise.

Some extensions of TDHF to incorporate part of the residual interaction have reached the level of realistic applications. For instance, the inclusion of pairing correlations allows to study the dynamics of superfluid systems. The latter is crucial in fission and enabled a series of recent breakthroughs in the description of the saddle to scission evolution in fissioning nuclei including non-adiabatic effects. A major outcome of these studies has been the ability to predict the total kinetic energy of the fission fragments without relying on any prescription for the definition of the scission point. Of course, there are still open problems. For instance, the treatment of the relative phase between colliding superfluid nuclei, which has been shown to impact the reaction outcome, may require beyond mean-field techniques.

Nowadays, various beyond mean-field approaches are also used to incorporate quantum fluctuations and to study their effect on the distributions of fragments formed in nuclear processes. This is done at the TDRPA level, or with a stochastic mean-field method which, in the limit of small fluctuations, leads to the TDRPA. Inclusion of these fluctuations is important for the description of the fragment properties in deep-inelastic collisions as well as in fission.

Some major problems remain. The main challenge is probably to find a way to treat quantum tunneling with a fully microscopic approach. Indeed, the current method to describe sub-barrier fusion using a potential extracted microscopically from mean-field approaches is only a temporary solution. The ultimate goal is to describe the fusion of heavy-nuclei via tunneling without invoking a nucleus-nucleus potential at all. Currently,

this is only possible at above barrier energies. The problem relies on the fact that more than one mean-fields are necessary to describe the transmitted and reflected fluxes simultaneously. A possible solution is to use the time-dependent generator coordinate method (TDGCM) where the collective wave-function is developed on TDHF mean-field trajectories. However, how to fix the collective coordinate? Using the path integral approach with complex time and invoking the stationary phase approximation might offer an alternative solution. Nevertheless many technical problems remain to be solved before one can hope to achieve realistic applications to fusion with this approach.

Another challenge is to develop an approach which accounts for each reaction channel properly, for instance in multi-nucleon transfer reactions. The difficulty with current mean-field approaches is that, despite the fact that the total state is a coherent superposition of different transfer channels, all these channels are assumed to evolve with the same mean-field. This might be a reasonable approximation for the transfer of few nucleons. However, this approach is doomed to fail for the description of transfer channels leading to fragments which are very different than the average ones. Here, a TDGCM description with a difference of chemical potentials between the fragments as collective coordinate might be a solution [309]. Another difficulty in describing transfer channels is to include the effect of clustering. The recent technique developed in [136] to identify the presence of clusters in the wave-function may help for this purpose.

Finally, we are still far from a consistent microscopic and non-adiabatic treatment of fission from the compound system to the post-scission configuration. The progress discussed in this review concern the later stage of fission, namely the evolution from saddle to scission. Time-dependent approaches are currently unable to describe the entire evolution from the compound nucleus. No need to say that, for spontaneous fission, the problem of tunneling in complex system is also present. A standard technique to describe fission is based on the TDGCM, where a collective wave-function is evolved on an adiabatic potential energy surface. A possible improvement will be to couple this approach with TDHF trajectories for the latter stage in order to account for the dynamical effects near scission.

Acknowledgments

The authors thank S. Ayik, M. Dasgupta, K. Godbey, L. Guo, K. Hagino, D.J. Hinde, D. Lacroix, J. Maruhn, T. Nakatsukasa, W. Nazarewicz, V.E. Oberacker, G. Scamps, B. Schuetrumpf, K. Sekizawa, E.C. Simpson, P.D. Stevenson, K. Vo-Phuoc, and E. Williams for useful discussions. N. Dubray, S. Ebata, T. Nakatsukasa, B. Schuetrumpf, K. Sekizawa, K. Vo-Phuoc, P.W. Wein, and S. Yan are also thanked for authorising the use of their figures. This work has been supported by the Australian Research Council Grants No. FT120100760 and DP160101254, and by the U.S. Department of Energy under grant No. [de-sc0013847](#) with Vanderbilt University. Part of this research was undertaken with the assistance of resources from the National Computational Infrastructure (NCI), which is supported by the Australian Government.

Appendix: Feynman rules

The Feynman rules for the n -th order contribution to the single-particle Green's function $G(x, y)$ in quantum many-body perturbation theory depends on the choice of the interaction. For an interaction of the form $\mathcal{V}(x, y) = V(\mathbf{x}, \mathbf{y})\delta(t_x - t_y)$, and omitting spin, these rules are (see, e.g., [21]):

1. Draw all topologically distinct connected diagrams with n interaction (wavy) lines and $2n + 1$ non-interacting propagators $G^0(x, y)$, running from y to x . Each vertex connects one interaction line with two propagators.
2. Label each vertex with a 4-dimensional space-time point $z = (\mathbf{z}, t_z)$.
3. Each wavy line represents an interaction $\mathcal{V}(x, y) = V(\mathbf{x}, \mathbf{y})\delta(t_x - t_y)$ with extremity at x and y .
4. Integrate all internal variables over space and time.
5. Each closed fermion loop gives a minus sign.
6. Assign a global factor $(i/\hbar)^n$ to each n -th order diagram
7. Green's functions with equal time variables must be interpreted as $G(\mathbf{x}t, \mathbf{x}t^+)$

References

- [1] J. Bardeen, L. N. Cooper, J. R. Schrieffer, Theory of Superconductivity, *Phys. Rev.* 108 (1957) 1175. doi:10.1103/PhysRev.108.1175.
- [2] M. Dasgupta, D. J. Hinde, N. Rowley, A. M. Stefanini, Measuring Barriers to Fusion, *Annu. Rev. Nucl. Part. Sci.* 48 (1998) 401–461. doi:10.1146/annurev.nucl.48.1.401.
- [3] K. Hagino, N. Takigawa, Subbarrier Fusion Reactions and Many-Particle Quantum Tunneling, *Prog. Theor. Phys.* 128 (2012) 1001–1060. doi:10.1143/PTP.128.1061.
- [4] W. H. Zurek, Decoherence and the Transition from Quantum to Classical, *Phys. Today* 44 (1991) 36. doi:10.1063/1.881293.
- [5] E. Joos, H. D. Zeh, C. Kiefer, D. Giulini, J. Kupsch, I. Stamatescu, Decoherence and the appearance of a classical world in quantum theory, Springer, Berlin, 2003, second Ed.
- [6] A. Bohr, B. Mottelson, Nuclear Structure, Vol. 2, W.A. Benjamin, Inc., 1975.
- [7] A. O. Caldeira, A. J. Leggett, Influence of Dissipation on Quantum Tunneling in Macroscopic Systems, *Phys. Rev. Lett.* 46 (1981) 211–214. doi:10.1103/PhysRevLett.46.211.
- [8] M. Lamehi-Rachti, W. Mittig, Quantum mechanics and hidden variables: A test of Bell’s inequality by the measurement of the spin correlation in low-energy proton–proton scattering, *Phys. Rev. D* 14 (1976) 2543–2555. doi:10.1103/PhysRevD.14.2543.
- [9] P. A. M. Dirac, Note on Exchange Phenomena in the Thomas Atom, *Math. Proc. Camb. Phil. Soc.* 26 (1930) 376. doi:10.1017/S0305004100016108.
- [10] P. Bonche, S. Koonin, J. W. Negele, One-dimensional nuclear dynamics in time-dependent Hartree-Fock approximation, *Phys. Rev. C* 13 (1976) 1226–1258. doi:10.1103/PhysRevC.13.1226.
- [11] C. Simenel, Particle-Number Fluctuations and Correlations in Transfer Reactions Obtained Using the Balian-Vénéroni Variational Principle, *Phys. Rev. Lett.* 106 (2011) 112502. doi:10.1103/PhysRevLett.106.112502.
- [12] R. Balian, M. Vénéroni, Time-Dependent Variational Principle for Predicting the Expectation Value of an Observable, *Phys. Rev. Lett.* 47 (1981) 1353. doi:10.1103/PhysRevLett.47.1353.
- [13] Y. Iwata, T. Otsuka, J. A. Maruhn, N. Itagaki, Suppression of Charge Equilibration Leading to the Synthesis of Exotic Nuclei, *Phys. Rev. Lett.* 104 (2010) 252501. doi:10.1103/PhysRevLett.104.252501.
- [14] J. R. Stone, P. Danielewicz, Y. Iwata, Proton and neutron density distributions at supranormal density in low- and medium-energy heavy-ion collisions, *Phys. Rev. C* 96 (2017) 014612. doi:10.1103/PhysRevC.96.014612.
- [15] J. W. Negele, The mean-field theory of nuclear-structure and dynamics, *Rev. Mod. Phys.* 54 (1982) 913–1015. doi:10.1103/RevModPhys.54.913.
- [16] C. Simenel, Nuclear quantum many-body dynamics, *Eur. Phys. J. A* 48 (2012) 152. doi:10.1140/epja/i2012-12152-0.
- [17] T. Nakatsukasa, K. Matsuyanagi, M. Matsuo, K. Yabana, Time-dependent density-functional description of nuclear dynamics, *Rev. Mod. Phys.* 88 (2016) 045004. doi:10.1103/RevModPhys.88.045004.
- [18] D. J. Thouless, Stability conditions and nuclear rotations in the Hartree-Fock theory, *Nucl. Phys.* 21 (1960) 225–232. doi:10.1016/0029-5582(60)90048-1.
- [19] D. Lacroix, S. Ayik, Stochastic quantum dynamics beyond mean field, *Eur. Phys. J. A* 50 (2014) 95. doi:10.1140/epja/i2014-14095-8.
- [20] J. P. Blaizot, G. Ripka, A variational principle for the calculation of transition amplitudes, *Phys. Lett. B* 105 (1981) 1. doi:10.1016/0370-2693(81)90026-5.
- [21] A. L. Fetter, J. D. Walecka, *Quantum Theory of Many-particle Systems*, Dover Books on Physics, Dover Publications, 2003.
URL <https://books.google.com.au/books?id=0wekf1s83b0C>
- [22] N. N. Bogoliubov, Kinetic Equations, *J. Phys. (USSR)* 10 (1946) 256.
- [23] H. Born, H. S. Green, A General Kinetic Theory of Liquids, *Proc. Roy. Soc. A* 188 (1946) 10. doi:10.1098/rspa.1946.0093.
- [24] J. G. Kirkwood, The Statistical Mechanical Theory of Transport Processes I. General Theory, *J. Chem. Phys.* 14 (1946) 180. doi:10.1063/1.1724117.
- [25] B. Avez, C. Simenel, P. Chomaz, Pairing vibrations study with the time-dependent Hartree-Fock-Bogoliubov theory, *Phys. Rev. C* 78 (2008) 044318. doi:10.1103/PhysRevC.78.044318.
- [26] S. Ebata, T. Nakatsukasa, T. Inakura, K. Yoshida, Y. Hashimoto, K. Yabana, Canonical-basis time-dependent Hartree-Fock-Bogoliubov theory and linear-response calculations, *Phys. Rev. C* 82 (2010) 034306. doi:10.1103/PhysRevC.82.034306.

- [27] G. Scamps, D. Lacroix, Effect of pairing on one- and two-nucleon transfer below the Coulomb barrier: A time-dependent microscopic description, *Phys. Rev. C* 87 (2013) 014605. doi:10.1103/PhysRevC.87.014605.
- [28] I. Stetcu, A. Bulgac, P. Magierski, K. J. Roche, Isovector giant dipole resonance from the 3D time-dependent density functional theory for superfluid nuclei, *Phys. Rev. C* 84 (2011) 051309. doi:10.1103/PhysRevC.84.051309.
- [29] C. H. Dasso, T. Dossing, H. C. Pauli, On the mass distribution in Time-Dependent Hartree-Fock calculations of heavy-ion collisions, *Z. Phys. A* 289 (1979) 395–398. doi:10.1007/BF01409391.
- [30] R. Balian, M. Vénéroni, Fluctuations in a time-dependent mean-field approach, *Phys. Lett. B* 136 (1984) 301–306. doi:10.1016/0370-2693(84)92008-2.
- [31] S. Ayik, A stochastic mean-field approach for nuclear dynamics, *Phys. Lett. B* 658 (2008) 174. doi:10.1016/j.physletb.2007.09.072.
- [32] K.-H. Kim, T. Otsuka, P. Bonche, Three-dimensional TDHF calculations for reactions of unstable nuclei, *J. Phys. G* 23 (1997) 1267. doi:10.1088/0954-3899/23/10/014.
- [33] A. S. Umar, V. E. Oberacker, Time-dependent response calculations of nuclear resonances, *Phys. Rev. C* 71 (2005) 034314. doi:10.1103/PhysRevC.71.034314.
- [34] T. Nakatsukasa, K. Yabana, Linear response theory in the continuum for deformed nuclei: Green's function vs time-dependent Hartree-Fock with the absorbing boundary condition, *Phys. Rev. C* 71 (2005) 024301. doi:10.1103/PhysRevC.71.024301.
- [35] J. A. Maruhn, P.-G. Reinhard, P. D. Stevenson, A. S. Umar, The TDHF Code Sky3D, *Comput. Phys. Commun.* 185 (2014) 2195–2216. doi:10.1016/j.cpc.2014.04.008.
- [36] A. S. Umar, V. E. Oberacker, J. A. Maruhn, Neutron transfer dynamics and doorway to fusion in time-dependent Hartree-Fock theory, *Eur. Phys. J. A* 37 (2008) 245–250. doi:10.1140/epja/i2008-10614-6.
- [37] R. P. Feynman, Space-Time Approach to Non-Relativistic Quantum Mechanics, *Rev. Mod. Phys.* 20 (1948) 367–387. doi:10.1103/RevModPhys.20.367.
- [38] S. Levit, Time-dependent mean-field approximation for nuclear dynamical problems, *Phys. Rev. C* 21 (1980) 1594–1602. doi:10.1103/PhysRevC.21.1594.
- [39] S. Levit, J. W. Negele, Z. Paltiel, Time-dependent mean-field theory and quantized bound states, *Phys. Rev. C* 21 (1980) 1603–1625. doi:10.1103/PhysRevC.21.1603.
- [40] R. Bass, Fusion of heavy nuclei in a classical model, *Nucl. Phys. A* 231 (1974) 45–63. doi:10.1016/0375-9474(74)90292-9.
- [41] R. Bass, *Nuclear Reactions with Heavy Ions*, Springer-Verlag, New York, 1980.
- [42] J. Błocki, J. Randrup, W. J. Swiatecki, C. F. Tsang, Proximity forces, *Ann. Phys.* 105 (1977) 427. doi:10.1016/0003-4916(77)90249-4.
- [43] J. Randrup, J. S. Vaagen, On the proximity treatment of the interaction between deformed nuclei, *Phys. Lett. B* 77 (1978) 170–173. doi:10.1016/0370-2693(78)90613-5.
- [44] M. Seiwert, W. Greiner, V. Oberacker, M. J. Rhoades-Brown, Test of the proximity theorem for deformed nuclei, *Phys. Rev. C* 29 (1984) 477–485. doi:10.1103/PhysRevC.29.477.
- [45] J. R. Birkelund, J. R. Huizenga, Fusion Reactions Between Heavy Nuclei, *Annu. Rev. Nucl. Part. Sci.* 33 (1983) 265–322. doi:10.1146/annurev.ns.33.120183.001405.
- [46] G. R. Satchler, W. G. Love, Folding model potentials from realistic interactions for heavy-ion scattering, *Phys. Rep.* 55 (1979) 183–254. doi:10.1016/0370-1573(79)90081-4.
- [47] G. Bertsch, J. Borysowicz, H. McManus, W. G. Love, Interactions for inelastic-scattering derived from realistic potentials, *Nucl. Phys. A* 284 (1977) 399–419. doi:10.1016/0375-9474(77)90392-X.
- [48] N. Takigawa, G. F. Bertsch, Semiclassical theory of quantum tunneling in multidimensional systems, *Phys. Rev. C* 29 (1984) 2358–2361. doi:10.1103/PhysRevC.29.2358.
- [49] A. B. Balantekin, N. Takigawa, Quantum tunneling in nuclear fusion, *Rev. Mod. Phys.* 70 (1998) 77–100. doi:10.1103/RevModPhys.70.77.
- [50] S. Landowne, S. C. Pieper, Coupled-channels fusion calculations for $^{58}\text{Ni}+^{58}\text{Ni}$, *Phys. Rev. C* 29 (1984) 1352–1357. doi:10.1103/PhysRevC.29.1352.
- [51] K. Hagino, N. Rowley, A. Kruppa, A program for coupled-channel calculations with all order couplings for heavy-ion fusion reactions, *Comput. Phys. Commun.* 123 (1999) 143–152. doi:10.1016/s0010-4655(99)00243-x.
- [52] H. Esbensen, Challenges in Coupled-Channels Calculations of Heavy-Ion Fusion Reactions, *Prog. Theor. Phys. Suppl.* 154 (2004) 11–20. doi:10.1143/PTPS.154.11.
- [53] A. V. Karpov, V. A. Rachkov, V. V. Samarin, Quantum coupled-channels model of nuclear fusion with a semiclassical consideration of neutron rearrangement, *Phys. Rev. C* 92 (2015) 064603. doi:10.1103/PhysRevC.92.064603.

- [54] L. R. Gasques, L. C. Chamon, D. Pereira, M. A. G. Alvarez, E. S. Rossi, C. P. Silva, B. V. Carlson, Global and consistent analysis of the heavy-ion elastic scattering and fusion processes, *Phys. Rev. C* 69 (2004) 034603. doi:10.1103/PhysRevC.69.034603.
- [55] L. C. Chamon, B. V. Carlson, L. R. Gasques, D. Pereira, C. De Conti, M. A. G. Alvarez, M. S. Hussein, M. A. C. Ribeiro, E. S. Rossi, C. P. Silva, Toward a global description of the nucleus-nucleus interaction, *Phys. Rev. C* 66 (2002) 014610. doi:10.1103/PhysRevC.66.014610.
- [56] T. Ichikawa, K. Matsuyanagi, Universal damping mechanism of quantum vibrations in deep sub-barrier fusion reactions, *Phys. Rev. C* 92 (2015) 021602. doi:10.1103/physrevc.92.021602.
- [57] Ş. Mişicu, H. Esbensen, Hindrance of Heavy-Ion Fusion due to Nuclear Incompressibility, *Phys. Rev. Lett.* 96 (2006) 112701. doi:10.1103/PhysRevLett.96.112701.
- [58] T. Ichikawa, K. Hagino, A. Iwamoto, Existence of a one-body barrier revealed in deep subbarrier fusion, *Phys. Rev. C* 75 (2007) 057603. doi:10.1103/physrevc.75.057603.
- [59] C. F. von Weizsäcker, Zur Theorie der Kernmassen, *Z. Phys. A* 96 (1935) 431–458. doi:10.1007/BF01337700.
- [60] H. A. Bethe, R. F. Bacher, Nuclear Physics A. Stationary States of Nuclei, *Rev. Mod. Phys.* 8 (1936) 82–229. doi:10.1103/RevModPhys.8.82.
- [61] K. A. Brueckner, J. R. Buchler, M. M. Kelly, New Theoretical Approach to Nuclear Heavy-Ion Scattering, *Phys. Rev.* 173 (1968) 944–949. doi:10.1103/physrev.173.944.
- [62] T. H. R. Skyrme, CVII. The nuclear surface, *Phil. Mag.* 1 (1956) 1043–1054. doi:10.1080/14786435608238186.
- [63] P.-G. Reinhard, A. S. Umar, P. D. Stevenson, J. Piekarewicz, V. E. Oberacker, J. A. Maruhn, Sensitivity of the fusion cross section to the density dependence of the symmetry energy, *Phys. Rev. C* 93 (2016) 044618. doi:10.1103/PhysRevC.93.044618.
- [64] V. Y. Denisov, W. Nörenberg, Entrance channel potentials in the synthesis of the heaviest nuclei, *Eur. Phys. J. A* 15 (2002) 375–388. doi:10.1140/epja/i2002-10039-3.
- [65] K. Washiyama, D. Lacroix, Energy dependence of the nucleus-nucleus potential close to the Coulomb barrier, *Phys. Rev. C* 78 (2008) 024610. doi:10.1103/PhysRevC.78.024610.
- [66] C. Simenel, B. Avez, Time-dependent Hartree-Fock description of heavy ions fusion, *Intl. J. Mod. Phys. E* 17 (2008) 31–40. doi:10.1142/S0218301308009525.
- [67] K. Vo-Phuoc, C. Simenel, E. C. Simpson, Dynamical effects in fusion with exotic nuclei, *Phys. Rev. C* 94 (2016) 024612. doi:10.1103/physrevc.94.024612.
- [68] O. Akyüz, A. Winther, Nuclear surface-surface interaction in the folding model, in: R. A. Broglia, R. A. Ricci (Eds.), *Nuclear Structure and Heavy-Ion Physics*, Proc. Int. School of Physics "Enrico Fermi", Varenna, North Holland, Amsterdam, 1982, p. 492.
- [69] C. Simenel, M. Dasgupta, D. J. Hinde, E. Williams, Microscopic approach to coupled-channels effects on fusion, *Phys. Rev. C* 88 (2013) 064604. doi:10.1103/PhysRevC.88.064604.
- [70] D. Bourgin, C. Simenel, S. Courtin, F. Haas, Microscopic study of $^{40}\text{Ca} + ^{58,64}\text{Ni}$ fusion reactions, *Phys. Rev. C* 93 (2016) 034604. doi:10.1103/PhysRevC.93.034604.
- [71] C. Simenel, P. Chomaz, Nonlinear vibrations in nuclei, *Phys. Rev. C* 68 (2003) 024302. doi:10.1103/PhysRevC.68.024302.
- [72] P. D. Stevenson, M. R. Strayer, J. R. Stone, W. G. Newton, Giant resonances from TDHF, *Intl. J. Mod. Phys. E* 13 (2004) 181–185. doi:10.1142/S0218301304001928.
- [73] J. A. Maruhn, P. G. Reinhard, P. D. Stevenson, J. Rikowska Stone, M. R. Strayer, Dipole giant resonances in deformed heavy nuclei, *Phys. Rev. C* 71 (2005) 064328. doi:10.1103/PhysRevC.71.064328.
- [74] P. D. Stevenson, D. Almeded, P.-G. Reinhard, J. A. Maruhn, Monopole giant resonances and TDHF boundary conditions, *Nucl. Phys. A* 788 (2007) 343C–348C. doi:10.1016/j.nuclphysa.2007.01.091.
- [75] C. Simenel, P. Chomaz, Couplings between dipole and quadrupole vibrations in tin isotopes, *Phys. Rev. C* 80 (2009) 064309. doi:10.1103/PhysRevC.80.064309.
- [76] P. D. Stevenson, S. Fracasso, Extracting structure information from TDHF, *J. Phys. G* 37 (2010) 064030. doi:10.1088/0954-3899/37/6/064030.
- [77] S. Fracasso, E. B. Suckling, P. D. Stevenson, Unrestricted Skyrme-tensor time-dependent Hartree-Fock model and its application to the nuclear response from spherical to triaxial nuclei, *Phys. Rev. C* 86 (2012) 044303. doi:10.1103/PhysRevC.86.044303.
- [78] G. Scamps, D. Lacroix, Systematics of isovector and isoscalar giant quadrupole resonances in normal and superfluid spherical nuclei, *Phys. Rev. C* 88 (2013) 044310. doi:10.1103/PhysRevC.88.044310.
- [79] C. Simenel, R. Keser, A. S. Umar, V. E. Oberacker, Microscopic study of $^{16}\text{O} + ^{16}\text{O}$ fusion, *Phys.*

- Rev. C 88 (2013) 024617. doi:10.1103/PhysRevC.88.024617.
- [80] G. Scamps, D. Lacroix, Systematic study of isovector and isoscalar giant quadrupole resonances in normal and superfluid deformed nuclei, Phys. Rev. C 89 (2014) 034314. doi:10.1103/PhysRevC.89.034314.
- [81] E. Chabanat, P. Bonche, P. Haensel, J. Meyer, R. Schaeffer, A Skyrme parametrization from subnuclear to neutron star densities Part II. Nuclei far from stabilities, Nucl. Phys. A 635 (1998) 231–256. doi:10.1016/S0375-9474(98)00180-8.
- [82] T. Kibédi, R. H. Spear, Reduced electric-octupole transition probabilities, $B(E3; 0_1^+ \rightarrow 3_1^-)$ —AN UPDATE, At. Data Nucl. Data Tables 80 (2002) 35. doi:10.1006/adnd.2001.0871.
- [83] P.-G. Reinhard, Lu Guo, J. Maruhn, Nuclear giant resonances and linear response, Eur. Phys. J. A 32 (2007) 19–23. doi:10.1140/epja/i2007-10366-9.
- [84] M. Fallot, P. Chomaz, M. V. Andrés, F. Catara, E. G. Lanza, J. A. Scarpaci, Anharmonic vibrations in nuclei, Nucl. Phys. A 729 (2003) 699. doi:10.1016/j.nuclphysa.2003.10.001.
- [85] K. Hagino, J. M. Yao, Semimicroscopic modeling of heavy-ion fusion reactions with multireference covariant density functional theory, Phys. Rev. C 91 (2015) 064606. doi:10.1103/PhysRevC.91.064606.
- [86] J. M. Yao, K. Hagino, Anharmonicity of multi-octupole-phonon excitations in ^{208}Pb : Analysis with multireference covariant density functional theory and subbarrier fusion of $^{16}\text{O} + ^{208}\text{Pb}$, Phys. Rev. C 94 (2016) 011303. doi:10.1103/PhysRevC.94.011303.
- [87] T. Fließbach, The reduced width amplitude in the reaction theory for composite particles, Z. Phys. A 272 (1975) 39–46. doi:10.1007/bf01408426.
- [88] T. Fließbach, The optical potential for the elastic heavy ion scattering, Z. Phys. 247 (1971) 117–126. doi:10.1007/bf01395288.
- [89] D. M. Brink, F. Stancu, Interaction potential between two ^{16}O nuclei derived from the Skyrme interaction, Nucl. Phys. A 243 (1975) 175–188. doi:10.1016/0375-9474(75)90027-5.
- [90] P. G. Zint, U. Mosel, Kinetic energy contributions to heavy ion potentials, Phys. Lett. B 56 (1975) 424–426. doi:10.1016/0370-2693(75)90402-5.
- [91] F. Beck, K.-H. Müller, H. S. Köhler, Momentum Dependence of the Ion-Ion Potential in a Microscopic Theory, Phys. Rev. Lett. 40 (1978) 837–840. doi:10.1103/physrevlett.40.837.
- [92] B. Sinha, S. A. Moszkowski, The nucleus-nucleus interaction potential using density-dependent delta interaction, Phys. Lett. B 81 (1979) 289–294. doi:10.1016/0370-2693(79)90337-X.
- [93] C. H. Dasso, G. Pollaro, Investigating the nucleus-nucleus potential at very short distances, Phys. Rev. C 68 (2003) 054604. doi:10.1103/physrevc.68.054604.
- [94] A. S. Umar, V. E. Oberacker, C. J. Horowitz, Microscopic sub-barrier fusion calculations for the neutron star crust, Phys. Rev. C 85 (2012) 055801. doi:10.1103/PhysRevC.85.055801.
- [95] R. Y. Cusson, P.-G. Reinhard, M. R. Strayer, J. A. Maruhn, W. Greiner, Density as a constraint and the separation of internal excitation energy in TDHF, Z. Phys. A 320 (1985) 475–482. doi:10.1007/BF01415725.
- [96] A. S. Umar, M. R. Strayer, R. Y. Cusson, P.-G. Reinhard, D. A. Bromley, Time-dependent Hartree-Fock calculations of $^4\text{He} + ^{14}\text{C}$, $^{12}\text{C} + ^{12}\text{C}(0^+)$, and $^4\text{He} + ^{20}\text{Ne}$ molecular formations, Phys. Rev. C 32 (1985) 172–183. doi:10.1103/PhysRevC.32.172.
- [97] C. Simenel, A. S. Umar, K. Godbey, M. Dasgupta, D. J. Hinde, How the Pauli exclusion principle affects fusion of atomic nuclei, Phys. Rev. C 95 (2017) 031601. doi:10.1103/physrevc.95.031601.
- [98] T. Ichikawa, K. Hagino, A. Iwamoto, Signature of Smooth Transition from Sudden to Adiabatic States in Heavy-Ion Fusion Reactions at Deep Sub-Barrier Energies, Phys. Rev. Lett. 103 (2009) 202701. doi:10.1103/PhysRevLett.103.202701.
- [99] C. Simenel, P. Chomaz, G. de France, Quantum Calculations of Coulomb Reorientation for Sub-Barrier Fusion, Phys. Rev. Lett. 93 (2004) 102701. doi:10.1103/PhysRevLett.93.102701.
- [100] A. S. Umar, V. E. Oberacker, Dynamical deformation effects in subbarrier fusion of $^{64}\text{Ni} + ^{132}\text{Sn}$, Phys. Rev. C 74 (2006) 061601. doi:10.1103/PhysRevC.74.061601.
- [101] A. S. Umar, V. E. Oberacker, Time dependent Hartree-Fock fusion calculations for spherical, deformed systems, Phys. Rev. C 74 (2006) 024606. doi:10.1103/PhysRevC.74.024606.
- [102] A. S. Umar, V. E. Oberacker, $^{64}\text{Ni} + ^{132}\text{Sn}$ fusion within the density-constrained time-dependent Hartree-Fock formalism, Phys. Rev. C 76 (2007) 014614. doi:10.1103/PhysRevC.76.014614.
- [103] A. S. Umar, V. E. Oberacker, Heavy-ion interaction potential deduced from density-constrained time-dependent Hartree-Fock calculation, Phys. Rev. C 74 (2006) 021601. doi:10.1103/PhysRevC.74.021601.
- [104] V. E. Oberacker, A. S. Umar, Microscopic analysis of sub-barrier fusion enhancement in $^{132}\text{Sn} + ^{40}\text{Ca}$ versus $^{132}\text{Sn} + ^{48}\text{Ca}$, Phys. Rev. C 87 (2013) 034611. doi:10.1103/PhysRevC.87.034611.

- [105] X. Jiang, J. A. Maruhn, S. Yan, Microscopic study of noncentral effects in heavy-ion fusion reactions with spherical nuclei, *Phys. Rev. C* 90 (2014) 064618. doi:10.1103/PhysRevC.90.064618.
- [106] A. S. Umar, C. Simenel, V. E. Oberacker, Energy dependence of potential barriers and its effect on fusion cross sections, *Phys. Rev. C* 89 (2014) 034611. doi:10.1103/PhysRevC.89.034611.
- [107] A. S. Umar, V. E. Oberacker, C. Simenel, Shape evolution and collective dynamics of quasifission in the time-dependent Hartree-Fock approach, *Phys. Rev. C* 92 (2015) 024621. doi:10.1103/PhysRevC.92.024621.
- [108] C. Simenel, Particle Transfer Reactions with the Time-Dependent Hartree-Fock Theory Using a Particle Number Projection Technique, *Phys. Rev. Lett.* 105 (2010) 192701. doi:10.1103/PhysRevLett.105.192701.
- [109] K. Sekizawa, K. Yabana, Time-dependent Hartree-Fock calculations for multinucleon transfer processes in $^{40,48}\text{Ca}+^{124}\text{Sn}$, $^{40}\text{Ca}+^{208}\text{Pb}$, and $^{58}\text{Ni}+^{208}\text{Pb}$ reactions, *Phys. Rev. C* 88 (2013) 014614. doi:10.1103/PhysRevC.88.014614.
- [110] J. Dobaczewski, J. Dudek, Time-odd components in the mean field of rotating superdeformed nuclei, *Phys. Rev. C* 52 (1995) 1827–1839. doi:10.1103/PhysRevC.52.1827.
- [111] K. Godbey, A. S. Umar, C. Simenel, Dependence of fusion on isospin dynamics, *Phys. Rev. C* 95 (2017) 011601(R). doi:10.1103/PhysRevC.95.011601.
- [112] M. Evers, M. Dasgupta, D. J. Hinde, D. H. Luong, R. Rafiei, R. du Rietz, C. Simenel, Cluster transfer in the reaction $^{16}\text{O}+^{208}\text{Pb}$ at energies well below the fusion barrier: A possible doorway to energy dissipation, *Phys. Rev. C* 84 (2011) 054614. doi:10.1103/PhysRevC.84.054614.
- [113] D. C. Rafferty, M. Dasgupta, D. J. Hinde, C. Simenel, E. C. Simpson, E. Williams, I. P. Carter, K. J. Cook, D. H. Luong, S. D. McNeil, K. Ramachandran, K. Vo-Phuoc, A. Wakhle, Multinucleon transfer in $^{16,18}\text{O}$, $^{19}\text{F}+^{208}\text{Pb}$ reactions at energies near the fusion barrier, *Phys. Rev. C* 94 (2016) 024607. doi:10.1103/physrevc.94.024607.
- [114] B. B. Back, H. Esbensen, C. L. Jiang, K. E. Rehm, Recent developments in heavy-ion fusion reactions, *Rev. Mod. Phys.* 86 (2014) 317–360. doi:10.1103/RevModPhys.86.317.
- [115] J. F. Liang, J. M. Allmond, C. J. Gross, P. E. Mueller, D. Shapira, R. L. Varner, M. Dasgupta, D. J. Hinde, C. Simenel, E. Williams, K. Vo-Phuoc, M. L. Brown, I. P. Carter, M. Evers, D. H. Luong, T. Ebadi, A. Wakhle, Examining the role of transfer coupling in sub-barrier fusion of $^{46,50}\text{Ti}+^{124}\text{Sn}$, *Phys. Rev. C* 94 (2016) 024616. doi:10.1103/physrevc.94.024616.
- [116] C. Simenel, P. Chomaz, G. de France, Quantum Calculation of the Dipole Excitation in Fusion Reactions, *Phys. Rev. Lett.* 86 (2001) 2971–2974. doi:10.1103/PhysRevLett.86.2971.
- [117] C. Simenel, P. Chomaz, G. de France, Fusion process studied with a preequilibrium giant dipole resonance in time-dependent Hartree-Fock theory, *Phys. Rev. C* 76 (2007) 024609. doi:10.1103/PhysRevC.76.024609.
- [118] V. E. Oberacker, A. S. Umar, J. A. Maruhn, P.-G. Reinhard, Dynamic microscopic study of pre-equilibrium giant resonance excitation and fusion in the reactions $^{132}\text{Sn} + ^{48}\text{Ca}$ and $^{124}\text{Sn} + ^{40}\text{Ca}$, *Phys. Rev. C* 85 (2012) 034609. doi:10.1103/PhysRevC.85.034609.
- [119] C. Simenel, D. J. Hinde, R. du Rietz, M. Dasgupta, M. Evers, C. J. Lin, D. H. Luong, A. Wakhle, Influence of entrance-channel magicity and isospin on quasi-fission, *Phys. Lett. B* 710 (2012) 607–611. doi:10.1016/j.physletb.2012.03.063.
- [120] A. S. Umar, C. Simenel, W. Ye, Transport properties of isospin asymmetric nuclear matter using the time-dependent Hartree-Fock method, *Phys. Rev. C* 96 (2017) 024625. doi:10.1103/PhysRevC.96.024625.
- [121] C. L. Jiang, K. E. Rehm, B. B. Back, H. Esbensen, R. V. F. Janssens, A. M. Stefanini, G. Montagnoli, Influence of heavy-ion transfer on fusion reactions, *Phys. Rev. C* 89 (2014) 051603(R). doi:10.1103/physrevc.89.051603.
- [122] J. J. Kolata, A. Roberts, A. M. Howard, D. Shapira, J. F. Liang, C. J. Gross, R. L. Varner, Z. Kohley, A. N. Villano, H. Amro, W. Loveland, E. Chavez, Fusion of $^{124,132}\text{Sn}$ with $^{40,48}\text{Ca}$, *Phys. Rev. C* 85 (2012) 054603. doi:10.1103/PhysRevC.85.054603.
- [123] A. S. Umar, V. E. Oberacker, $^{64}\text{Ni}+^{64}\text{Ni}$ fusion reaction calculated with the density-constrained time-dependent Hartree-Fock formalism, *Phys. Rev. C* 77 (2008) 064605. doi:10.1103/PhysRevC.77.064605.
- [124] A. S. Umar, V. E. Oberacker, Density-constrained time-dependent Hartree-Fock calculation of $^{16}\text{O}+^{208}\text{Pb}$ fusion cross-sections, *Eur. Phys. J. A* 39 (2009) 243–247. doi:10.1140/epja/i2008-10712-5.
- [125] K. Goeke, F. Grümmer, P.-G. Reinhard, Three-dimensional nuclear dynamics in the quantized ATDHF approach, *Ann. Phys.* 150 (1983) 504–551. doi:10.1016/0003-4916(83)90025-8.
- [126] G. H. Rawitscher, Approximate Independence of Optical-Model Elastic Scattering Calculations on

- the Potential at Small Distances, Phys. Rev. 135 (1964) B605–B612. doi:10.1103/PhysRev.135.B605.
- [127] J. Thomas, Y. T. Chen, S. Hinds, D. Meredith, M. Olson, Sub-barrier fusion of the oxygen isotopes: A more complete picture, Phys. Rev. C 33 (1986) 1679–1689. doi:10.1103/PhysRevC.33.1679.
- [128] I. Tserruya, Y. Eisen, D. Pelte, A. Gavron, H. Oeschler, D. Berndt, H. L. Harney, Total fusion cross section for the $^{16}\text{O}+^{16}\text{O}$ system, Phys. Rev. C 18 (1978) 1688–1699. doi:10.1103/PhysRevC.18.1688.
- [129] B. Fernandez, C. Gaarde, J. S. Larsen, S. Pontoppidan, F. Videbaek, Fusion cross sections for the $^{16}\text{O} + ^{16}\text{O}$ reaction, Nucl. Phys. A 306 (1978) 259–284. doi:10.1016/0375-9474(78)90327-5.
- [130] S.-C. Wu, C. A. Barnes, Fusion and elastic scattering cross sections for the $^{16}\text{O} + ^{16}\text{O}$ reactions near the Coulomb barrier, Nucl. Phys. A 422 (1984) 373–396. doi:10.1016/0375-9474(84)90523-2.
- [131] J. J. Kolata, R. M. Freeman, F. Haas, B. Heusch, A. Gallmann, Gross and intermediate-width structure in the interaction of ^{16}O with ^{16}O , Phys. Rev. C 19 (1979) 2237–2245. doi:10.1103/PhysRevC.19.2237.
- [132] C. R. Morton, A. C. Berriman, M. Dasgupta, D. J. Hinde, J. O. Newton, K. Hagino, I. J. Thompson, Coupled-channels analysis of the $^{16}\text{O}+^{208}\text{Pb}$ fusion barrier distribution, Phys. Rev. C 60 (1999) 044608. doi:10.1103/PhysRevC.60.044608.
- [133] G. Montagnoli, A. M. Stefanini, C. L. Jiang, H. Esbensen, L. Corradi, S. Courtin, E. Fioretto, A. Goasduff, F. Haas, A. F. Kifle, C. Michelagnoli, D. Montanari, T. Mijatović, K. E. Rehm, R. Silvestri, P. P. Singh, F. Scarlassara, S. Szilner, X. D. Tang, C. A. Ur, Fusion of $^{40}\text{Ca} + ^{40}\text{Ca}$ and other Ca + Ca systems near and below the barrier, Phys. Rev. C 85 (2012) 024607. doi:10.1103/PhysRevC.85.024607.
- [134] H. A. Aljuwair, R. J. Ledoux, M. Beckerman, S. B. Gazes, J. Wiggins, E. R. Cosman, R. R. Betts, S. Saini, O. Hansen, Isotopic effects in the fusion of ^{40}Ca with $^{40,44,48}\text{Ca}$, Phys. Rev. C 30 (1984) 1223–1227. doi:10.1103/PhysRevC.30.1223.
- [135] X. Jiang, J. A. Maruhn, S. W. Yan, Configuration transition effect in heavy-ion fusion reactions with deformed nuclei, EPL 112 (2015) 12001. doi:10.1209/0295-5075/112/12001.
- [136] B. Schuetrumpf, W. Nazarewicz, Cluster formation in precompound nuclei in the time-dependent framework, Phys. Rev. C 96 (2017) 064608. doi:10.1103/PhysRevC.96.064608.
- [137] L. R. Gasques, A. V. Afanasjev, M. Beard, J. Lubian, T. Neff, M. Wiescher, D. G. Yakovlev, São Paulo potential as a tool for calculating S factors of fusion reactions in dense stellar matter, Phys. Rev. C 76 (2007) 045802. doi:10.1103/PhysRevC.76.045802.
- [138] M. J. Rudolph, Z. Q. Gosser, K. Brown, S. Hudan, R. T. de Souza, A. Chbihi, B. Jacquot, M. Famiano, J. F. Liang, D. Shapira, D. Mercier, Near- and sub-barrier fusion of ^{20}O incident ions with ^{12}C target nuclei, Phys. Rev. C 85 (2012) 024605. doi:10.1103/PhysRevC.85.024605.
- [139] R. T. deSouza, S. Hudan, V. E. Oberacker, A. S. Umar, Confronting measured near- and sub-barrier fusion cross sections for $^{20}\text{O}+^{12}\text{C}$ with a microscopic method, Phys. Rev. C 88 (2013) 014602. doi:10.1103/PhysRevC.88.014602.
- [140] V. Singh, J. Vadas, T. K. Steinbach, B. B. Wiggins, S. Hudan, R. T. deSouza, Zidu Lin, C. J. Horowitz, L. T. Baby, S. A. Kuvin, Vandana Tripathi, I. Wiedenhöver, A. S. Umar, Fusion enhancement at near and sub-barrier energies in $^{19}\text{O}+^{12}\text{C}$, Phys. Lett. B 765 (2017) 99–103. doi:10.1016/j.physletb.2016.12.017.
- [141] T. K. Steinbach, J. Vadas, J. Schmidt, C. Haycraft, S. Hudan, R. T. deSouza, L. T. Baby, S. A. Kuvin, I. Wiedenhöver, A. S. Umar, V. E. Oberacker, Sub-barrier enhancement of fusion as compared to a microscopic method in $^{18}\text{O} + ^{12}\text{C}$, Phys. Rev. C 90 (2014) 041603. doi:10.1103/PhysRevC.90.041603.
- [142] A. Astier, P. Petkov, M.-G. Porquet, D. S. Delion, P. Schuck, Novel Manifestation of α -Clustering Structures: New $\alpha + ^{208}\text{Pb}$ States in ^{212}Po Revealed by Their Enhanced $E1$ Decays, Phys. Rev. Lett. 104 (2010) 042701. doi:10.1103/PhysRevLett.104.042701.
- [143] A. S. Umar, J. A. Maruhn, N. Itagaki, V. E. Oberacker, Microscopic Study of the Triple- α Reaction, Phys. Rev. Lett. 104 (2010) 212503. doi:10.1103/PhysRevLett.104.212503.
- [144] Y. Iwata, K. Iida, N. Itagaki, Synthesis of thin, long heavy nuclei in ternary collisions, Phys. Rev. C 87 (2013) 014609. doi:10.1103/PhysRevC.87.014609.
- [145] Y. Iwata, T. Ichikawa, N. Itagaki, J. A. Maruhn, T. Otsuka, Examination of the stability of a rod-shaped structure in ^{24}Mg , Phys. Rev. C 92 (2015) 011303. doi:10.1103/PhysRevC.92.011303.
- [146] B. Schuetrumpf, W. Nazarewicz, P.-G. Reinhard, Time-dependent density functional theory with twist-averaged boundary conditions, Phys. Rev. C 93 (2016) 054304. doi:10.1103/PhysRevC.93.054304.

- [147] D. M. Brink, F. Stancu, Time-dependent Hartree-Fock and the one-body dissipation for head-on collisions, *Phys. Rev. C* 24 (1981) 144–147. doi:[10.1103/physrevc.24.144](https://doi.org/10.1103/physrevc.24.144).
- [148] K. Washiyama, D. Lacroix, S. Ayik, One-body energy dissipation in fusion reactions from mean-field theory, *Phys. Rev. C* 79 (2009) 024609. doi:[10.1103/PhysRevC.79.024609](https://doi.org/10.1103/PhysRevC.79.024609).
- [149] K. Wen, F. Sakata, Z.-X. Li, X.-Z. Wu, Y.-X. Zhang, S.-G. Zhou, Non-Gaussian Fluctuations and Non-Markovian Effects in the Nuclear Fusion Process: Langevin Dynamics Emerging from Quantum Molecular Dynamics Simulations, *Phys. Rev. Lett.* 111 (2013) 012501. doi:[10.1103/PhysRevLett.111.012501](https://doi.org/10.1103/PhysRevLett.111.012501).
- [150] A. S. Umar, V. E. Oberacker, J. A. Maruhn, P.-G. Reinhard, Microscopic calculation of precompound excitation energies for heavy-ion collisions, *Phys. Rev. C* 80 (2009) 041601. doi:[10.1103/PhysRevC.80.041601](https://doi.org/10.1103/PhysRevC.80.041601).
- [151] A. S. Umar, V. E. Oberacker, J. A. Maruhn, P.-G. Reinhard, Entrance channel dynamics of hot and cold fusion reactions leading to superheavy elements, *Phys. Rev. C* 81 (2010) 064607. doi:[10.1103/PhysRevC.81.064607](https://doi.org/10.1103/PhysRevC.81.064607).
- [152] J. Skalski, Adiabatic fusion barriers from self-consistent calculations, *Phys. Rev. C* 76 (2007) 044603. doi:[10.1103/PhysRevC.76.044603](https://doi.org/10.1103/PhysRevC.76.044603).
- [153] N. Schunck, L. M. Robledo, Microscopic theory of nuclear fission: a review, *Rep. Prog. Phys.* 79 (2016) 116301. doi:[10.1088/0034-4885/79/11/116301](https://doi.org/10.1088/0034-4885/79/11/116301).
- [154] M. Matsuo, T. Nakatsukasa, K. Matsuyanagi, Adiabatic Selfconsistent Collective Coordinate Method for Large Amplitude Collective Motion in Nuclei with Pairing Correlations, *Prog. Theor. Phys.* 103 (2000) 959–979. doi:[10.1143/ptp.103.959](https://doi.org/10.1143/ptp.103.959).
- [155] K. Wen, T. Nakatsukasa, Self-consistent collective coordinate for reaction path and inertial mass, *Phys. Rev. C* 94 (2016) 054618. doi:[10.1103/PhysRevC.94.054618](https://doi.org/10.1103/PhysRevC.94.054618).
- [156] K. Wen, T. Nakatsukasa, Adiabatic self-consistent collective path in nuclear fusion reactions, *Phys. Rev. C* 96 (2017) 014610. doi:[10.1103/PhysRevC.96.014610](https://doi.org/10.1103/PhysRevC.96.014610).
- [157] P. Ring, P. Schuck, *The Nuclear Many-Body Problem*, Springer-Verlag, New York, 1980. doi:[10.1007/978-3-642-61852-9](https://doi.org/10.1007/978-3-642-61852-9).
- [158] J. Dobaczewski, W. Nazarewicz, T. R. Werner, J. F. Berger, C. R. Chinn, J. Decharge, Mean-field description of ground-state properties of drip-line nuclei: Pairing and continuum effects, *Phys. Rev. C* 53 (1996) 2809–2840. doi:[10.1103/PhysRevC.53.2809](https://doi.org/10.1103/PhysRevC.53.2809).
- [159] J. Terasaki, P.-H. Heenen, H. Flocard, P. Bonche, 3D solution of Hartree-Fock-Bogoliubov equations for drip-line nuclei, *Nucl. Phys. A* 600 (1996) 371–386. doi:[10.1016/0375-9474\(96\)00036-X](https://doi.org/10.1016/0375-9474(96)00036-X).
- [160] M. V. Stoitsov, J. Dobaczewski, P. Ring, S. Pittel, Quadrupole deformations of neutron-drip-line nuclei studied within the Skyrme Hartree-Fock-Bogoliubov approach, *Phys. Rev. C* 61 (2000) 034311. doi:[10.1103/PhysRevC.61.034311](https://doi.org/10.1103/PhysRevC.61.034311).
- [161] M. Bender, P.-H. Heenen, P.-G. Reinhard, Self-consistent mean-field models for nuclear structure, *Rev. Mod. Phys.* 75 (2003) 121–180. doi:[10.1103/RevModPhys.75.121](https://doi.org/10.1103/RevModPhys.75.121).
- [162] M. V. Stoitsov, J. Dobaczewski, W. Nazarewicz, S. Pittel, D. J. Dean, Systematic study of deformed nuclei at the drip lines and beyond, *Phys. Rev. C* 68 (2003) 054312. doi:[10.1103/PhysRevC.68.054312](https://doi.org/10.1103/PhysRevC.68.054312).
- [163] D. Vretenar, A. Afanasjev, G. Lalazissis, P. Ring, Relativistic Hartree–Bogoliubov theory: static and dynamic aspects of exotic nuclear structure, *Phys. Rep.* 409 (2005) 101–259. doi:[10.1016/j.physrep.2004.10.001](https://doi.org/10.1016/j.physrep.2004.10.001).
- [164] A. Blazkiewicz, V. E. Oberacker, A. S. Umar, M. Stoitsov, Coordinate space Hartree-Fock-Bogoliubov calculations for the zirconium isotope chain up to the two-neutron drip line, *Phys. Rev. C* 71 (2005) 054321. doi:[10.1103/PhysRevC.71.054321](https://doi.org/10.1103/PhysRevC.71.054321).
- [165] A. Staszczak, A. Baran, J. Dobaczewski, W. Nazarewicz, Microscopic description of complex nuclear decay: Multimodal fission, *Phys. Rev. C* 80 (2009) 014309. doi:[10.1103/PhysRevC.80.014309](https://doi.org/10.1103/PhysRevC.80.014309).
- [166] J. Sadhukhan, K. Mazurek, A. Baran, J. Dobaczewski, W. Nazarewicz, J. A. Sheikh, Spontaneous fission lifetimes from the minimization of self-consistent collective action, *Phys. Rev. C* 88 (2013) 064314. doi:[10.1103/PhysRevC.88.064314](https://doi.org/10.1103/PhysRevC.88.064314).
- [167] J. Sadhukhan, J. Dobaczewski, W. Nazarewicz, J. A. Sheikh, A. Baran, Pairing-induced speedup of nuclear spontaneous fission, *Phys. Rev. C* 90 (2014) 061304. doi:[10.1103/PhysRevC.90.061304](https://doi.org/10.1103/PhysRevC.90.061304).
- [168] J. Sadhukhan, W. Nazarewicz, N. Schunck, Microscopic modeling of mass and charge distributions in the spontaneous fission of ^{240}Pu , *Phys. Rev. C* 93 (2016) 011304. doi:[10.1103/PhysRevC.93.011304](https://doi.org/10.1103/PhysRevC.93.011304).
- [169] J. W. Negele, S. E. Koonin, P. Möller, J. R. Nix, A. J. Sierk, Dynamics of induced fission, *Phys. Rev. C* 17 (1978) 1098–1115. doi:[10.1103/PhysRevC.17.1098](https://doi.org/10.1103/PhysRevC.17.1098).

- [170] C. Simenel, A. S. Umar, Formation and dynamics of fission fragments, *Phys. Rev. C* 89 (2014) 031601(R). doi:10.1103/PhysRevC.89.031601.
- [171] G. Scamps, C. Simenel, D. Lacroix, Superfluid dynamics of ^{258}Fm fission, *Phys. Rev. C* 92 (2015) 011602(R). doi:10.1103/PhysRevC.92.011602.
- [172] C. L. Zhang, B. Schuetrumpf, W. Nazarewicz, Nucleon localization and fragment formation in nuclear fission, *Phys. Rev. C* 94 (2016) 064323. doi:10.1103/PhysRevC.94.064323.
- [173] J. Sadhukhan, C. Zhang, W. Nazarewicz, N. Schunck, Formation and distribution of fragments in the spontaneous fission of ^{240}Pu , *Phys. Rev. C* 96 (2017) 061301. doi:10.1103/PhysRevC.96.061301.
- [174] H. Tao, J. Zhao, Z. P. Li, T. Nikšić, D. Vretenar, Microscopic study of induced fission dynamics of ^{226}Th with covariant energy density functionals, *Phys. Rev. C* 96 (2017) 024319. doi:10.1103/PhysRevC.96.024319.
- [175] S. Ebata, T. Nakatsukasa, Pairing Effects in Nuclear Fusion Reaction, *JPS Conf. Proc.* 1 (2012) 013038. doi:10.7566/JPSCP.1.013038.
- [176] S. Ebata, T. Nakatsukasa, Repulsive aspects of pairing correlation in nuclear fusion reaction, *JPS Conf. Proc.* 6 (2014) 020056. doi:10.7566/JPSCP.1.013038.
- [177] G. Scamps, D. Lacroix, Effect of pairing on transfer and fusion reactions, *EPJ Web Conf.* 86 (2015) 00042. doi:10.1051/epjconf/20158600042.
- [178] Y. Hashimoto, G. Scamps, Gauge angle dependence in time-dependent Hartree-Fock-Bogoliubov calculations of $^{20}\text{O} + ^{20}\text{O}$ head-on collisions with the Gogny interaction, *Phys. Rev. C* 94 (2016) 014610. doi:10.1103/PhysRevC.94.014610.
- [179] P. Magierski, K. Sekizawa, G. Wlazłowski, Novel Role of Superfluidity in Low-Energy Nuclear Reactions, *Phys. Rev. Lett.* 119 (2017) 042501. doi:10.1103/PhysRevLett.119.042501.
- [180] G. Scamps, Examining empirical evidence of the effect of superfluidity on the fusion barrier, *Phys. Rev. C* 97 (2018) 044611. doi:10.1103/PhysRevC.97.044611.
- [181] M. Matsuo, Continuum linear response in coordinate space Hartree-Fock-Bogoliubov formalism for collective excitations in drip-line nuclei, *Nucl. Phys. A* 696 (2001) 371. doi:10.1016/S0375-9474(01)01133-2.
- [182] E. Khan, N. Sandulescu, M. Grasso, N. Van Giai, Continuum quasiparticle random phase approximation and the time-dependent Hartree-Fock-Bogoliubov approach, *Phys. Rev. C* 66 (2002) 024309. doi:10.1103/PhysRevC.66.024309.
- [183] Y. Hashimoto, Linear responses in time-dependent Hartree-Fock-Bogoliubov method with Gogny interaction, *Eur. Phys. J. A* 48 (2012) 55. doi:10.1140/epja/i2012-12055-0.
- [184] S. Jin, A. Bulgac, K. Roche, G. Wlazłowski, Coordinate-space solver for superfluid many-fermion systems with the shifted conjugate-orthogonal conjugate-gradient method, *Phys. Rev. C* 95 (2017) 044302. doi:10.1103/PhysRevC.95.044302.
- [185] A. Bulgac, P. Magierski, K. J. Roche, I. Stetcu, Induced Fission of ^{240}Pu within a Real-Time Microscopic Framework, *Phys. Rev. Lett.* 116 (2016) 122504. doi:10.1103/physrevlett.116.122504.
- [186] G. Wlazłowski, K. Sekizawa, P. Magierski, A. Bulgac, M. M. Forbes, Vortex Pinning and Dynamics in the Neutron Star Crust, *Phys. Rev. Lett.* 117 (2016) 232701. doi:10.1103/PhysRevLett.117.232701.
- [187] G. Scamps, Y. Hashimoto, Transfer probabilities for the reactions $^{14,20}\text{O} + ^{20}\text{O}$ in terms of multiple time-dependent Hartree-Fock-Bogoliubov trajectories, *Phys. Rev. C* 96 (2017) 031602. doi:10.1103/PhysRevC.96.031602.
- [188] J. Dobaczewski, H. Flocard, J. Treiner, Hartree-Fock-Bogolyubov description of nuclei near the neutron-drip line, *Nucl. Phys. A* 422 (1984) 103–139. doi:10.1016/0375-9474(84)90433-0.
- [189] E. Terán, V. E. Oberacker, A. S. Umar, Axially symmetric Hartree-Fock-Bogoliubov calculations for nuclei near the drip lines, *Phys. Rev. C* 67 (2003) 064314. doi:10.1103/PhysRevC.67.064314.
- [190] N. N. Bogoliubov, A New method in the theory of superconductivity. I, *Sov. Phys. JETP* 7 (1958) 41.
- [191] J. Blaizot, G. Ripka, *Quantum Theory of Finite Systems*, MIT Press, Cambridge, MA, 1985.
- [192] A. Bulgac, *Hartree-Fock-Bogoliubov Approximation for Finite Systems*, arXiv:nucl-th/9907088. URL <http://arXiv:nucl-th/9907088>
- [193] A. Bulgac, Y. Yu, Renormalization of the Hartree-Fock-Bogoliubov Equations in the Case of a Zero Range Pairing Interaction, *Phys. Rev. Lett.* 88 (2002) 042504. doi:10.1103/PhysRevLett.88.042504.
- [194] J. Blocki, H. Flocard, Simple dynamical models including pairing residual interaction, *Nucl. Phys. A* 273 (1976) 45–60. doi:10.1016/0375-9474(76)90299-2.

- [195] P.-G. Reinhard, M. Bender, K. Rutz, J. A. Maruhn, An HFB scheme in natural orbitals, *Z. Phys. A* 358 (1997) 277–278. doi:10.1007/s002180050328.
- [196] G. Scamps, D. Lacroix, G. F. Bertsch, K. Washiyama, Pairing dynamics in particle transport, *Phys. Rev. C* 85 (2012) 034328. doi:10.1103/PhysRevC.85.034328.
- [197] H. Flocard, S. E. Koonin, M. S. Weiss, Three-dimensional time-dependent Hartree-Fock calculations: Application to $^{16}\text{O}+^{16}\text{O}$ collisions, *Phys. Rev. C* 17 (1978) 1682–1699. doi:10.1103/PhysRevC.17.1682.
- [198] Y. Tanimura, D. Lacroix, G. Scamps, Collective aspects deduced from time-dependent microscopic mean-field with pairing: Application to the fission process, *Phys. Rev. C* 92 (2015) 034601. doi:10.1103/PhysRevC.92.034601.
- [199] Y. Tanimura, D. Lacroix, S. Ayik, Microscopic Phase-Space Exploration Modeling of ^{258}Fm Spontaneous Fission, *Phys. Rev. Lett.* 118 (2017) 152501. doi:10.1103/PhysRevLett.118.152501.
- [200] A. Wakhle, K. Hammerton, Z. Kohley, D. J. Morrissey, K. Stiefel, J. Yurkon, J. Walshe, K. J. Cook, M. Dasgupta, D. J. Hinde, D. J. Jeung, E. Prasad, D. C. Rafferty, C. Simenel, E. C. Simpson, K. Vo-Phuoc, J. King, W. Loveland, R. Yanez, Capture cross sections for the synthesis of new heavy nuclei using radioactive beams, *Phys. Rev. C* 97 (2018) 021602. doi:10.1103/PhysRevC.97.021602.
- [201] S. Ebata, T. Nakatsukasa, T. Inakura, Systematic investigation of low-lying dipole modes using the canonical-basis time-dependent Hartree-Fock-Bogoliubov theory, *Phys. Rev. C* 90 (2014) 024303. doi:10.1103/PhysRevC.90.024303.
- [202] P. M. Goddard, P. D. Stevenson, A. Rios, Fission dynamics within time-dependent Hartree-Fock: deformation-induced fission, *Phys. Rev. C* 92 (2015) 054610. doi:10.1103/PhysRevC.92.054610.
- [203] P. M. Goddard, P. D. Stevenson, A. Rios, Fission dynamics within time-dependent Hartree-Fock. II. Boost-induced fission, *Phys. Rev. C* 93 (2016) 014620. doi:10.1103/PhysRevC.93.014620.
- [204] G. Scamps, C. Simenel, On the origin of asymmetric fission of actinides, arXiv:1804.03337. URL <https://arxiv.org/abs/1804.03337>
- [205] N. Dubray, H. Goutte, J.-P. Delaroche, Structure properties of ^{226}Th and $^{256,258,260}\text{Fm}$ fission fragments: Mean-field analysis with the Gogny force, *Phys. Rev. C* 77 (2008) 014310. doi:10.1103/PhysRevC.77.014310.
- [206] H. Goutte, J. F. Berger, P. Casoli, D. Gogny, Microscopic approach of fission dynamics applied to fragment kinetic energy and mass distributions in ^{238}U , *Phys. Rev. C* 71 (2005) 024316. doi:10.1103/PhysRevC.71.024316.
- [207] D. Regnier, N. Dubray, N. Schunck, M. Verrière, Fission fragment charge and mass distributions in $^{239}\text{Pu}(n, f)$ in the adiabatic nuclear energy density functional theory, *Phys. Rev. C* 93 (2016) 054611. doi:10.1103/PhysRevC.93.054611.
- [208] N. Dubray, D. Regnier, Numerical search of discontinuities in self-consistent potential energy surfaces, *Comput. Phys. Commun.* 183 (2012) 2035–2041. doi:10.1016/j.cpc.2012.05.001.
- [209] E. K. Hulet, J. F. Wild, R. J. Dougan, R. W. Lougheed, J. H. Landrum, A. D. Dougan, M. Schadel, R. L. Hahn, P. A. Baisden, C. M. Henderson, R. J. Dupzyk, K. Sümmerer, G. R. Bethune, Biomodal symmetrical fission observed in the heaviest elements, *Phys. Rev. Lett.* 56 (1986) 313–316. doi:10.1103/PhysRevLett.56.313.
- [210] C. Golabek, C. Simenel, Collision Dynamics of Two ^{238}U Atomic Nuclei, *Phys. Rev. Lett.* 103 (2009) 042701. doi:10.1103/PhysRevLett.103.042701.
- [211] D. J. Kedziora, C. Simenel, New inverse quasifission mechanism to produce neutron-rich transfermium nuclei, *Phys. Rev. C* 81 (2010) 044613. doi:10.1103/PhysRevC.81.044613.
- [212] A. Wakhle, C. Simenel, D. J. Hinde, M. Dasgupta, M. Evers, D. H. Luong, R. du Rietz, E. Williams, Interplay between Quantum Shells and Orientation in Quasifission, *Phys. Rev. Lett.* 113 (2014) 182502. doi:10.1103/PhysRevLett.113.182502.
- [213] V. E. Oberacker, A. S. Umar, C. Simenel, Dissipative dynamics in quasifission, *Phys. Rev. C* 90 (2014) 054605. doi:10.1103/PhysRevC.90.054605.
- [214] K. Hammerton, Z. Kohley, D. J. Hinde, M. Dasgupta, A. Wakhle, E. Williams, V. E. Oberacker, A. S. Umar, I. P. Carter, K. J. Cook, J. Greene, D. Y. Jeung, D. H. Luong, S. D. McNeil, C. S. Palshetkar, D. C. Rafferty, C. Simenel, K. Stiefel, Reduced quasifission competition in fusion reactions forming neutron-rich heavy elements, *Phys. Rev. C* 91 (2015) 041602(R). doi:10.1103/PhysRevC.91.041602.
- [215] A. S. Umar, V. E. Oberacker, C. Simenel, Fusion and quasifission dynamics in the reactions $^{48}\text{Ca}+^{249}\text{Bk}$ and $^{50}\text{Ti}+^{249}\text{Bk}$ using a time-dependent Hartree-Fock approach, *Phys. Rev. C* 94 (2016) 024605. doi:10.1103/PhysRevC.94.024605.
- [216] K. Sekizawa, K. Yabana, Time-dependent Hartree-Fock calculations for multinucleon transfer and quasifission processes in the $^{64}\text{Ni}+^{238}\text{U}$ reaction, *Phys. Rev. C* 93 (2016) 054616. doi:

- [10.1103/PhysRevC.93.054616](https://doi.org/10.1103/PhysRevC.93.054616).
- [217] C. Yu, L. Guo, Angular momentum dependence of quasifission dynamics in the reaction $^{48}\text{Ca}+^{244}\text{Pu}$, *Sci. China Phys.* 60 (2017) 092011. [doi:10.1007/s11433-017-9063-3](https://doi.org/10.1007/s11433-017-9063-3).
- [218] M. Morjean, D. J. Hinde, C. Simenel, D. Y. Jeung, M. Airiau, K. J. Cook, M. Dasgupta, A. Drouart, D. Jacquet, S. Kalkal, C. S. Palshetkar, E. Prasad, D. Rafferty, E. C. Simpson, L. Tassan-Got, K. Vo-Phuoc, E. Williams, Evidence for the Role of Proton Shell Closure in Quasifission Reactions from X-Ray Fluorescence of Mass-Identified Fragments, *Phys. Rev. Lett.* 119 (2017) 222502. [doi:10.1103/PhysRevLett.119.222502](https://doi.org/10.1103/PhysRevLett.119.222502).
- [219] J. Töke, R. Bock, G. X. Dai, A. Gobbi, S. Gralla, K. D. Hildenbrand, J. Kuzminski, W. F. J. Müller, A. Olmi, H. Stelzer, B. B. Back, S. Bjørnholm, Quasi-fission: The mass-drift mode in heavy-ion reactions, *Nucl. Phys. A* 440 (1985) 327–365. [doi:10.1016/0375-9474\(85\)90344-6](https://doi.org/10.1016/0375-9474(85)90344-6).
- [220] L. Guo, T. Nakatsukasa, Time-dependent Hartree-Fock studies of the dynamical fusion threshold, *EPJ Web Conf.* 38 (2012) 09003. [doi:10.1051/epjconf/20123809003](https://doi.org/10.1051/epjconf/20123809003).
- [221] K. Washiyama, Microscopic analysis of fusion hindrance in heavy nuclear systems, *Phys. Rev. C* 91 (2015) 064607. [doi:10.1103/PhysRevC.91.064607](https://doi.org/10.1103/PhysRevC.91.064607).
- [222] R. du Rietz, E. Williams, D. J. Hinde, M. Dasgupta, M. Evers, C. J. Lin, D. H. Luong, C. Simenel, A. Wakhle, Mapping quasifission characteristics and timescales in heavy element formation reactions, *Phys. Rev. C* 88 (2013) 054618. [doi:10.1103/PhysRevC.88.054618](https://doi.org/10.1103/PhysRevC.88.054618).
- [223] S. E. Koonin, K. T. R. Davies, V. Maruhn-Rezwani, H. Feldmeier, S. J. Krieger, J. W. Negele, Time-dependent Hartree-Fock calculations for $^{16}\text{O} + ^{16}\text{O}$ and $^{40}\text{Ca} + ^{40}\text{Ca}$ reactions, *Phys. Rev. C* 15 (1977) 1359–1374. [doi:10.1103/PhysRevC.15.1359](https://doi.org/10.1103/PhysRevC.15.1359).
- [224] Sonika, B. J. Roy, A. Parmar, U. K. Pal, H. Kumawat, V. Jha, S. K. Pandit, V. V. Parkar, K. Ramachandran, K. Mahata, A. Pal, S. Santra, A. K. Mohanty, K. Sekizawa, Multinucleon transfer study in $^{206}\text{Pb}(^{18}\text{O}, x)$ at energies above the Coulomb barrier, *Phys. Rev. C* 92 (2015) 024603. [doi:10.1103/physrevc.92.024603](https://doi.org/10.1103/physrevc.92.024603).
- [225] G. Scamps, C. Rodríguez-Tajes, D. Lacroix, F. Farget, Time-dependent mean-field determination of the excitation energy in transfer reactions: Application to the reaction ^{238}U on ^{12}C at 6.14 MeV/nucleon, *Phys. Rev. C* 95 (2017) 024613. [doi:10.1103/PhysRevC.95.024613](https://doi.org/10.1103/PhysRevC.95.024613).
- [226] K. Sekizawa, Microscopic description of production cross sections including deexcitation effects, *Phys. Rev. C* 96 (2017) 014615. [doi:10.1103/physrevc.96.014615](https://doi.org/10.1103/physrevc.96.014615).
- [227] K. Sekizawa, Enhanced nucleon transfer in tip collisions of $^{238}\text{U} + ^{124}\text{Sn}$, *Phys. Rev. C* 96 (2017) 041601(R). [doi:10.1103/PhysRevC.96.041601](https://doi.org/10.1103/PhysRevC.96.041601).
- [228] D. Regnier, D. Lacroix, G. Scamps, Y. Hashimoto, Microscopic description of pair transfer between two superfluid Fermi systems: Combining phase-space averaging and combinatorial techniques, *Phys. Rev. C* 97 (2018) 034627. [doi:10.1103/PhysRevC.97.034627](https://doi.org/10.1103/PhysRevC.97.034627).
- [229] E. Williams, K. Sekizawa, D. J. Hinde, C. Simenel, M. Dasgupta, I. P. Carter, K. J. Cook, D. Y. Jeung, S. D. McNeil, C. S. Palshetkar, D. C. Rafferty, K. Ramachandran, A. Wakhle, Exploring Zeptosecond Quantum Equilibration Dynamics: From Deep-Inelastic to Fusion-Fission Outcomes in $^{58}\text{Ni} + ^{60}\text{Ni}$ Reactions, *Phys. Rev. Lett.* 120 (2018) 022501. [doi:10.1103/PhysRevLett.120.022501](https://doi.org/10.1103/PhysRevLett.120.022501).
- [230] A. S. Umar, V. E. Oberacker, Center-of-mass motion and cross-channel coupling in the time-dependent Hartree-Fock theory, *J. Phys. G* 36 (2009) 025101. [doi:10.1088/0954-3899/36/2/025101](https://doi.org/10.1088/0954-3899/36/2/025101).
- [231] J. Randrup, Transport of angular momentum in damped nuclear reactions, *Nucl. Phys. A* 383 (1982) 468–508. [doi:10.1016/0375-9474\(82\)90087-2](https://doi.org/10.1016/0375-9474(82)90087-2).
- [232] A. Valor, P.-H. Heenen, P. Bonche, Configuration mixing of mean-field wave functions projected on angular momentum and particle number: Application to ^{24}Mg , *Nucl. Phys. A* 671 (2000) 145. [doi:10.1016/S0375-9474\(99\)00830-1](https://doi.org/10.1016/S0375-9474(99)00830-1).
- [233] M. Anguiano, J. L. Egido, L. M. Robledo, Particle number projection with effective forces, *Nucl. Phys. A* 696 (2001) 467–493. [doi:10.1016/s0375-9474\(01\)01219-2](https://doi.org/10.1016/s0375-9474(01)01219-2).
- [234] M. Samyn, S. Goriely, M. Bender, J. M. Pearson, Further explorations of Skyrme-Hartree-Fock-Bogoliubov mass formulas. III. Role of particle-number projection, *Phys. Rev. C* 70 (2004) 044309. [doi:10.1103/PhysRevC.70.044309](https://doi.org/10.1103/PhysRevC.70.044309).
- [235] J. Dobaczewski, M. V. Stoitsov, W. Nazarewicz, P.-G. Reinhard, Particle-number projection and the density functional theory, *Phys. Rev. C* 76 (2007) 054315. [doi:10.1103/physrevc.76.054315](https://doi.org/10.1103/physrevc.76.054315).
- [236] M. Bender, P.-H. Heenen, Configuration mixing of angular-momentum and particle-number projected triaxial Hartree-Fock-Bogoliubov states using the Skyrme energy density functional, *Phys. Rev. C* 78 (2008) 024309. [doi:10.1103/PhysRevC.78.024309](https://doi.org/10.1103/PhysRevC.78.024309).
- [237] K. Sekizawa, K. Yabana, Particle-number projection method in time-dependent Hartree-Fock

- theory: Properties of reaction products, Phys. Rev. C 90 (2014) 064614. doi:10.1103/PhysRevC.90.064614.
- [238] C. L. Jiang, K. E. Rehm, H. Esbensen, D. J. Blumenthal, B. Crowell, J. Gehring, B. Glagola, J. P. Schiffer, A. H. Wuosmaa, Multineutron transfer in $^{58}\text{Ni} + ^{124}\text{Sn}$ collisions at sub-barrier energies, Phys. Rev. C 57 (1998) 2393–2400. doi:10.1103/physrevc.57.2393.
- [239] L. Corradi, J. H. He, D. Ackermann, A. M. Stefanini, A. Pisent, S. Beghini, G. Montagnoli, F. Scarlassara, G. F. Segato, G. Pollarolo, C. H. Dasso, A. Winther, Multinucleon transfer reactions in $^{40}\text{Ca} + ^{124}\text{Sn}$, Phys. Rev. C 54 (1996) 201–205. doi:10.1103/physrevc.54.201.
- [240] N. Wang, L. Guo, New neutron-rich isotope production in $^{154}\text{Sm} + ^{160}\text{Gd}$, Phys. Lett. B 760 (2016) 236–241. doi:10.1016/j.physletb.2016.06.073.
- [241] W. von Oertzen, A. Vitturi, Pairing correlations of nucleons and multi-nucleon transfer between heavy nuclei, Rep. Prog. Phys. 64 (2001) 1247. doi:10.1088/0034-4885/64/10/202.
- [242] L. Corradi, G. Pollarolo, S. Szilner, Multinucleon transfer processes in heavy-ion reactions, J. Phys. G 36 (2009) 113101. doi:10.1088/0954-3899/36/11/113101.
- [243] L. Bonneau, Fission modes of ^{256}Fm and ^{258}Fm in a microscopic approach, Phys. Rev. C 74 (2006) 014301. doi:10.1103/PhysRevC.74.014301.
- [244] R. Balian, M. Vénéroni, Correlations and fluctuations in static and dynamic mean-field approaches, Ann. Phys. 216 (1992) 351. doi:10.1016/0003-4916(92)90181-K.
- [245] M. Tohyama, Two-body collision effects on the low-L fusion window in $^{16}\text{O} + ^{16}\text{O}$ reactions, Phys. Lett. B 160 (1985) 235–238. doi:10.1016/0370-2693(85)91317-6.
- [246] M. Tohyama, A. S. Umar, Quadrupole resonances in unstable oxygen isotopes in time-dependent density-matrix formalism, Phys. Lett. B 549 (2002) 72–78. doi:10.1016/S0370-2693(02)02885-X.
- [247] M. Assié, D. Lacroix, Probing Neutron Correlations through Nuclear Breakup, Phys. Rev. Lett. 102 (2009) 202501. doi:10.1103/PhysRevLett.102.202501.
- [248] M. Tohyama, A. S. Umar, Two-body dissipation effects on the synthesis of superheavy elements, Phys. Rev. C 93 (2016) 034607. doi:10.1103/PhysRevC.93.034607.
- [249] K. Wen, M. C. Barton, A. Rios, P. D. Stevenson, Two-body dissipation effect in nuclear fusion reactions, Phys. Rev. C 98 (2018) 014603. doi:10.1103/PhysRevC.98.014603.
URL <https://link.aps.org/doi/10.1103/PhysRevC.98.014603>
- [250] K. T. R. Davies, V. Maruhn-Rezwani, S. E. Koonin, J. W. Negele, Test of the Time-Dependent Mean-Field Theory in Kr-Induced Strongly Damped Collisions, Phys. Rev. Lett. 41 (1978) 632. doi:10.1103/PhysRevLett.41.632.
- [251] J. B. Marston, S. E. Koonin, Mean-Field Calculations of Fluctuations in Nuclear Collisions, Phys. Rev. Lett. 54 (1985) 1139–1141. doi:10.1103/PhysRevLett.54.1139.
- [252] P. Bonche, H. Flocard, Dispersion of one-body operators with the Balian-Veneroni variational principle, Nucl. Phys. A 437 (1985) 189–207. doi:10.1016/0375-9474(85)90232-5.
- [253] T. Troudet, D. Vautherin, Mass dispersion through particle emission from a vibrating nucleus, Phys. Rev. C 31 (1985) 278. doi:10.1103/PhysRevC.31.278.
- [254] J. M. A. Broomfield, P. D. Stevenson, Mass dispersions from giant dipole resonances using the Balian-Vénéroni variational approach, J. Phys. G 35 (2008) 095102. doi:10.1088/0954-3899/35/9/095102.
- [255] J. M. A. Broomfield, Calculations of Mass Distributions using the Balian-Vénéroni Variational Approach, Ph.D. thesis, University of Surrey (2009).
- [256] M. Zielinska-Pfabé, C. Grégoire, Dispersions in semiclassical dynamics, Phys. Rev. C 37 (1988) 2594. doi:10.1103/PhysRevC.37.2594.
- [257] C. Martin, D. Vautherin, A variational derivation of semiclassical mean-field evolution equations for a hot Fermi gas, Phys. Lett. B 260 (1991) 1. doi:10.1016/0370-2693(91)90959-T.
- [258] C. Martin, Variational approximation for two-time correlation functions in Φ^4 theory: Optimization of the dynamics, Phys. Rev. D 52 (1995) 7121. doi:10.1103/PhysRevD.52.7121.
- [259] M. Benarous, H. Flocard, Time-Dependent Variational Approach for Boson Systems, Ann. Phys. 273 (1999) 242. doi:10.1006/aphy.1998.5901.
- [260] A. Boudjemâa, M. Benarous, Variational self-consistent theory for trapped Bose gases at finite temperature, Eur. Phys. J. D 59 (2010) 427. doi:10.1140/epjd/e2010-00177-5.
- [261] A. Boudjemâa, Self-consistent theory of a bose-einstein condensate with impurity at finite temperature, J. Phys. A 48 (4) (2015) 045002.
URL <http://stacks.iop.org/1751-8121/48/i=4/a=045002>
- [262] J. C. Roynette, H. Doubre, N. Frascaria, J. C. Jacmart, N. Poffé, M. Riou, On the time scale of $^{40}\text{Ca} + ^{40}\text{Ca}$ strongly damped reactions, Phys. Lett. B 67 (1977) 395. doi:10.1016/0370-2693(77)90428-2.

- [263] S. Ayik, K. Washiyama, D. Lacroix, Fluctuation and dissipation dynamics in fusion reactions from a stochastic mean-field approach, *Phys. Rev. C* 79 (2009) 054606. doi:10.1103/PhysRevC.79.054606.
- [264] K. Washiyama, S. Ayik, D. Lacroix, Mass dispersion in transfer reactions with a stochastic mean-field theory, *Phys. Rev. C* 80 (2009) 031602. doi:10.1103/PhysRevC.80.031602.
- [265] B. Yilmaz, S. Ayik, D. Lacroix, K. Washiyama, Nucleon exchange mechanism in heavy-ion collisions at near-barrier energies, *Phys. Rev. C* 83 (2011) 064615. doi:10.1103/PhysRevC.83.064615.
- [266] S. Ayik, N. Er, O. Yilmaz, A. Gokalp, Quantal effects on spinodal instabilities in charge asymmetric nuclear matter, *Nucl. Phys. A* 812 (2008) 44–57. doi:10.1016/j.nuclphysa.2008.08.007.
- [267] S. Ayik, O. Yilmaz, N. Er, A. Gokalp, P. Ring, Spinodal instabilities in nuclear matter in a stochastic relativistic mean-field approach, *Phys. Rev. C* 80 (2009) 034613. doi:10.1103/PhysRevC.80.034613.
- [268] S. Ayik, O. Yilmaz, F. Acar, B. Danisman, N. Er, A. Gokalp, Investigations of instabilities in nuclear matter in stochastic relativistic models, *Nucl. Phys. A* 859 (2011) 73–86. doi:10.1016/j.nuclphysa.2011.04.004.
- [269] O. Yilmaz, S. Ayik, A. Gokalp, Quantal description of instabilities in nuclear matter in a stochastic relativistic model, *Eur. Phys. J. A* 47 (2011) 123. doi:10.1140/epja/i2011-11123-3.
- [270] O. Yilmaz, S. Ayik, F. Acar, S. Saatci, A. Gokalp, Investigations of spinodal dynamics in asymmetric nuclear matter within a stochastic relativistic model, *Eur. Phys. J. A* 49 (2013) 33. doi:10.1140/epja/i2013-13033-8.
- [271] S. Ayik, B. Yilmaz, O. Yilmaz, A. S. Umar, G. Turan, Multinucleon transfer in central collisions of $^{238}\text{U} + ^{238}\text{U}$, *Phys. Rev. C* 96 (2017) 024611. doi:10.1103/PhysRevC.96.024611.
- [272] D. Lacroix, D. Gambacurta, S. Ayik, Quantal corrections to mean-field dynamics including pairing, *Phys. Rev. C* 87 (2013) 061302. doi:10.1103/PhysRevC.87.061302.
- [273] B. Yilmaz, S. Ayik, D. Lacroix, O. Yilmaz, Nucleon exchange in heavy-ion collisions within a stochastic mean-field approach, *Phys. Rev. C* 90 (2014) 024613. doi:10.1103/physrevc.90.024613.
- [274] S. Ayik, B. Yilmaz, O. Yilmaz, Multinucleon exchange in quasifission reactions, *Phys. Rev. C* 92 (2015) 064615. doi:10.1103/physrevc.92.064615.
- [275] S. Ayik, O. Yilmaz, B. Yilmaz, A. S. Umar, A. Gokalp, G. Turan, D. Lacroix, Quantal description of nucleon exchange in a stochastic mean-field approach, *Phys. Rev. C* 91 (2015) 054601. doi:10.1103/PhysRevC.91.054601.
- [276] S. Ayik, O. Yilmaz, B. Yilmaz, A. S. Umar, Quantal nucleon diffusion: Central collisions of symmetric nuclei, *Phys. Rev. C* 94 (2016) 044624. doi:10.1103/PhysRevC.94.044624.
- [277] T. Skyrme, The effective nuclear potential, *Nucl. Phys.* 9 (1958) 615–634. doi:10.1016/0029-5582(58)90345-6.
- [278] P. Klüepfel, P.-G. Reinhard, T. J. Bürvenich, J. A. Maruhn, Variations on a theme by Skyrme: A systematic study of adjustments of model parameters, *Phys. Rev. C* 79 (2009) 034310. doi:10.1103/PhysRevC.79.034310.
- [279] M. Kortelainen, T. Lesinski, J. More, W. Nazarewicz, J. Sarich, N. Schunck, M. V. Stoitsov, S. Wild, Nuclear energy density optimization, *Phys. Rev. C* 82 (2010) 024313. doi:10.1103/PhysRevC.82.024313.
- [280] M. Kortelainen, J. McDonnell, W. Nazarewicz, P.-G. Reinhard, J. Sarich, N. Schunck, M. V. Stoitsov, S. M. Wild, Nuclear energy density optimization: Large deformations, *Phys. Rev. C* 85 (2012) 024304. doi:10.1103/PhysRevC.85.024304.
- [281] Y. M. Engel, D. M. Brink, K. Goeke, S. J. Krieger, D. Vautherin, Time-dependent Hartree-Fock theory with Skyrme’s interaction, *Nucl. Phys. A* 249 (1975) 215–238. doi:10.1016/0375-9474(75)90184-0.
- [282] T. Lesinski, M. Bender, K. Bennaceur, T. Duguet, J. Meyer, Tensor part of the Skyrme energy density functional: Spherical nuclei, *Phys. Rev. C* 76 (2007) 014312. doi:10.1103/PhysRevC.76.014312.
- [283] J. Dobaczewski, J. Dudek, S. G. Rohoziński, T. R. Werner, Point symmetries in the Hartree-Fock approach. I. Densities, shapes, and currents, *Phys. Rev. C* 62 (2000) 014310. doi:10.1103/PhysRevC.62.014310.
- [284] A. S. Umar, M. R. Strayer, P.-G. Reinhard, Resolution of the Fusion Window Anomaly in Heavy-Ion Collisions, *Phys. Rev. Lett.* 56 (1986) 2793–2796. doi:10.1103/PhysRevLett.56.2793.
- [285] P.-G. Reinhard, A. S. Umar, K. T. R. Davies, M. R. Strayer, S.-J. Lee, Dissipation and forces in time-dependent Hartree-Fock calculations, *Phys. Rev. C* 37 (1988) 1026–1035. doi:10.1103/PhysRevC.37.1026.

- [286] A. S. Umar, M. R. Strayer, P.-G. Reinhard, K. T. R. Davies, S.-J. Lee, Spin-orbit force in time-dependent Hartree-Fock calculations of heavy-ion collisions, *Phys. Rev. C* 40 (1989) 706–714. doi:10.1103/PhysRevC.40.706.
- [287] J. A. Maruhn, P.-G. Reinhard, P. D. Stevenson, M. R. Strayer, Spin-excitation mechanisms in Skyrme-force time-dependent Hartree-Fock calculations, *Phys. Rev. C* 74 (2006) 027601. doi:10.1103/PhysRevC.74.027601.
- [288] A. S. Umar, V. E. Oberacker, Three-dimensional unrestricted time-dependent Hartree-Fock fusion calculations using the full Skyrme interaction, *Phys. Rev. C* 73 (2006) 054607. doi:10.1103/PhysRevC.73.054607.
- [289] E. B. Suckling, P. D. Stevenson, The effect of the tensor force on the predicted stability of super-heavy nuclei, *EPL* 90 (2010) 12001. doi:10.1209/0295-5075/90/12001.
- [290] G.-F. Dai, L. Guo, E.-G. Zhao, S.-G. Zhou, Dissipation dynamics and spin-orbit force in time-dependent Hartree-Fock theory, *Phys. Rev. C* 90 (2014) 044609. doi:10.1103/PhysRevC.90.044609.
- [291] N. Loebl, J. A. Maruhn, P.-G. Reinhard, Equilibration in the time-dependent Hartree-Fock approach probed with the Wigner distribution function, *Phys. Rev. C* 84 (2011) 034608. doi:10.1103/PhysRevC.84.034608.
- [292] N. Loebl, A. S. Umar, J. A. Maruhn, P.-G. Reinhard, P. D. Stevenson, V. E. Oberacker, Single-particle dissipation in a time-dependent Hartree-Fock approach studied from a phase-space perspective, *Phys. Rev. C* 86 (2012) 024608. doi:10.1103/PhysRevC.86.024608.
- [293] G. Dai, L. Guo, E. Zhao, S. Zhou, Effect of tensor force on dissipation dynamics in time-dependent Hartree-Fock theory, *Sci. China Phys.* 57 (2014) 1618–1622. doi:10.1007/s11433-014-5536-8.
- [294] M. C. Barton, P. D. Stevenson, [Magnetic Dipole Transitions with the Full Skyrme Interaction](#), arXiv:1709.07823. URL <https://arxiv.org/abs/1709.07823>
- [295] L. Guo, C. Simenel, L. Shi, C. Yu, [The role of tensor force in heavy-ion fusion dynamics](#), *Phys. Lett. B* 782 (2018) 401 – 405. doi:<https://doi.org/10.1016/j.physletb.2018.05.066>. URL <http://www.sciencedirect.com/science/article/pii/S0370269318304301>
- [296] P. D. Stevenson, E. B. Suckling, S. Fracasso, M. C. Barton, A. S. Umar, Skyrme tensor force in heavy ion collisions, *Phys. Rev. C* 93 (2016) 054617. doi:10.1103/physrevc.93.054617.
- [297] Y. Iwata, J. A. Maruhn, Enhanced spin-current tensor contribution in collision dynamics, *Phys. Rev. C* 84 (2011) 014616. doi:10.1103/PhysRevC.84.014616.
- [298] D. Almhed, P. D. Stevenson, Isovector giant monopole resonances in spherical nuclei, *J. Phys. G* 31 (2005) S1819. doi:10.1088/0954-3899/31/10/079.
- [299] P.-G. Reinhard, P. D. Stevenson, D. Almhed, J. A. Maruhn, M. R. Strayer, Role of boundary conditions in dynamic studies of nuclear giant resonances and collisions, *Phys. Rev. E* 73 (2006) 036709. doi:10.1103/PhysRevE.73.036709.
- [300] B. Avez, C. Simenel, Structure and direct decay of Giant Monopole Resonances, *Eur. Phys. J. A* 49 (2013) 76. doi:10.1140/epja/i2013-13076-9.
- [301] L. Guo, J. A. Maruhn, P.-G. Reinhard, Y. Hashimoto, Conservation properties in the time-dependent Hartree Fock theory, *Phys. Rev. C* 77 (2008) 041301. doi:10.1103/PhysRevC.77.041301.
- [302] U. De Giovannini, D. Varsano, M. A. L. Marques, H. Appel, E. K. U. Gross, A. Rubio, *Ab initio* angle- and energy-resolved photoelectron spectroscopy with time-dependent density-functional theory, *Phys. Rev. A* 85 (2012) 062515. doi:10.1103/PhysRevA.85.062515.
- [303] K. Boucke, H. Schmitz, H.-J. Kull, Radiation conditions for the time-dependent Schrödinger equation: Application to strong-field photoionization, *Phys. Rev. A* 56 (1997) 763–771. doi:10.1103/PhysRevA.56.763.
- [304] M. Mangin-Brinet, J. Carbonell, C. Gignoux, Exact boundary conditions at finite distance for the time-dependent Schrödinger equation, *Phys. Rev. A* 57 (1998) 3245–3255. doi:10.1103/PhysRevA.57.3245.
- [305] C. I. Pardi, P. D. Stevenson, Continuum time-dependent Hartree-Fock method for giant resonances in spherical nuclei, *Phys. Rev. C* 87 (2013) 014330. doi:10.1103/PhysRevC.87.014330.
- [306] C. I. Pardi, P. D. Stevenson, K. Xu, Extension of the continuum time-dependent Hartree-Fock method to proton states, *Phys. Rev. E* 89 (2014) 033312. doi:10.1103/PhysRevE.89.033312.
- [307] B. Schuetrumpf, W. Nazarewicz, Twist-averaged boundary conditions for nuclear pasta Hartree-Fock calculations, *Phys. Rev. C* 92 (2015) 045806. doi:10.1103/PhysRevC.92.045806.
- [308] M. Tohyama, A. S. Umar, Dipole resonances in oxygen isotopes in time-dependent density-matrix theory, *Phys. Lett. B* 516 (2001) 415–420. doi:10.1016/S0370-2693(01)00925-X.

- [309] C. Simenel, Challenges in description of heavy-ion collisions with microscopic time-dependent approaches, *J. Phys. G* 41 (2014) 094007. doi:[10.1088/0954-3899/41/9/094007](https://doi.org/10.1088/0954-3899/41/9/094007).